Development and Testing of Passive Walking Assistive Exoskeleton with Upward Force Assist

Author: **Zlatko Lovrenovic**

A thesis submitted to the

Faculty of Graduate and Postdoctoral Studies

In partial fulfillment of the requirement for the degree of

Masters of Applied Science in Biomedical Engineering

Ottawa – Carleton Institute for Biomedical Engineering

Department of Mechanical Engineering

Faculty of Engineering

University of Ottawa

ABSTRACT

An aging population and rising prevalence in obesity, arthritis and diabetes are resulting in a great number of elders that are suffering from mobility challenges. Walking assist exoskeletons have the potential to help preserve mobility in elders. The most common type of exoskeleton relies on heavily, complex and expensive components to help their user walk effortlessly. Recent research on walking assist exoskeletons has shifted towards the creation of an entirely mechanical system called passive walking assist exoskeleton.

This research aims to design, model and test a passive walking assist exoskeleton that reduces the felt weight of the user during gait. The assist is achieved by the action of a seat mechanism which constantly produces an upward force on the pelvis of the user. This thesis details the entire composition and assembly of such device. The proposed device was modelled in order to predict the assistance provided by the seat mechanism when standing and walking with the device. A human-sized prototype was built and tested in order to mechanically validate the proposed design. The test results validated the proposed seat mechanism which produces the desired upward force, but the use of the exoskeleton in its current state hindered the natural gait pattern of the user.

ACKNOWLEDGMENTS

I would like to express my sincere gratitude and thanks to the many people who helped, encouraged and supported me in the completion of this difficult endeavour. It was a long journey filled with multiple ups and downs, but overall proved to be a great opportunity for personal growth.

Firstly, I would like to thank my thesis supervisor, Dr. Marc Doumit, whose expertise and guidance has been crucial throughout this journey. He proved to be an incredible mentor.

Secondly, I want to thank the faculty and staff members at the University of Ottawa for their commitment to offer post-graduate studies of the highest standards. An additional thank you to the machine shop technicians whose advices and help came very handy.

Thirdly, I want to give a special thanks to my family and closest friends who provided the major inspiration and support for this thesis. They helped me see the light at the end of the tunnel. I wish to dedicate this work to them to express my gratitude for their unshakable believe in my abilities. I am truly blessed to have them in my life.

TABLE OF CONTENTS:

LIST OF FIGURES

LIST OF TABLES

NOMENCLATURE:

Symbol	Description
θ_A	Tilt angle of wire rope on front end of SU.
θ_B	Tilt angle of wire rope on back end of SU.
θ_C	Tilt angle of wire rope wrapped over large pulley of HJU.
θ_D	Tilt angle of wire rope wrapped over small pulley of HJU.
Θ_{KJU}	Angle of KJU in locking position (º).
θ_{SFU}	Angle of SFU in locking position (º).
θ_{SLU}	Angle of SLU (º).
θ_{TLU}	Angle of TLU (º).
ω_{SFU}	Angular velocity of SFU (rad/s).
α_{SFU}	Angular acceleration of SFU (rad/s^2).
ΔL_{AB}	Length variation of segment AB between case 2 and case 1 in standing (m).
ΔL_{CD}	Length variation of segment CD between case 2 and case 1 in standing (m).
$\Delta L_{SPRING\ INITIAL}$	Initial spring extension (m).
ΔL_{SPRING}	Extension of extension spring (m)
ΔY_{SEAT}	Vertical displacement of seat (m)
η	Energy efficiency for walking
$a_{COM\ X}$	Horizontal acceleration of COM (m/s^2)
$a_{COM\ Y}$	Vertical acceleration of COM (m/s^2)
BRHEL	Berkeley Robotics and Human Engineering Laboratory
BW	Bodyweight (N)
CAD	Computer assisted design
COG	Center of gravity of human body.
COM	Center of mass of body segment.
COP	Center of pressure of GRF
COT	Cost of transport of walking (W)
CPG	Central Pattern Generator.
CPU	Central Processing Unit.
D_{PULLEY}	Diameter of larger pulley (m)
DOF	Degree of freedom of joint.
$\dot{E}_{METABOLIC}$	Metabolic rate of walking.
EWU	Elastic wire rope unit.
F_{AXIAL}	Compressive axial force at SLU (N)
F_{CX} and F_{CY}	Reaction forces at hip joint unit attachment (N)
F_{DX} and F_{DY}	Reaction forces at thigh link unit attachment (N)
F_{EX} and F_{EY}	Reaction forces at small pulley attachment (N)
F_{GX} and F_{GY}	Reaction forces at knee joint center (N)
F_{RSU}	Compressive force transmitted in rubber stopper unit (N)
F_{SEAT}	Force applied on seat (N).
F_{SHEAR}	Shear force at SLU (N)
$F_{USER\ Y}$	Upward force on SU interface (N)
$F_{USER\ X}$	Horizontal force on SU interface (N)
FBD	Free Body Diagram.
FPU	Foot Plate Unit.
GC	Gait cycle.
GRF	Ground reaction forces (N).
H	Height of person (m).
H_{TOTAL}	Total height of device.
HJU	Hip Joint Unit.
HDPE	High density poly-ethylene.
HULC	Human Universal Load Carrier
I	Second moment of inertia (kg/m^2).
K_{SPRING}	Stiffness of spring (N/m).
KJU	Knee Joint Unit
$L_{AB\ 1}$	Length of segment AB for case 1 in standing (m).
$L_{AB\ 2}$	Length of segment AB for case 2 in standing (m).
L_{AE}	Length of wire rope of each EWU (m).
$L_{C/BUTT}$	Distance between point C and point BUTT in MATLAB simulation (m).
L_{CD}	Distance between point C and point D in MATLAB simulation (m).
$L_{CD\ 1}$	Length of segment CD for case 1 in standing (m).

$L_{CD\ 2}$	Length of segment CD for case 2 in standing (m).
$L_{D/BUTT}$	Distance between point D and point BUTT in MATLAB simulation (m).
$L_{EF\ 1}$	Length of extension spring for case 1 in standing (m).
$L_{EF\ 2}$	Length of extension spring for case 2 in standing (m).
L_{FPU}	Length of FPU (m).
L_{SLU}	Length of SLU (m).
L_{SU}	Length of SU (m).
L_{TLU}	Length of TLU (m)
$L_{TOTAL\ 1}$	Length of wire rope and extension spring of EWU (m).
M_C	Moment at hip joint unit attachment (Nm)
M_G	Moment at knee joint unit (Nm)
M_{SFU}	Mass of seat frame unit (kg).
M_{SU}	Mass of seat unit (kg).
P_{SEAT}	Pressure on seat interface (mmHg)
PAM	Pneumatic Artificial Muscle.
ROM	Range of motion of joint. (º)
RSU	Rubber Stopper Unit
SA_{SU}	Surface area of SU (m^2)
SFU	Seat Frame Unit
SLU	Shank Link Unit
SU	Seat Unit
T_{EWU}	Tension force in EWU (N)
TC	Trigger Cable
TLU	Thigh Link Unit
Vco_2	Consumption rate of carbon dioxide
Vo_2	Consumption rate of oxygen
$Y_{SEAT\ 1}$	Vertical position of SU for case 1 in standing (m).
$Y_{SEAT\ 2}$	Vertical position of SU for case 2 in standing (m)
$Y_{SEAT\ INITIAL}$	Initial vertical position of SU (m).
W_{FOOT}	Width between FPU (m).
W_{SFU}	Weight of seat frame unit (N)
W_{SLU}	Weight of shank link unit (N)
W_{SU}	Width of SU (m).
W_{SU}	Weight of seat unit (N)
W_{TLU}	Weight of thigh link unit (N).
W_{TOTAL}	Total width, depth of device (m).
WAE	Walking Assist Exoskeleton

CHAPTER 1. INTRODUCTION

1.1 INTRODUCTION

The ability to walk freely and safely is perhaps the most common indicator of mobility and independence. Regrettably, a large portion of the population is experiencing a loss in their walking abilities due to aging and/or chronic health conditions such as obesity, diabetes and arthritis. There is an urgent need to develop systems that will help preserve mobility for elderly and people in needs. One promising solution venue is walking assistive exoskeletons (WAE). The following thesis details the development and testing of a novel WAE.

1.2 RATIONALE

Mobility defines the ability to move freely and easily from one place to another. A person capable of walking on their own without major muscular effort is considered to hold a functional level of mobility [1]. Unfortunately, most people will experience a form of loss of mobility in their lifetime that will hinder their walking abilities. Loss of mobility defines any limitations of movement due to a physiological impairment. Aging is the most common cause of loss of mobility. As people age, they gradually counter challenges in walking effectively and effortlessly such their autonomy and productivity are significantly reduced. Consequently, they become dependent on the assistance of others to get around. Such a scenario is expected to become a growing concern in our society due to the fact that the elderly population is growing at a rapid rate. According to Statistics Canada, life expectancy in men is projected to rise from 78.8 to 84.0 years old, while women life expectancy is expected to rise from 83.3 to 87.3 years old by the year 2036 [2]. The same projection predicts that the population of 65 years and over will rise from 5.18 to 10.38 million. The U.S. Census Bureau projects that the American population aged 65 and over will be 83.72 million by 2050 [3]. These projections reveal that a larger number of elders is expected to be affected by a loss of mobility. Aging may be combined with the effects of prominent medical conditions such as obesity, arthritis, and diabetes to further restrain mobility. Obesity is known to hinder mobility due to the excess load carried by the musculoskeletal system. In fact, energy expenditure for ground level walking are higher in obese individuals [4],[5]. Health Canada estimates that 34.2 % of the population will be overweight and 21.2 % will be obese by 2019 [6]. In the United States, trends based on the National Health and Nutrition Examination Survey estimates that by 2030,

51.2 % of the American population will be obese [7]. Arthritis is another rising health problem that affects mobility. People with advanced arthritis have pronounced pain in their lower limb joints. Studies indicate that arthritis-related pain in lower limbs decreases physical activity which leads to the development of mobility limitations [8]. According to the Canadian Community Health Survey, 4.8 million Canadians were affected by arthritis in 2000 and the number is expected to surpass 6 million by 2026 [9]. In the United States, the number of reported arthritis is projected to rise from 52.5 to 78.0 million from now to 2040 [10]. Diabetes is a third rising health concern that affects mobility in elders. Studies report greater decline in basic functions and onset of severe disabilities in elders with diabetes [11],[12]. According to the Canadian Diabetes Association, the current prevalence of diabetes is expected to increase 44 % by the year 2025 [13]. The increasing prevalence of obesity, arthritis and diabetes combined with an aging population implies that loss of mobility among elders will become a serious social and economic issue in the near future. Such a scenario reveals the urgency to develop solutions in preserving mobility. One proven solution venue is through the development of WAE.

Such device is a mechanical system worn by a user and intended to reduce the physiological and metabolic cost of walking [5]. Typically, WAE are intended for individuals able to move on their own. Thus, the device does not replace the legs of the user, but instead enhance their abilities to achieve mobility. There are two categories of WAE: powered and passive. On one end, powered exoskeletons use portable batteries, actuators, sensors and control units to help the user walking. On the other end, passive WAE only employ mechanical components to assist the user. The present successful generation of WAE are mostly powered in their design. Complexity, bulkiness, limited operation time and excessive cost are some drawbacks of such class of WAE. This justifies current research interest which is focused on developing passive devices. A recent example is the Ankle Exoskeleton developed by Collins & al which recorded a reduction of 7.2 % in metabolic cost during gait trials on healthy participants [14]. Such result reveals the potential of creating simple, cost effective, easy to use and customisable WAE to assist user.

1.3 OBJECTIVES

The following thesis aims to achieve two objectives. The first objective is to design a passive WAE that assist the user by reducing its felt weight during locomotion. This is achieved through the use of solely mechanical components with no portable power source. The second objective is to analytically and experimentally validate the proposed exoskeleton design. This objective implies an analytical model development and a fabrication of a prototype for human testing.

1.4 THESIS CONTRIBUTIONS

This thesis has led to the following 5 research contributions.

1. Comprehensive literature review that shed the light on the challenges of current WAE and the requirements in formulating an assist strategy for a passive WAE.

2. Proposed a novel exoskeleton seat mechanism that provides an upward force without impeding the user gait. The mechanism ensures that the assist force is vertical such not to impede user stability while standing. Unlike existing mechanism that relies on sensors and actuators, the mechanism is composed of solely mechanical components.

3. Two analytical models were developed to predict the behaviour of the proposed WAE. The standing model determines the effect of increasing spring stiffness on assistance to the user, while the walking model predicts how the device moves during gait and more importantly when peak assistance is provided by the seat mechanism.

4. Proposed a novel passive WAE structure shown by Figure 1-1. The proposed design is simple, light, easy to use and more affordable in comparison to currently available powered WAE.

5. A prototype of the proposed design was fabricated and tested in a gait lab by the researcher. The prototype is made primarily of aluminium and high density polyethylene (HDPE). During testing, loads cells were used to measure the loads generated by the seat mechanism when standing and walking with the device. Motion capture technologies were used to track the motion of the user when walking with and without the device in order to detect if gait was compromised.

Figure 1-1: CAD model of proposed passive WAE, isometric view.

1.5 SCOPE AND LIMITATIONS

The development of a WAE represents a long and strenuous process made of 4 steps: design, modelling, prototyping, and testing. The primary focus of this thesis centered on the design and modelling for a passive system. All prototypes and tests were completed only for the purpose of providing additional support to the proposed design.

1.6 THESIS OUTLINE

This thesis is organized into six chapters. Chapter 1 states the driving motivation in the development of a passive WAE, the objectives and contributions of the thesis.

Chapter 2 presents the results of a literature review divided into two sections: gait cycle and current state of WAE. The first section describes the many variables used to quantify human walking and how these variables are used in the design of WAE. The second section makes the distinctions between current WAE and discusses the major challenges faced by current WAE.

Chapter 3 details the design and modelling of a passive WAE. The major inspiration in the design process is unveiled followed by a description of the seat mechanism. An overall description of the final design is given followed by description of the multiple sub-assemblies of the device. The chapter also showcase the modeling conducted in MATLAB to predict the mechanical response of the proposed device when standing and walking.

Chapter 4 details the fabrication of a human sized prototype intended for testing. The manufacturing and assembly of the final prototype are disclosed. Chapter 4 follows by a description of the testing apparatus used to evaluate the performance of the prototype. Lastly, relevant results of preliminary mechanical tests are presented.

Chapter 5 unveils the results collected during human standing and walking trials. The data measured by all testing equipment is discussed and compared to theoretical values obtained from the MATLAB models.

Chapter 6 concludes the thesis by unveiling the major accomplishments achieved and by listing the potential improvements for the current prototype.

CHAPTER 2: LITERATURE REVIEW

Chapter 2 presents the findings of a literature review. The chapter is divided into two sections: gait analysis and current state of WAE. The first section describes how walking is quantified using various measurements and how these measurements are used in developing WAE. The presented measurements are kinematics, kinetics and energetics. The second section of the literature review gives an overlook on the current state of WAE. The distinctions between passive and powered WAE are made by providing examples for the two categories. It is followed by a discussion on the challenges faced by current WAE.

2.1 GAIT ANALYSIS

The development of WAE requires an in depth understanding of walking such as to devise the proper strategy as to how to assist the user. Gait analysis defines the quantitative study of human walking. Gait analysis views walking as a synchronized, cyclic and controlled sequence of limb motions. The starting and ending point in gait analysis corresponds to two consecutive contacts of one foot with the ground, also referred as heel strike. The time period between two heel strikes is called the gait cycle (GC). One GC is divided into two phases, stance (60 % of GC) and swing (40 % of GC). Stance defines the interval when the studied foot is in contact with the ground, while swing is the interval when the studied foot is in the air. Figure 2-1 depicts a visual schematic of the GC in the sagittal plane.

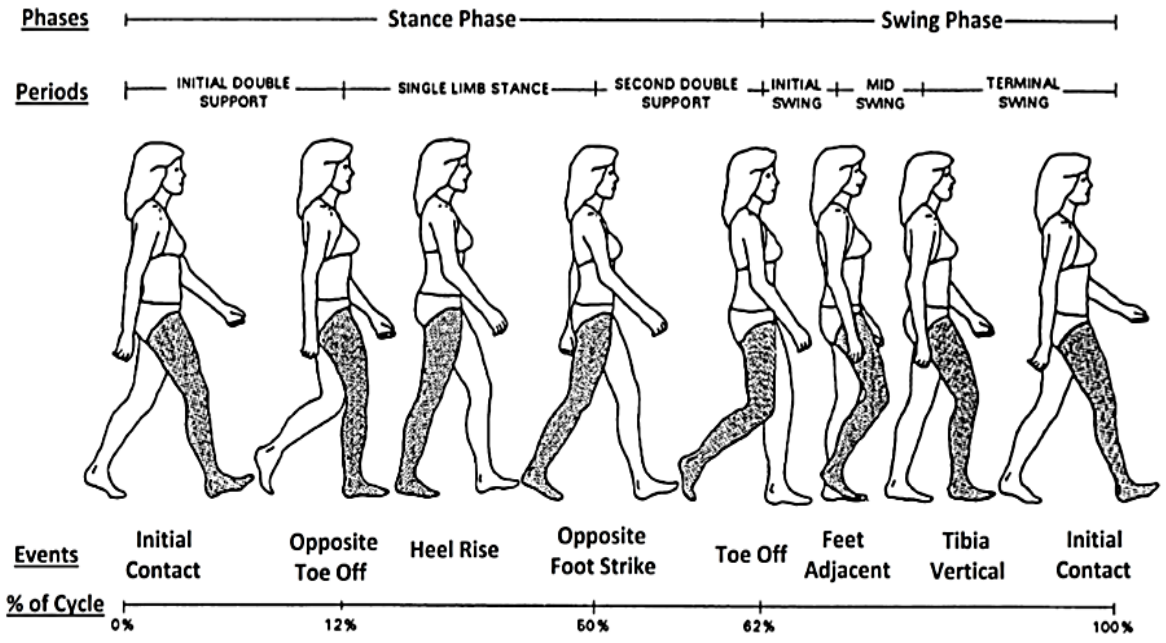

Figure 2-1: Illustration of GC for right leg [15].

Gait analysis focuses mainly on the motion of the lower limbs. Upper body motion is often ignored, since it does not directly contribute to the action of walking [16]. Stance is divided into three periods: initial double limb support, single limb support and second double limb support. Swing is divided into three periods: initial swing, mid swing and terminal swing. Table 2-1 details the time duration and functions of those 6 GC periods.

Table 2-1: Description of 6 GC periods.

Period	% GC	Functions
Initial Double Limb Support	0-12	Loading of support leg. Shock absorption. Weight transfer between legs.
Single Limb Support	12-50	Support of body. Forward progression of COG.
Second Double Limb Support	50-62	Unloading of support leg. Preparation for swing.
Initial Swing	62-75	Foot clearance.
Mid Swing	75-85	Limb advancement.
Terminal Swing	85-100	Deceleration of moving leg. Preparation of foot strike Preparation of weight transfer.

Scholars also use another terminology to divide the GC. This approach divides stance into 5 smaller time periods, where each period describes a specific motion of lower limbs. These smaller periods are called the sub phases of the GC. Table 2-2 details the starting and ending point of the sub phases.

Table 2-2: Description of sub phase of GC.

Sub-phases	% GC	Start	End
Initial Contact	0-2	Foot strike.	-
Loading Response	0-10	Foot strike.	Opposite toe off.
Mid Stance	10-30	Opposite toe off.	Body weight aligned with forefoot.
Terminal Stance	30-50	Heel rise.	Opposite foot strike.
Pre Swing	50-60	Opposite foot strike.	Ipsilateral toe-off.
Initial Swing	60-73	Toe off.	Swinging foot is opposite to other foot.
Mid Swing	73-87	Swinging foot is opposite to other foot.	Vertical tibia
Terminal Swing	87-100	Vertical tibia.	Foot touches ground.

2.1.1 ANTHROPOMETRY

Anthropometry is a branch of Anthropology which focuses on measurements of human body segments. Anthropometry is extensively used in gait analysis to approximate properties of body segments such as their length (L), mass (M), position of center of mass (COM) and second moment of inertia (I). It is also a useful tool in the development of personalized WAE meaning an exoskeleton that fits the anatomical needs of its user. Figure 2-2 presents an

anthropometric model that expresses the length of body segments as a function of the person's body height (*H*).

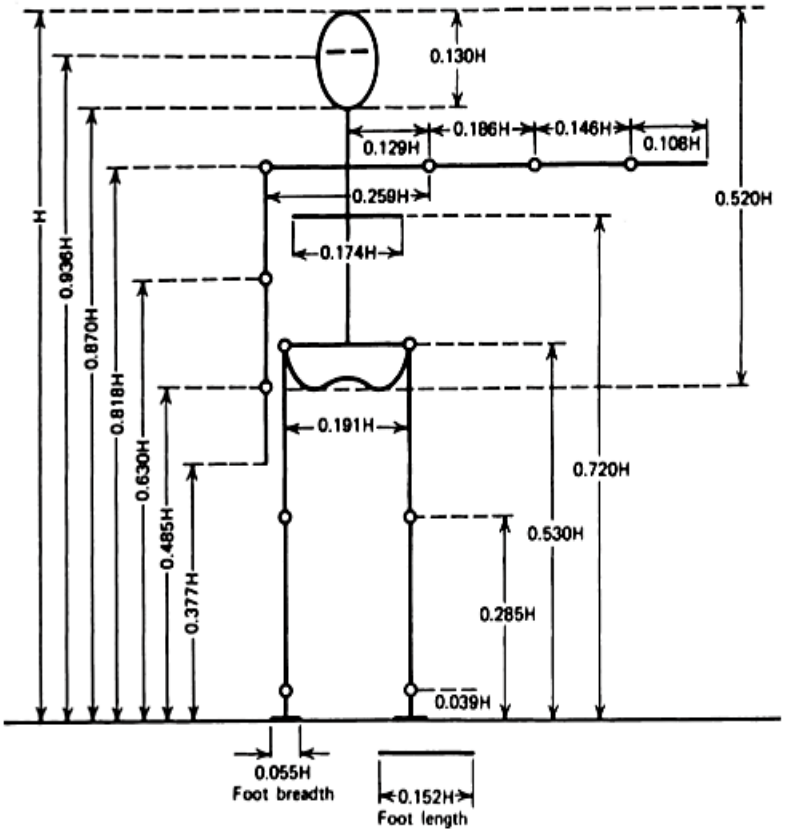

Figure 2-2: Length of body segments expressed as a fraction of H [17].

In Figure 2-2, the human body is modelled as an assembly of rigid segments connected about anatomical joints. This approach in modeling the human body is called the rigid link model. Table 2-3 provides anthropometric measurements of 4 body segments expressed in terms of *M* and *L*.

Table 2-3: Mass and inertial properties of lower limbs [17].

Segment	Mass /Body Mass	Center of Mass / Segment Length	Radius of Gyration / Segment Length	
	(Fraction of M)	(Proximal)	(COG)	(Proximal)
Foot	0.0145	0.5	0.475	0.690
Shank	0.0465	0.433	0.302	0.528
Thigh	0.1	0.433	0.323	0.540
Leg	0.061	0.606	0.416	0.735

2.1.2. GAIT KINEMATICS

Gait kinematics presents the movement of body segments during locomotion. It studies the linear and angular displacements of lower body segments about the three joints: hip, knee and ankle. Motion capture technologies are often used to acquire gait kinematics. In such an approach, the position of reflective markers placed on anatomical landmarks is recorded during motion. The data are processed to find displacement, velocity and acceleration. Figure 2-3 unveils the normal angular motion of the hip, knee and ankle about the sagittal plane during gait.

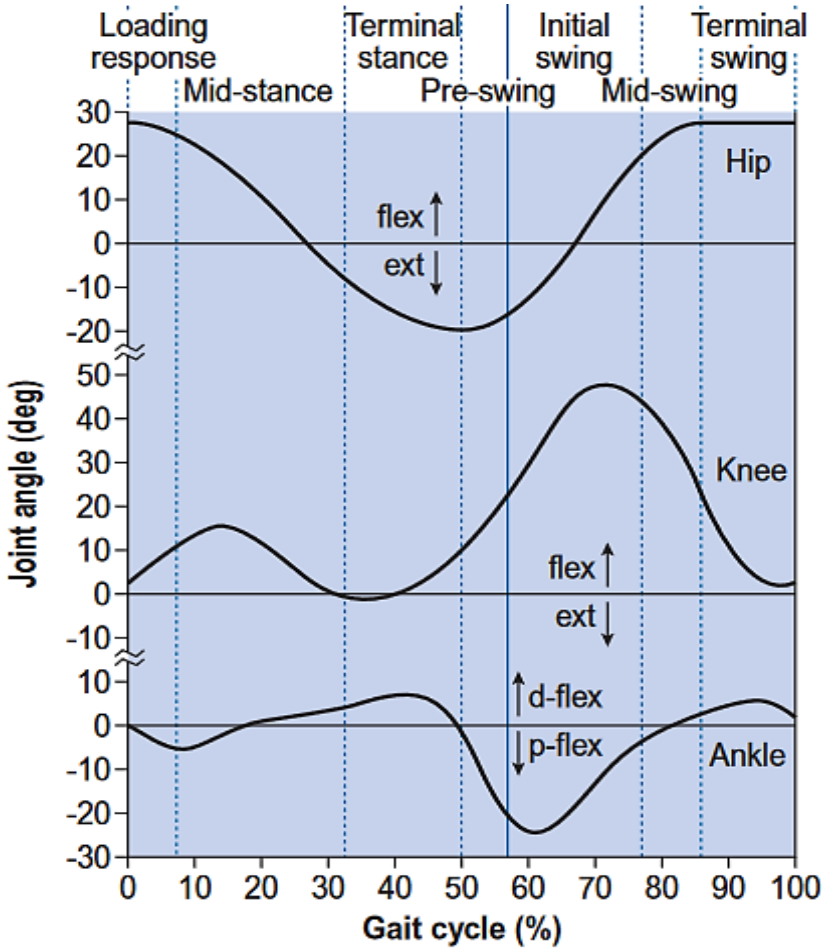

. **Figure 2-3**: Sagittal plane motion of hip (top), knee (center) and ankle (bottom) during gait [18].

Figure 2-3 reveals that the three joints move differently during gait. The hip comes through a single flexion and extension cycle. The average range of motion (ROM) of the hip is 40º,average peak flexion is 30º and average peak extension is 10º [16]. The knee goes

through two cycles of flexion and extension with an average ROM of 60º [16]. During stance, the knee flexes during loading response and early midstance and extends in later mid stance. Average peak flexion during stance is 18º [16]. During swing, peak flexion reaches 67º and drops to 5º at end of swing [16]. The ankle alternates twice between plantarflexion and dorsiflexion. In stance, the ankle reaches a first plantarflexion peak of 5º followed by peak dorsiflexion of 10º and ends with a second plantarflexion peak of 20º [16]. During swing, the ankle only dorsiflexes to ensure foot clearance and to prepare for the next step. The use of a WAE should not hinder hip, knee and ankle motion to ensure that the user can walk in a controlled and comfortable manner. If the device mechanically blocks or limits certain motions, the exoskeleton will impose kinematic constraints on its user.

2.1.3 GAIT KINETICS

Gait kinetics focuses on determining the internal and external forces causing the synchronized motion of lower limbs during walking. The external forces involved in walking are the ground reaction force (GRF) and the mass of body segments. As shown, the mass of body segments can be approximated by using anthropometry. The GRF corresponds to the total force applied by the studied foot on the ground. GRF are measured with the use of force plates. Figure 2-4 unveils GRF recorded for ground level walking. Note that, the value of GRF is normalized in terms of bodyweight (BW).

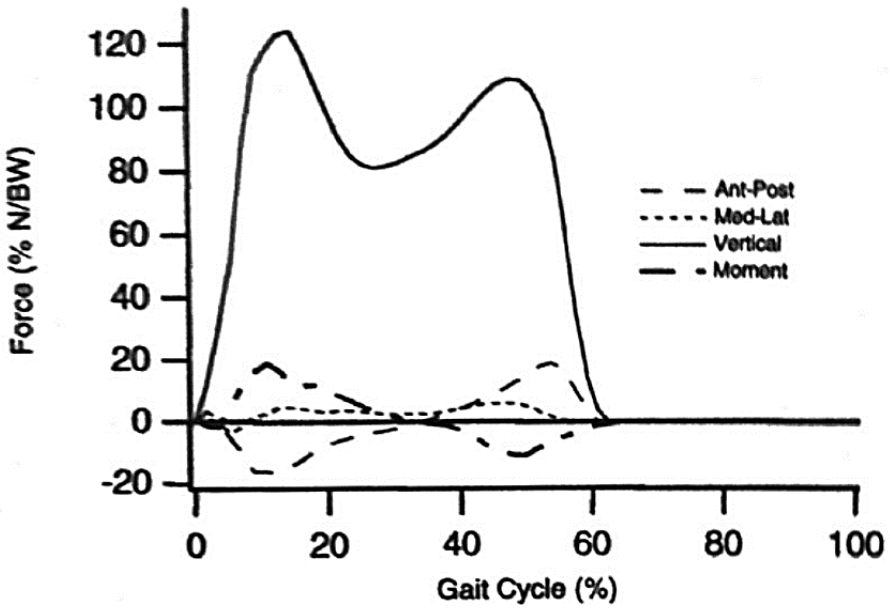

Figure 2-4: GRF during ground level gait about three directions: vertical (solid line), anterior-posterior (dotted line) and medial-lateral (dashed line) [15].

Figure 2-4 shows the 'butterfly' profile for the vertical GRF. The first peak corresponds to the upward acceleration of the center of gravity (COG) during early stance. The lower peak results from the body going over the supporting leg during mid stance. The second peak is due to the deceleration of the body during late stance in preparation of swing. In Figure 2-4, the highest value in vertical GRF accounts for about 1.2 BW. Note that, the 'butterfly' profile is affected by walking speed. In 1997, Cook & al. showed that at a walking speed of 0.9 m/s, the vertical GRF did not show three distinct peaks and remained close to stable throughout the stance [19]. From Figure 2-4, the medial / lateral GRF is much smaller in magnitude and peaks at about 0.05 BW. Medial / lateral GRF acts to accelerate the COG towards the side of the swinging leg. The anterior/posterior GRF moves from a negative to a positive value. The negative half corresponds to a braking action of the foot, while the positive half correspond to the propulsion action of the foot. It peaks with a value of about 0.2 BW in both directions.

For internal forces, muscles are the major internal contributor in the production of motion. Internal loading values are often approximated with the use of Inverse Dynamics, since direct measurements are too invasive. In the Inverse Dynamics approach, all the internal forces such as muscles, ligaments and joint contact forces are regrouped and simplified by a

net joint force and a moment acting about the center of the studied joint. With such simplification, it is not possible to identify the contribution of each muscle. A positive value of moment is an indication of an internal flexor moment, while a negative moment is associated with an internal extensor moment. Note that a positive moment does not imply that only flexor muscles are acting, but rather than the net actuation comes from flexor muscles. Joint power about each joint can be computed by multiplying moment with angular velocity. Joint power gives an indication on the type of action muscles are producing. Positive power generates motion, while negative power brakes or absorbs motion. Figure 2-5 presents the moment and power plots of the hip, knee and ankle for one GC. Note that, both moment and power values are normalized with body mass.

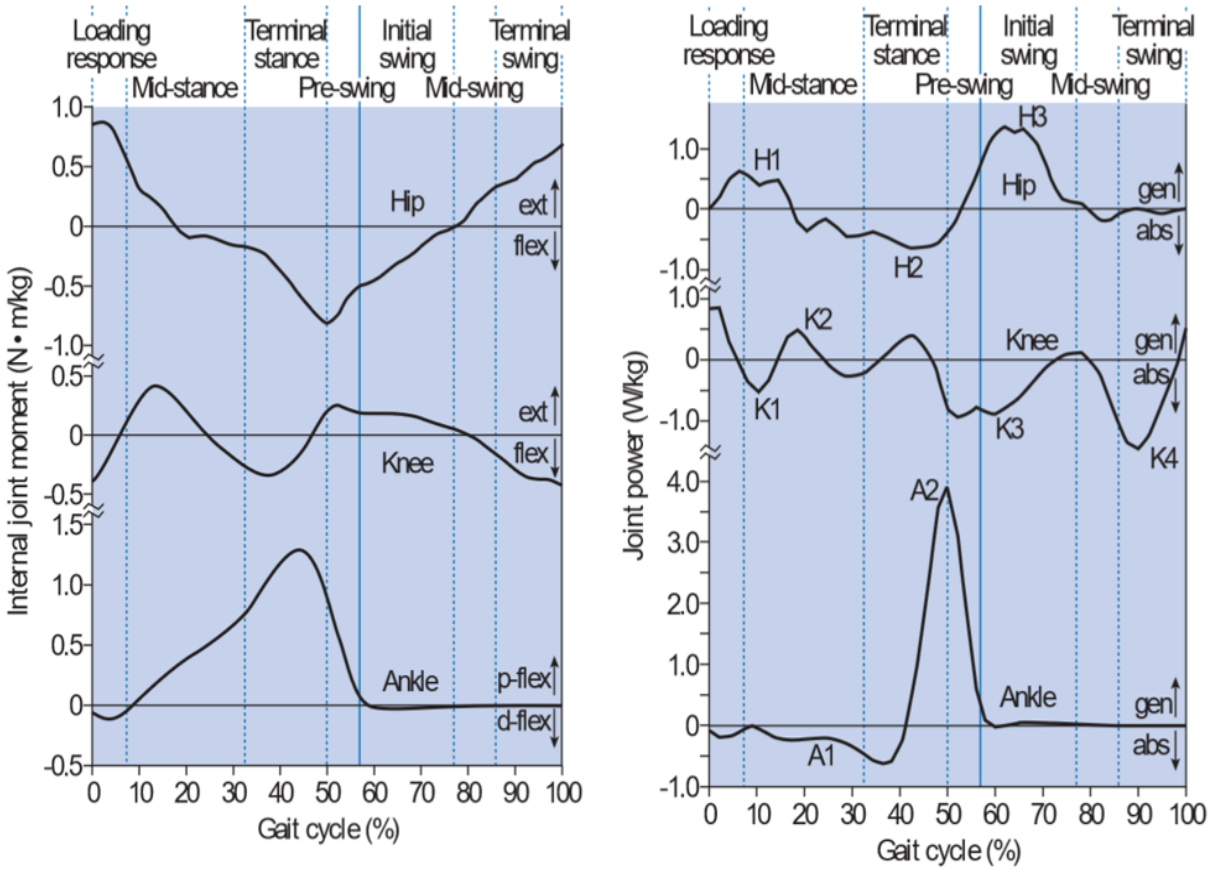

Figure 2-5: Joint moment (left) and joint power (right) of the ankle, knee and hip during gait [18].

From Figure 2-5, it is visually apparent that leg muscles act differently on the three joints. A detailed description of Figure 2-5 can be found in APPENDIX A. Table 2-4 reveals

the maximum positive and negative values of moment and power for three joints in Figure 2-5.

Table 2-4: Maximum values of moment and power for hip, knee and ankle.

Joint	Moment (Nm/kg)	Power (W/kg)
Hip	0.80 / -0.80	1.25 / -0.50
Knee	0.50 / -0.40	0.80 / -1.50
Ankle	1.25 / -0.10	4.00 / -0.80

Moment and power plots are extensively used in the development of WAE. These plots reveal the merit in producing either positive or negative assistive torques about lower limb joints during gait. The intended result with such assistive approach is that the WAE reduces muscular work. For that approach to work properly, it is crucial that the torque created by the exoskeleton is synchronized with the torque produced by muscles. Otherwise, the user will be fighting the torque of the exoskeleton.

2.1.4 GAIT ENERGETICS

Gait energetics studies the energy required for a person to walk. People walk in manner to minimize the displacement of their COG and to avoid deviating from their natural gait [15]. Walking can be regarded as the direct result of energy conversion. It starts at the cellular level where intake food is chemically converted to ATP to later be used by tissues, mainly muscles, to produce motion and heat. Energy efficiency in walking (η) is expressed as overall muscular mechanical work over net metabolic energy. It is given by (2-1) [15].

$$\eta = \frac{Mechanical\ work}{walking\ metabolic\ cost - resting\ metabolic\ cost} \tag{2-1}$$

In 1977, G.A. Cavagna and M. Kaneko measured η to be about 24 % for ground level walking at a comfortable speed [20]. Energy consumed by tissues is hard to measure and thus metabolic cost is often expressed in terms of metabolic rate ($\dot{E}_{METABOLIC}$). The consumption rate of oxygen (VO_2) and the output rate of carbon dioxide (VCO_2) during walking are most commonly used to approximate $\dot{E}_{METABOLIC}$ given by (2-2) where both VO_2 and VCO_2 are expressed in ml/s .

$$\dot{E}_{METABOLIC} = 16.58\,\dot{V}O_2 + 4.51\,\dot{V}CO_2 \quad (2\text{-}2)$$

Another measurement calculated in gait energetics is the cost of transport (COT) which corresponds to ratio of $\dot{E}_{METABOLIC}$ over the product of BW and travelled distance (d). COT values provide an approximate on the amount of energy required for a person to move. It is given by (2-3).

$$COT = \frac{\dot{E}_{METABOLISM}}{BW \times d} \quad (2\text{-}3)$$

Many gait parameters are known to increase or decrease COT and $\dot{E}_{METABOLIC}$ values. In 2007, Browning & al. found that adding weights on legs resulted in increasing COT values [21]. In 2014, P.Huang and D.Kuo found that energy expenditure increases by 7.6 W for each 1 kg payload carried in a backpack [22]. Step length and walking speed are two other gait parameters known to impact gait energetics. COT values increase with cadences values [23], [24], [25]. Increasing step length during walking has been found to increase COT values [26], [27]. In 2003, Gottschall and Kram measured the effect of applying a forward (assisting) and backward (impeding) force on the pelvis during locomotion [28]. Figure 2-6 shows their results for $\dot{E}_{METABOLIC}$ versus the application of a horizontal force.

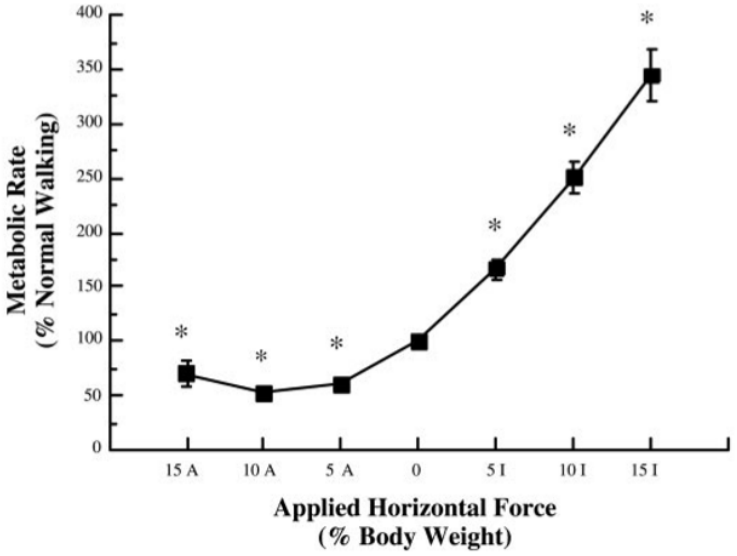

Figure 2-6: Normalized metabolic rate versus applied horizontal forces [28]..

In Figure 2-6, $\dot{E}_{METABOLIC}$ increases in a linear trend with the application of an impending force. Conversely, the application of a forward force leads to a decrease in $\dot{E}_{METABOLIC}$ values. In 1992, Farley and McMahon [29] studied the effect of reducing felt weight on $\dot{E}_{METABOLIC}$ using the experimental apparatus shown by Figure 2-7.

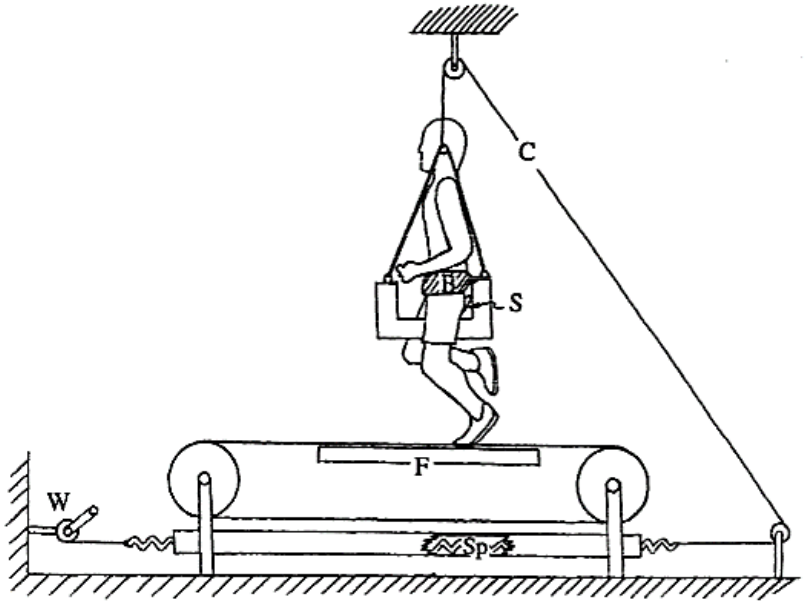

Figure 2-7: Experimental apparatus for producing reduced felt weight to participant walking on treadmill [29].

In Figure 2-7, a spring, cable and horse saddle were used to apply an upward force on the pelvis of the participant when walking on a treadmill. Their study found that $\dot{E}_{METABOLIC}$ decreases in almost a linear manner with increased reduction of felt weight. A decrease in $\dot{E}_{METABOLIC}$ of 25 % was recorded when reducing the felt weigh of the participant by 50 %. Such result supports the creation of WAE intended to reduce felt weight of user during locomotion.

2.1.5 KINEMATICS OF COG

The COG of the human body is located slightly anterior to the second sacral vertebra. The movement of the COG plays a crucial role in gait energetics. It is ideal that the COG maintain its height so that potential energy remained constant during gait. However, the COG undergoes sinusoidal variations during gait as shown by Figure 2-8.

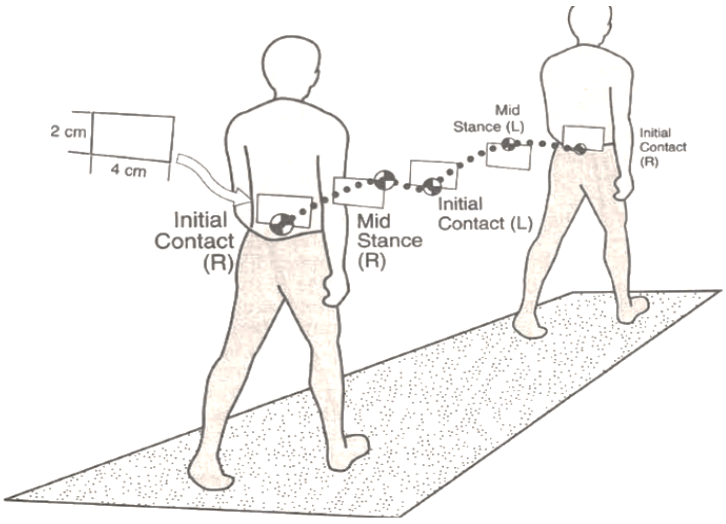

Figure 2-8: Illustration of COG progression during gait [16].

Figure 2-8 reveals that the COG travels vertically in a double sinusoidal profile with average amplitude of 2.5 cm [16]. Lowest positions are reached during double limb support, while highest positions are reached during single limb support. The horizontal displacement of the COG follows a single sinusoidal profile with an average amplitude of 4.5 cm [16]. Such small variations in vertical and horizontal displacements of the COG are the result of 6 optimization strategies of the human body. Three strategies concern the motion of the ankle,

knee and hip to vary the effective length of each leg during gait. The remaining three optimization strategies relate to the displacement of the pelvis during gait as shown by Figure 2-9.

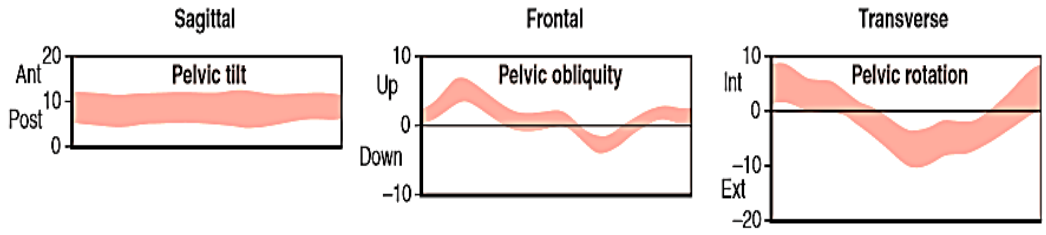

Figure 2-9: Displacement of pelvis about the sagittal (left), frontal (middle) and transverse (right) planes during gait [32].

From Figure 2-9, the average ROM about the sagittal, frontal and transverse plane for the pelvis are respectively 4º, 7º and 10º. An assistive device used during walking should avoid interfering or restraining the pelvis, otherwise gait energetics will be compromised.

2.1.6 ELDERLY GAIT

Gait varies as people age due to gradual physiological changes they experience. A prominent physiological change is the loss of muscle mass and muscle strength. A weaker musculature implies that in order for an elder to walk in the same manner as a young adult, their leg muscles need to be more engaged. In 1988, Waters & al. measured an increase in oxygen consumption in elders versus young adults walking at same speeds [31]. A second physiological change that elders experience and that affects their mobility is the structural weakening of their lower limb joints. A lifetime of repeated loadings can result in the permanent wear of articulating tissues. The wear may onset diseases such as osteoarthritis that hinders ROM in joints [32]. A third physiological change experienced by elders is the gradual reduction in sensory feedback. Elders develop gradual visual, hearing and touch impairments that compromise the required sensory feedback needed for efficient walking. The degree at which gait is modified in an elder depends on various factors such as their medical history, diet and lifestyle. However, there are some general gait deviations that have been observed. Elders walk at lower speeds than young adults [33], [34], [35], [36]. Stride length was measured to be smaller in elders versus young adults, while cadence values remained

unchanged [37], [38], [39]. Time spent in double limb support in stance is increased from 18 % to 26 % GC [40]. Hip, knee and ankle kinematics are also modified with aging. ROM in ankle is reduced from 29.3° to 24.9°[41]. ROM in knee is reduced from 59° to 55° [42]. Inversely, ROM of the hip is increased from 32° to 40° [39]. Peak plantar flexion at the ankle is reduced by 4° explained by weaker calf muscles [42],[43]. Gait kinetics are also affected by aging. Lower ankle motion combined with weaker calf muscles result in lower values of ankle moment and power at push-off [44], [45]. Hip pull-off power is increased during swing to compensate for the reduction in push off power at the ankle [42]. Power absorption in the knee at push off is found to be higher for elders [42]. Vertical and anterior / posterior GRF in elders shows lower peaks [46],[39].

2.2 CURRENT STATE OF WAE

WAE are mechanical devices that are worn by a user which reduce the metabolic and physiological cost associated with walking. There are two general approaches on how these devices assist their user. The first approach consists in introducing assistive torques about lower limb joints. For this approach, the exoskeleton creates a torque that enhances the torque generated by leg muscles. The assisting torque may help in generating or braking joint motion. The second assistive strategy consists in giving the user a feeling of reduced gravity. Such approach is achieved by producing an upward force directed towards the COG of the user. How each WAE provides assistance depends entirely on their design. WAE are intended to help users still able to move on their own. In other words, the machine does not replace the legs of the user, but instead compliments them during gait. At the present, WAE are not recognized as medical devices by Health Canada of the Food Drug Administration. WAE are often classified into two general categories: powered WAE and passive WAE. The following section of the literature review provides few examples of both categories. For each device, a detailed description on the design, assistance strategy and recorded performance of the device is given. The section concludes with a discussion of the challenges facing current WAE.

2.2.1 POWERED WAE

A powered WAE is a system that relies on a portable power source and actuators to convert electric, pneumatic or hydraulic energy into mechanical work to obtain a controlled motion of their support structure [47]. Powered WAE employ various sensors to detect joint

motion and discern GC sub phases. The sensors data are acquired by control units that formulate the proper response of actuators. Examples of powered WAE are the Human Universal Load Carrier (HULC), the Honda Bodyweight Support Assist and the Honda Stride Management.

2.2.1.1 HULC

The HULC as shown in Figure 2-10, is a powered WAE currently offered by Ekso Bionics and licensed exclusively to Lockheed Martin. The product originated at the Berkeley Robotics and Human Engineering Laboratory (BRHEL). The intended use of the device is to help soldiers walk with minimal effort for extended periods of time while wearing their combat gear. To do so, the device employs hydraulic cylinders to offset payloads along the support structure of the device and introduces assistive torques at the knee and hip.

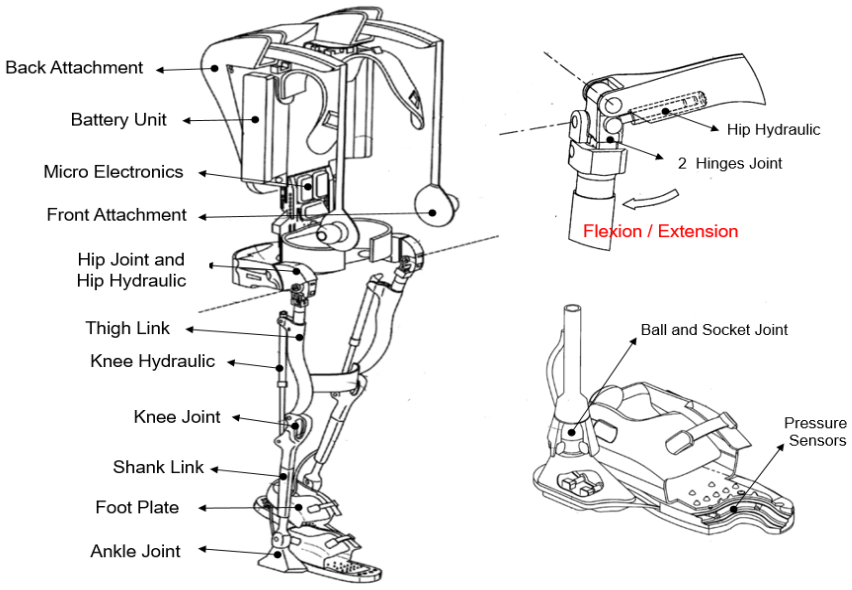

Figure 2-10: Drawing of current generation of HULC (left), of HULC hip joint assembly (top right) and HULC foot assembly [48].

The HULC support structure runs parallel to the legs of the user and is made mostly of titanium. The latest HULC version runs on lithium polymer batteries. The HULC offers limited motion to the hip and knee. The knee can only move about the sagittal plane, while the hip can move about both sagittal and frontal planes. The device provides full motion to the ankle. For each leg support structure, two linear hydraulic cylinders are found. The first

actuator is placed at the knee, while the second is placed at the hip. Both actuators generate controlled extension or flexion torques. The HULC uses two types of sensors to discern GC sub phases: pressure transducers within the foot unit and angular displacements sensors placed at the knee and hip. Data acquired by sensors are analyzed by a single board processor to activate both actuators in a way to maximize payload carriage and augment joint torques. The manufacturer claims that the HULC offers a walking range of 20 km, a maximum walking speed of 4 km/hr and can be fitted on any user measuring between 5'4" and 6'2". The price tag of most recent model is estimated to be 250 000 $ [49]. The product weights 24 kg without batteries. Tests on the use of the HULC without payloads recorded reduction in oxygen consumption ranging from 5 to 12 % when walking at 3.2 km/hr [50].

2.2.1.2 HONDA BODYWEIGHT SUPPORT ASSIST

The Bodyweight Support Assist as shown by Figure 2-11 is a powered WAE developed by Honda. The device is intended to preserve mobility for elders. The assistive strategy of the device consists in producing an upward force on the pelvis of the user via a seat interface. The upward force is created by the controlled extending and bending motion of the support structure.

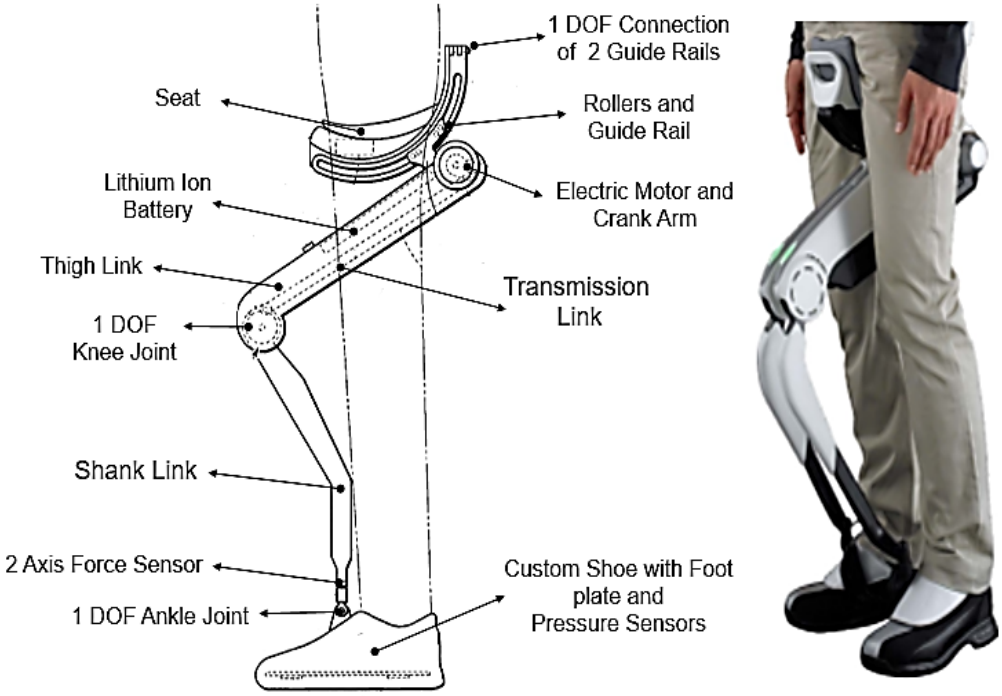

Figure 2-11: Drawing of current generation of Honda Bodyweight Support Assist (left) and photograph of person wearing the device (right) [51], [52].

The device is made of three assemblies: feet, support legs and seat. Fitting the device is divided into two steps. First step, the user places their feet in the foot assembly. Second step, the user raises the support legs and places the seat under their groin region. Note that, the support legs remain between the legs of the user throughout gait. Full ROM is offered at the ankle of the device. The knee of each support leg provides 1 DOF about the sagittal plane. The roller and guide rails design found under the seat assembly gives full ROM to the hip. The upward assistive force is produced by the work of two electric DC motors and two transmission mechanisms. During stance, only the electric motor paired to the standing support leg is active. When the electric motor is activated, it drives the transmission mechanism to either straighten up or bend the whole device so that the seat is constantly pushing against the pelvis of the user. In doing so, an up-lifting force is transmitted at the seat interface. During swing, the electric motor is turned off to provide sufficient leg motion. At the same time, the second motor is engaged to give support on the opposite supporting leg. Pressure transducers are placed in the sole of the custom shoe to detect GRF. Force sensors are placed at each ankle connection to measure the amount of load taken by each support leg. A CPU process sensors data and controls the electric motors. The control strategy is designed

to offer maximum reduction in felt weight during single limb support. The whole system is powered by portable lithium ion batteries and weighs 6.5 kg. Honda claims the exoskeleton offers a 2 hours use time and a maximum speed of 4.5 km/hr. The device was tested on healthy participants and measured a peak reduction of felt weight of 20 % BW during mid stance [52]. The Bodyweight Support Assist has yet to be available to the general public and thus no estimates have been published on the price of the device.

2.2.1.3 HONDA STRIDE MANAGEMENT ASSIST

The Stride Management Assist as shown in Figure 2-12, is a powered WAE developed by Honda. The assistive strategy of the device relies on introducing assistive torques about the hips of the user.

Figure 2-12: Honda Stride Management Assist with description of components [53].

The device is made of four components: waist frame, control unit, actuator unit and thigh frame. The waist frame is wrapped around the pelvis, while the thigh frames are attached to the thighs. Two brushless DC motors are found in the actuator unit. Each motor is coupled to a planetary gear train. The device uses angular displacement sensors to track the natural rhythmic motion of the thighs of the user. A central pattern generator (CPG) located in the control unit reads the information of angular displacement sensors. The CPG controls the two electric motors in a way to produce two simultaneous and complementary torques. At early midstance, an extension torque is offered to the supporting leg, while a flexion torque is

offered to the swinging leg. Portable lithium ions batteries power the system. The weight of the device with batteries is 2.8 kg. Honda claims that the device offers an operating time of 2 hours for a person walking at 4.5 km/hr. The use of device was found to reduce oxygen consumption by 7.06 %for healthy participants walking at comfortable speeds [54]. A randomized clinical trial on stroke patients concluded that wearing the device increases walking speed and stride length [53].

2.2.2 PASSIVE WAE

Passive WAE are devices that compliment gait using solely mechanical components such as springs, levers, pulleys and clutches. Some passive designs implement elastic components that store and release energy as the person is walking. Other passive designs create a support structure that offset the BW of the user when walking. Examples of current passive WAE are the Passive Ankle Exoskeleton, the XPED2, the MoonWalker and the Bodyweight Support Exoskeleton with Compliant Knee.

2.2.2.1 PASSIVE ANKLE EXOSKELETON

The Passive Ankle Exoskeleton as shown by Figure 2-13, was by developed by Collins et al. [14]. The assistive strategy of the device consists in replicating the elastic stretch and recoil of the Achilles tendon and calf muscles during stance [55]. In doing so, the device aims to reduce the high energetic requirements of the calf muscles at push off.

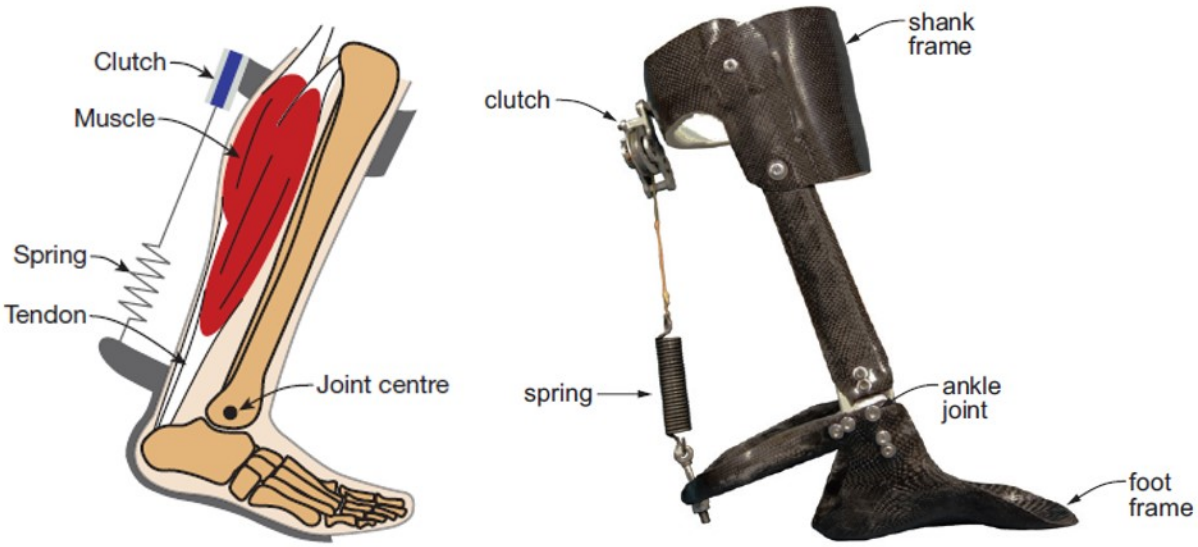

Figure 2-13: Schematic of the passive ankle exoskeleton (left) and photograph of the prototype used during walking trials (right) [14].

Figure 2-13 reveals that the device is made of 4 components: a carbon fiber frame, an extension spring, a rigid cable and a mechanical clutch. The upper portion of the frame wraps over the top portion of the calf muscles of the user. The lower portion of the frame takes a foot orthosis shape and is placed inside the shoe of the user. The upper and lower portion of the frame are connected by a 1 degree of freedom (DOF) joint that only provides plantarflexion and dorsiflexion. The rigid cable and extension spring are the energy storing and releasing components of the device. Energy is stored and released based on the rotation of the shank during stance. At heel strike, the clutch is engaged and the slack in the cable is taken during loading response. As the shank rotates during mid stance and terminal stance, the spring stretches storing potential energy. During pre-swing, the stored energy is released and the clutch is disengaged. The use of the device was tested on healthy participants walking on a treadmill. The two prototypes used during testing weight 0.408 kg and 0.508 kg. Test results revealed reduction in $\dot{E}_{METABOLIC}$ value of 7.2 % for a spring stiffness of 180 Nm [14].

2.2.2.2 XPED2

Dijk & al. [56] created a passive WAE called the XPED2 shown by Figure 2-14. The assistive strategy of the device consists in reducing joint torques by making use of elastic elements called exotendons. Exotendons were developed by A. J. van den Bogert [57] and

they consist of long elastic cables that replicate the mechanical behaviour of poly-articular muscle-tendons units found in horses. In such animal, muscles-tendons units can effectively store and transfer power across multiple joints. The XPED2 was built to test the implementation of exotendon on a WAE.

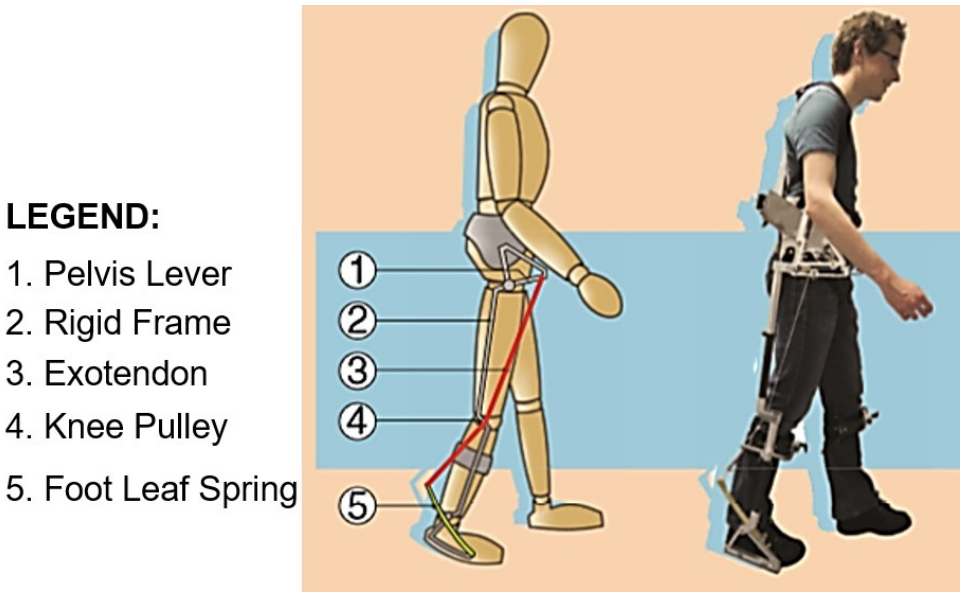

Figure 2-14: Schematic of XPED2 concept with components identified (left) and photograph of user wearing the XPED2 (right) [56].

The XPED2 employs a rigid frame that runs parallel to the legs of the user. The frame is attached to the pelvis and shanks via use of straps. On the top end of the frame, a rotatable lever is placed about the hip. On the bottom end of the frame, a leaf spring extends from the sole of the foot to the back of the shank. At the knee, a hinge joint and pulley are found. An arrangement of Dyneema cables is used to create the exotendon that will store and transfer energy across joints. The exotendon starts at the pelvis lever, goes over the pulley at the knee and ends on the foot leaf spring. The cable configuration is such that the exotendon is stretched for hip extension and ankle dorsiflexion. The cable loosens for the opposite set of motions. Thus, the cable stores elastic energy during single limb support and releases the stored energy during second double limb support. Since the exotendon is placed with an offset from the center of hip, knee and ankle, the stretching of the exotendon creates three assistive torques. The total weight of the exoskeleton is 6.91 kg. Joint torques were reduced by 12.1 %, $\dot{E}_{METABOLIC}$ values increased by 27.3 % between walking with and without the XPED2 [56].

2.2.2.3 MOONWALKER

The MoonWalker shown in Figure 2-15, is a quasi-passive WAE created by S. Krut & al. A quasi-passive device means that external power is only use to control certain components. The device provides assistance by supporting a portion of the BW of the user. The approach behind the design of the MoonWalker was to adapt a conventional body weight support (BWS) used in gait rehabilitation and transform it into a mobile structure [58].

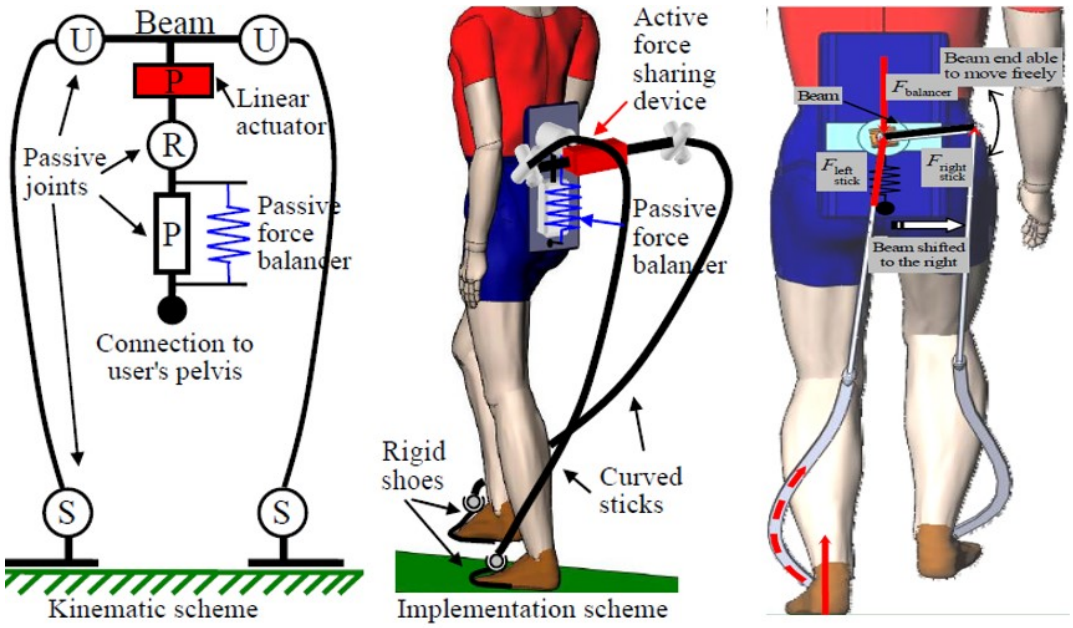

Figure 2-15: Schematics of the MoonWalker (left and center) and force distribution in MoonWalker for left leg in stance (right) [58].

The device consists of four units: two leg structures, two custom shoes, a force balancer and a force sharing mechanism. The two leg structures are curved in order to not interfere with the legs of the user during gait. Spherical joints are found on the ankle connection and provide full ROM. The upper end of each leg structure connects to a rigid beam which is part of the force sharing mechanism. During locomotion, a linear actuator moves the rigid beam towards the supporting leg. By doing so, part of GRF will be transmitted through the support leg and directed towards the pelvis of the user. Pressure sensors placed in the sole of the custom shoe are used to detect GRF. An external computer reads sensing readings and controls the motion of the linear actuator. A revolute joint connects the force sharing mechanism and force balancer. The force balancer is mounted on a rigid plate and attached to a harness worn by the

user. The force balancer is made of a spring and prismatic joint. The function of the force balancer is provide sufficient vertical displacement to the pelvis while transmitting the upward force created in the standing leg structure. Initial prototype testing provided an uplifting force of 320 N during mid stance [58]. Video recordings on the use of the device unveils that the system is very noisy, the harness unit moves greatly and gait is unsteady [59].

2.2.2.4 BODYWEIGHT SUPPORT EXOSKELETON WITH COMPLIANT KNEE

Lee and Wang developed a passive WAE shown by Figure 2-6, intended to reduce the internal knee loadings of people affected by a mild form of osteoarthritis [60]. The assistive strategy of the device consists in offering a compliant leg support structure that offsets BW.

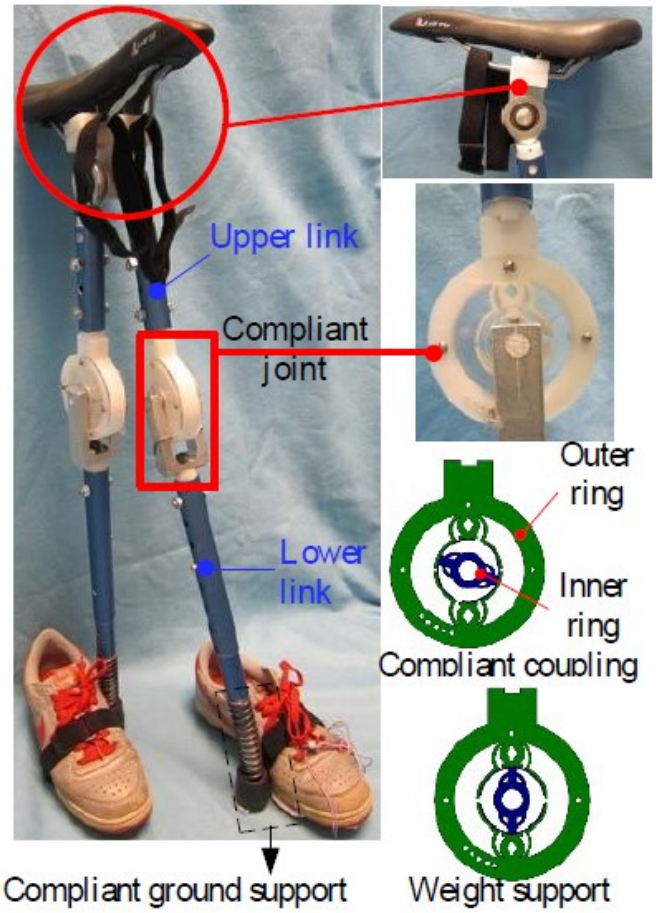

Figure 2-16: Bodyweight support exoskeleton (left), seat unit (top right) and of compliant knee (middle right). Illustration of two functions of compliant knee (bottom right) [60].

The device is placed between the legs of the user. The user places their weight on the bicycle seat throughout gait. The two leg structures are made of two adjustable links: thigh and shank. Both leg structures connect to the bicycle seat via a 2 DOF joint. The 2 DOF joint offers sagittal and frontal motion to the hip. Adjustable straps are wrapped on the upper thighs of user in order to maintain the seat placed between the legs of the user. A compliant knee is found on each support leg and it is made of two custom rings. The knee unit only allows motion about the sagittal plane. The outer ring connects to the thigh link and the inner ring connects to the shank link. The design of these rings is such that they are rigid in one direction and deformable in another. During initial contact, the upper link reaches an overextended position of 5º. In such position, the two rings are aligned in the weight support position; see Figure 2-16. At such a position, the leg structure behaves as a rigid lever. A stiff compression spring is placed on the lower end of the shank link which offsets the load applied on the bicycle seat. In pre-swing, the compliant knee moves to the compliant coupling positon (see Figure 2-16) to provide proper motion during swing. The user wears a custom shoe made with a support plate on the medial side. It is on this support plate that the compression spring is placed. The total weight of the device is 2.36 kg. Pressure sensors were used in ground level walking trials to detect the amount of BW taken by each support leg. A peak reduction of 27 % BW was recorded during midstance. However, the use of device increased swing from 40 % GC to 53 %. K.-M. Lee and D. Wang recently collaborated with two other researchers to further improve their design. No results on the newest prototype have yet to be published.

2.2.3 CHALLENGES OF CURRENT WAE

Current WAE are faced by multiple challenges largely attributed to technological and conceptual limitations. One technological limitation concerning powered WAE is that they require a large number of parts to operate. Their complexity does not always yield to a net reduction in COT values due to the weight of components. Section 2.1.5 demonstrated that carried weights have a negative effect on gait energetics. Thus, part number and total weight on a powered WAE need to be minimized. Another technological limitation exclusive to current powered WAE is the lack of compliant actuators. Very few available actuators can reproduce the mechanical behaviour of muscles. It creates a problem in properly pairing the torques produced by the exoskeleton and the torque produces by leg muscles. In the event of

improper synchronization between torques, the exoskeleton does not help motion but rather hinders it. Pneumatic artificial muscles (PAM) are viewed to be the actuators that best replicate the action of muscles [61]. Their implementation to WAE is challenging due to the need of a portable air supply and a proper control algorithm [62]. Passive WAE are also faced with this problem of properly synchronizing torques when their design employs energy storing and releasing components. It is difficult to create a reliable timing mechanism to ensure optimal energy release considering the fact that gait varies among individuals. Another technological problem concerns how motion is tracked in powered WAE. The proper control of actuators in powered WAE depends on properly discerning how the user intends to move. Few devices directly measure the intentions of the user. Instead, powered WAE take measurements via the use of displacement and/or force sensors. There is no gold standard on how sensor data relate to the intentions of the user [63]. Powered WAE are exposed to the problem of limited usage since they rely on portable batteries to function. Finally, powered WAE can be viewed as inaccessible technologies since their cost surpasses largely what an average person can afford.

A second type of limitations relates to the conventional strategies on how WAE are designed and modelled. Inverse Dynamics is often used to explain how best to assist muscles during gait. However, such a mathematical approach is based on major simplifications in the sense that the moments and powers computed only represents net values [64]. The approach cannot discern which muscle is acting and with what amount of force. Inverse Dynamics needs to be combine with updated models on biological tissues in order to better quantify walking. Next, very few models exist on how to quantify and evaluate the interactions between the interfaces of an exoskeleton and the limbs of the user. Adjustable straps and rigid pads are often used in pairing an exoskeleton. Their use are known to create pressure points that surpass the pressure thresholds of tissues [49]. The application of an externally applied pressure of over 50 mmHg on lower limbs tissues was found to seriously obstruct blood flow and created permanent discomfort while using exoskeletons [65],[66]. Note that, if a user feels any discomfort wearing a device, he or she may be tempted to modify the initial fit of the device to release discomfort. By doing so, misalignment may be created between the device and the legs of the user. J.M. Hilder and A.E. Wall [67] investigated the effect of misalignment in powered exoskeleton and found that misalignment creates undesired forces on skin tissues.

CHAPTER 3: DESIGN AND MODELLING OF PASSIVE WAE

Chapter 3 details the design and modelling of a passive WAE that aims to reduce felt weight during gait. The chapter starts off by presenting the concept and scope of the design. Next, the list of design criteria and restrictions is presented A special consideration is given to the development of a seat mechanism to produce reduction in felt weight. An overview of the final design follows, where all assemblies are described. The chapter ends by presenting the modelling achieved in MATLAB to quantify the assistance given by the seat mechanism to the user during standing and walking with the device.

3.1 DESIGN CONCEPT

The Honda Bodyweight Support Assist served as the genesis for this thesis. The initial goal was to mimic this powered WAE by developing an entirely passive system. The Honda Bodyweight Support Assist system was particularly considered due to three factors.

First is the originality of its assistive strategy. The majority of recent WAE relied on the production of assistive torques to help the user. Such an approach as explained in Section 2.2.3 presents the challenge of properly pairing the torque created by the device with the motion of the user. Furthermore, there is not a clear consensus on the optimal way to enhance walking via assistive torques. On the other hand, Section 2.1.4 unveiled that the approach of producing an upward force directed towards the pelvis of the user yields to a reduction in COT values. Interestingly, only a small number of WAE have considered such an approach. The Honda Bodyweight Support Assist is without doubt the best example of a powered WAE based on such strategy. On the passive side, the MoonWalker and the Bodyweight Support Exoskeleton with Compliant Knee are two devices built on the same assistive strategy.

The second factor considered for selecting the Honda system as a reference design is the effectiveness of its structural design. The support legs and seat unit of the device appear to not interfere with the walking pattern of the user. Video recordings of the Honda device reveals that leg motion is smooth and progressive as opposed to the use of the MoonWalker.

The third factor considered is the recent optimistic results achieved in research by passive devices as opposed to powered ones. Section 2.2.3 highlights the many problems faced by powered WAE and why they do not represent a viable solution to help user for now. The complexity of powered WAE makes them hard to fit, hard to use without supervision and too expensive. Thus, there is merit in trying to simplify a powered WAE.

3.2 SCOPE OF DESIGN

The process of designing any assistive device is a complex task that requires the expertise of many professionals, access to multiple resources and years of hard work. In an academic context, time and resources are in limited supply. Therefore, the limitations for this project were initially defined in order to ensure that a feasible WAE would be developed. The following points define the scope for the development of a passive WAE.

- Design an entirely passive WAE. The device must not have any form of external power.
- The assistive strategy of the device relies on reducing felt weight during gait. To do so, the WAE will use a seat mechanism that creates an upward force. The assistance provided by the seat mechanism should be comparable to the performance of the Honda system.
- The thesis aims to develop a proof of concept prototype rather than a final product. The thesis focus on the development of a seat mechanism that reduces felt weight of user during gait.
- The structure of the proposed WAE should mimic the Honda Bodyweight Support Assist and not exceed 6.5 kg in mass.
- The ideal user of the proposed device is an individual that is affected by mild or medium walking impairments. However, due to human testing challenges, this research will consider a healthy participant in the design and testing of a WAE.
- The production cost of the WAE must be optimized. Simple mechanical parts and affordable building materials must be considered.

3.3 DESIGN CRITERIA AND RESTRICTIONS

To help guide the design process, a list of criteria and restrictions were identified. A criterion represents a characteristic in the design that can be optimized. A restriction represents a characteristic in the design associated to a limit value and that must be respected imperatively.

List of **criteria:**

1. **Weight**: The parts and building materials are selected to create the lightest exoskeleton possible.
2. **Comfort**: The interface surfaces between the user and exoskeleton should minimize pressure points and discomfort. The number of attachment used should be limited.
3. **Skills required**: Easy to learn how to fit, stand and walk with the device.
4. **Affordability**: The cost of the device is minimized by creating a simple design, using affordable materials and simple manufacturing processes.
5. **Aesthetic**: The shape of device provides a physical appeal so that the user has a desire to use the WAE.

6. **Upward Assistive Force**: The uplifting assistive force is activated in early stance and released during terminal stance in a smooth manner.

List of **restrictions**:

1. Passive Device
2. Minimal assistive force of 20 % BW at midstance.
3. Mass of the device should not exceed 6.5 kg.
4. Assistive mechanism should not create undesirable or sudden responses.
5. The user's stability is maintained when using the device.
6. Removal of exoskeleton takes less than 30 seconds.
7. The device is fully operated and controlled by the user.

3.4 ASSISTANCE STRATEGY

At the start of the thesis, a decision was made to focus on creating a passive WAE that will help its user by offering a reduction in felt weight. Such assistance would be achieved by a mechanism that would produce an upward force on a seat interface where the user constantly applies their weight. There are two major reasons why such approach was considered.

1. Timing the assistance of the exoskeleton no longer becomes an issue, in contrast to WAE that are based on assistive torques. The mechanism responsible for creating an upward force can be active throughout gait just as long as the user applies their weight on the seat.
2. The device can provide assistance when the user is standing and walking. In contrast to WAE based on assistive torques, the user needs to walk in a particular pattern for its components to offer assistance.

Prior to creating various design concepts, several brainstorming sessions were undertaken in order to develop the best strategy on how to reduce felt weight via a seat interface. The sport of slacklining was used as major inspiration for formulating such an assistance. Figure 3-1 unveils the concept behind slacklining.

Figure 3-1: Force diagram for slacklining [68].

In slacklining, the weight of person is supported by the tension generated in an elastic cord. Considering this concept, a seat that would rest on two elastic cables that are constantly stretched by the weight of the user is proposed. Figure 3-2 presents the schematic for the design of converting slacklining concept to an exoskeleton.

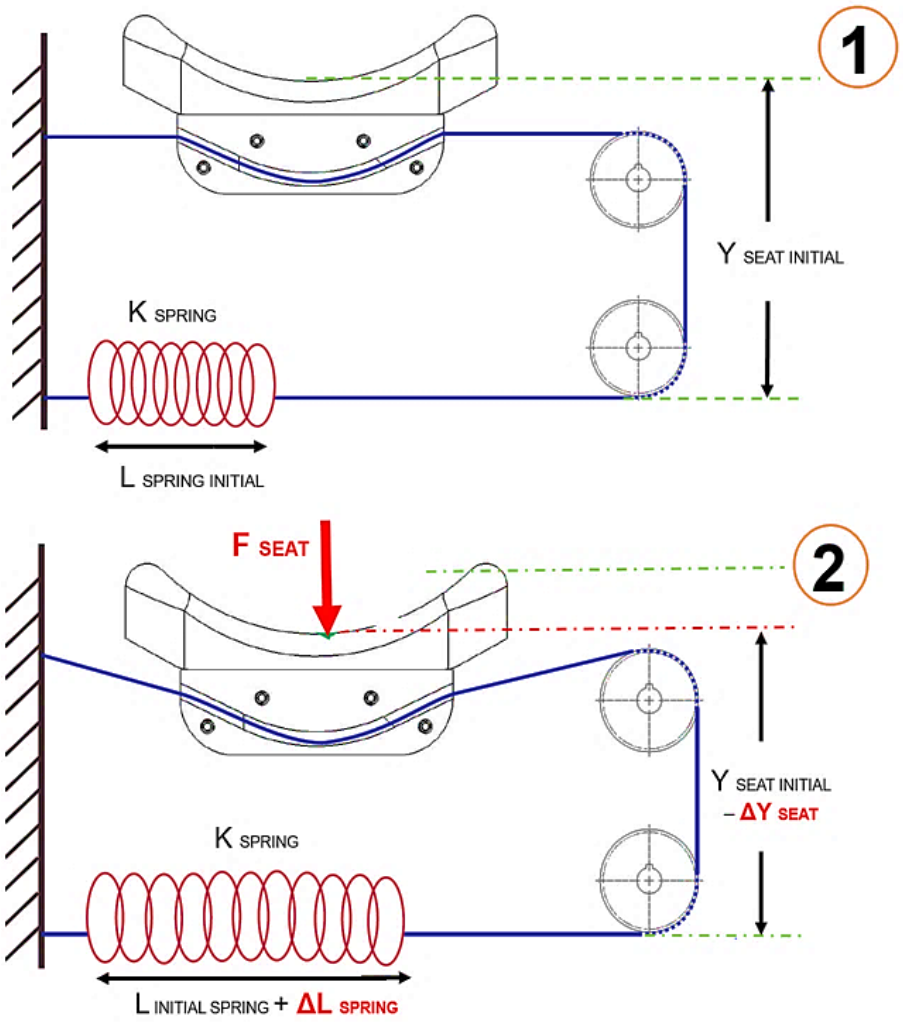

Figure 3-2: Schematic of adapted slacklining concept for exoskeleton for initial position (top) and seat position (bottom).

In Figure 3-2, there is a wire rope that passes through a seat via an internal groove. The wire rope then loops over two pulleys and connects to an extension spring of constant stiffness (K_{SPRING}). Thus, the tension in the wire rope is directly related to the spring extension and stiffness. The combination of wire rope and extension spring acts as an elastic wire unit (EWU). The EWU is the analogue of the elastic cord in slacklining. In position 1 of Figure 3-2, the spring in the EWU is stretched to overcome the weight of the seat. When someone stands on the seat, the seat is lowered to position 2 in Figure 3-2. The displacement of the seat from position 1 to position 2 corresponds to $\Delta Y_{SEAT.}$ In order for the seat to move by ΔY_{SEAT}, the spring in the EWU will get stretched by a value of ΔL_{SPRING} which increases the tension in the

wire rope of the EWU. The increased tension supports a portion of the BW of the user that corresponds to the downward force found on the seat interface (F_{SEAT}). Based on Newton's third principle, the user receives an opposite upward force on their pelvis equivalent to F_{SEAT}. The following seat mechanism will be implemented on a passive exoskeleton. With such mechanism, the amount of upward force provided is determinate by the values of ΔY_{SEAT}, ΔL_{SPRING} and K_{SPRING}.

3.5 DESIGN CONCEPTS

The next step in the design process was to propose various conceptual designs for a passive WAE that implements the seat mechanism. After several brainstorming sessions, multiple design concepts were sketched on paper and kept for further examination. These sketches can be found in APPENDIX A. Next, each concept idea underwent an evaluation process to determine the best one. The evaluation process consisted in assigning a relative score on how each concept idea fulfilled each design criteria (see Section 3.3). The conceptual design with the highest score was selected. The evaluation process table can be found in APPENDIX A.

3.6 FINAL DESIGN OVERVIEW

The production of multiple prototypes helped in further improving the initial selected conceptual design (see Section 4-1) and producing a final design. SolidWorks (Dassault Système, France) was used to produce the CAD model of the final design shown by Figure 3-3. The device is made primarily of aluminium and HDPE. The exoskeleton mass is 5.68 kg and is made of 9 units identified in Figure 3-3. Each unit provides a specific set of functions. Table 3-1 defines these 9 units and present their mass.

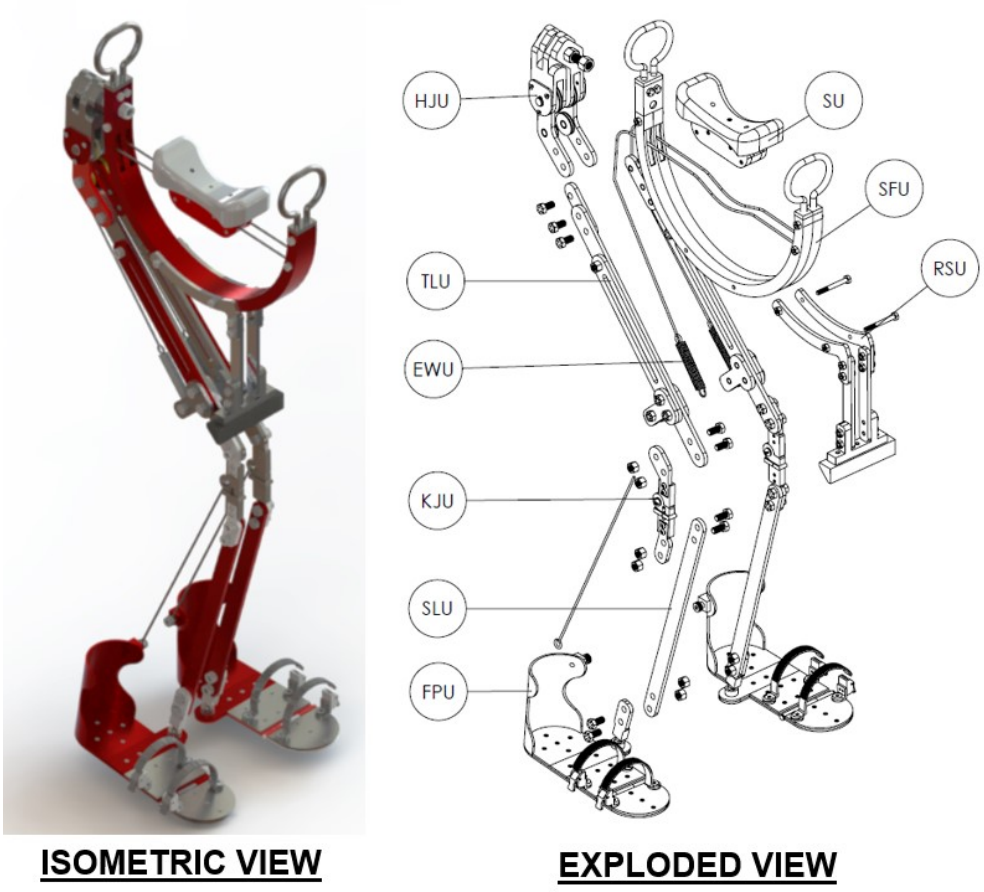

Figure 3-3: Isometric view (left) and exploded view (right) of CAD model of proposed passive WAE.

Table 3-1: Nomenclature of units of proposed passive WAE.

ID	Description Name	Qty.	Mass (g)
SU	Seating Unit	1	431
SFU	Seat Frame Unit	1	884
RSU	Rubber Stopper Unit	1	429
HJU	Hip Joint Unit	1	681
TLU	Thigh Link Unit	2	437
EWU	Elastic Wire Unit	2	29
KJU	Knee Joint Unit	2	183
SLU	Shank Link Unit	2	165
FPU	Foot Plate Unit	2	784

The structure of the final design resembles the Honda Bodyweight Support Assist. The device is placed between the legs of the user. The exoskeleton can be viewed as two support legs and curved top frame (SFU) on which the seat mechanism of Section 3.4 is implemented.

The seat mechanism corresponds to the combination of SU and EWU. The wire rope of each EWU extends from the front of the SFU, passes through the SU, wraps over two pulleys located on the HJU and connects to an extension spring attached to the TLU. When the SU is lowered by the weight of the user, the tension in the EWU is increased and upward force is produced. For a standing scenario, both EWU (left and right) produce equal upward force on the SU. For a walking scenario, the action of each EWU on the SU will alternate depending which support leg is in stance. The support leg corresponds to the combination of the TLU, KJU, SLU and FPU. Each support leg employs a locking mechanism in their KJU. During stance, the KJU is locked to ensure that the SU and EWU provide their intended assistance. The KJU is unlocked via a trigger cable activated by the shank rotation of the user during late stance. On the top portion, each support leg is connected to the HJU which provides sagittal and front rotation to the hip. On the bottom portion of each support leg, the user straps their feet to the FPU. There are only two interfaces between the user and the device and they are found at each FPU and SU. Fitting the device is a quick process. First step, both KJU are unlocked and the user places the device between their legs. Second step, the user securely attaches their feet to each FPU. Third step, the user raises the whole exoskeleton using the two handles found on the SFU. The device is raised until both KJU are locked and the SU is placed under their groin region. The RSU is a key unit in the final design. It is placed under the SFU and interacts with both TLU during gait. Its function is to limit the rotation of the SFU with respect to the HJU. Otherwise, applying weight on the SU results in the forward collapse of the SFU and no assistance would be gained.

3.6.1 GENERAL DIMENSIONS

The proposed design was developed with the prior knowledge that it would be used by a single user measuring 1.78 m and with a body mass of 82 kg. Anthropometry was used in dimensioning the device so that it would fit the size of the user. The Anthropometric data computed can be found in Appendix A. Figure 3-4 and Table 3-2 detail the general dimensions of the final design when the device is in its standing position.

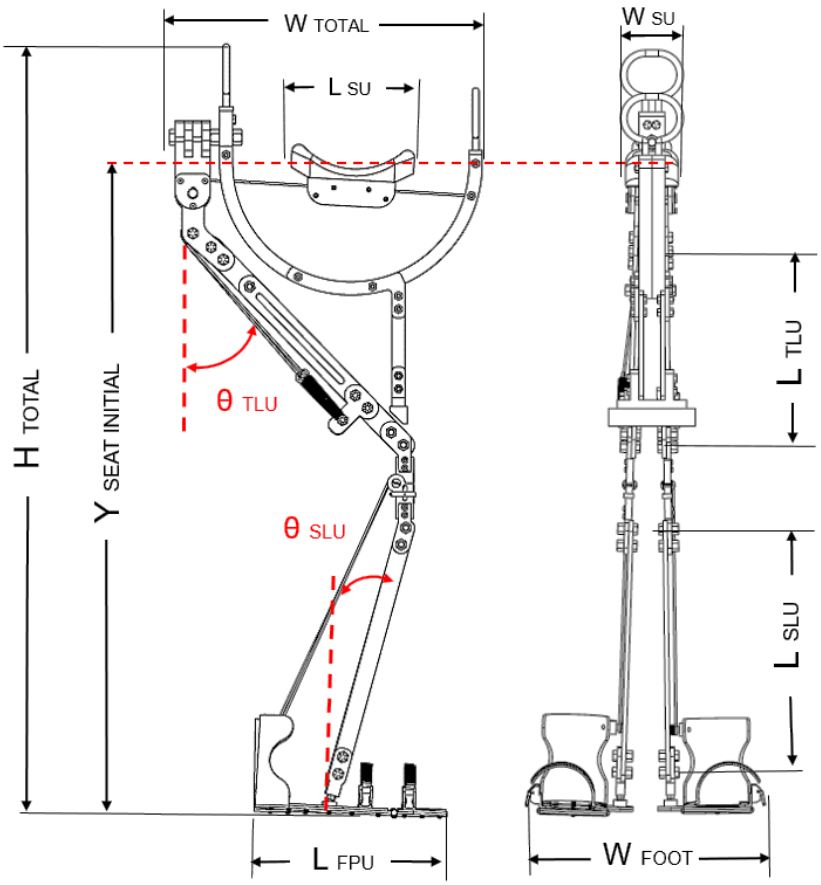

Figure 3-4: Schematic of general dimensions of final design.

Table 3-2: General dimensions of final design.

Nomenclature	Description	Value
H_{TOTAL}	Total height of device.	1100 mm
$Y_{SEAT\ INITIAL}$	Initial vertical position of SU.	926 mm
W_{TOTAL}	Total width, depth of device.	450 mm
L_{SU}	Length of SU.	180 mm
W_{SU}	Width of SU.	50 mm
L_{TLU}	Length of TLU.	390 mm
θ_{TLU}	Angle of TLU.	44º
L_{SLU}	Length of SLU.	360 mm
θ_{SLU}	Angle of SFU.	15º
W_{FOOT}	Width between FPU.	310 mm
L_{FPU}	Length of FPU.	278 mm

3.6.2 GAIT CYCLE BREAKDOWN

To fully comprehend how the proposed WAE assists its user, an illustration of the GC was created shown by Figure 3-5. Figure 3-5 depicts how the 9 units move in space and when assistance is provided by the SU and EWU.

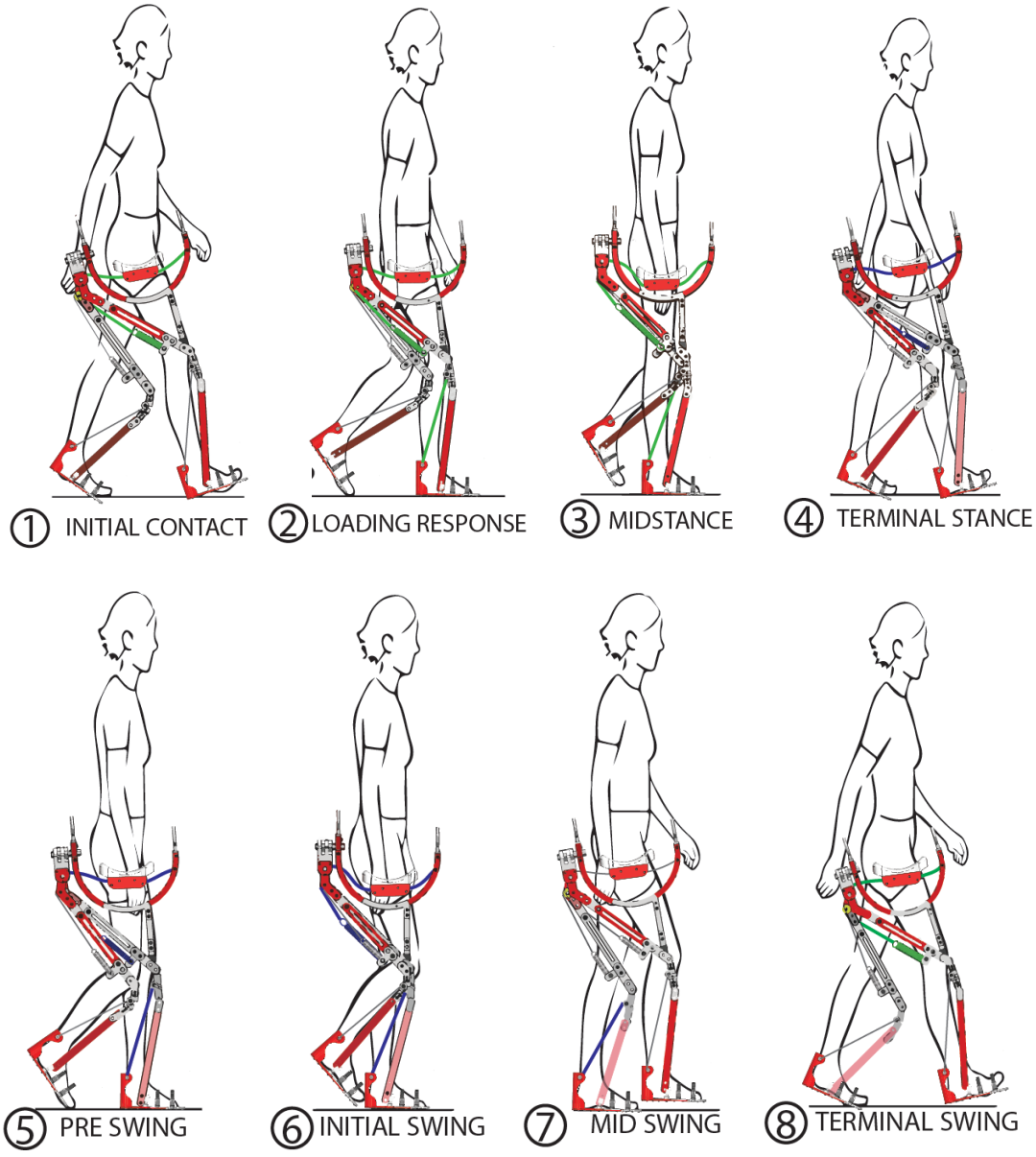

Figure 3-5: Illustration of one GC for use of proposed WAE.

In Figure 3-5, a colour code, green and blue, was used to highlight key action on the device. When the EWU is colored in green, it implies that the right support leg and right EWU produce most of the upward assistance. When the EWU is colored blue, it is the opposite conclusion. The trigger cable responsible for unlocking the KJU was also colored. When the trigger cable is colored, it means that it is being stretched. Once again, a trigger cable colored in green corresponds to the stretch of the right trigger cable. A trigger cable colored in blue targets the left trigger cable.

Figure 3-5 shows that the distance between the SU and the SFU changes during gait. When the distance is smaller, it implies that the SU and EWU produce greater upward force at the SU interface. Figure 3-5 also reveals that the motion of the WAE is entirely driven by the feet and pelvis of the user. The SU remains between both legs and is constantly loaded by the weight of the user. The FPU are moved by the feet of the user. When the KJU is locked during stance, the support leg behaves as a rigid lever, meaning that it will rotate about the ankle joint due to forward progression of the pelvis of the user. In sum, the support leg creates a pendulum motion with peak vertical position at midstance. At such position, the SU is at lowest position with respect to the SFU and the EWU is most stretched creating highest upward force at the SU interface. The device alternates motion between two support legs which implies that peak assistance is reached twice during gait. Near terminal stance, the KJU of the standing support leg is unlocked to provide sufficient motion in swing.

Figure 3-5 reveals the importance of the RSU. When the user places their weight on the SU, the SFU rotates downward until resting on one or both TLU. At early stance, it rests on the right TLU. Near the end of mid stance, the left support leg will raise the RSU to shift support. Note that such motion represents an abrupt change in support, but it is required. Otherwise, the right KJU could not be unlocked due to still being highly loaded. The abrupt change of support occurs at 30 % GC and 80 % GC.

A brief summary of each GC sub phases follows:

1) Initial Contact: The right KJU is locked. The right support leg is inclined and aligned with the right leg of the user. The SU is close to its highest position meaning that the

assistance of the right side is small. The left KJU is unlocked. The left support leg is in swing. The RSU rests on the right TLU.

2) Loading Response: The right support leg rotates forward. In doing so, the SU is lowered with respect to the SFU increasing upward force produced. The right trigger cable begins to be stretch which starts to pull on the unlocking pin of the KJU. The RSU remains on the right TLU. The left support leg continues to swing with the TLU moving forward and the KJU continuing to flex.

3) Mid Stance: The right support leg continues to move forward and reaches an upright position. At such a position, the SU and EWU provide the highest upward force. The right trigger cable is further stretched and pulls more on the unlocking pin of the KJU. The left TLU continues to move forward and is about to hit the RSU to take over support.

4) Terminal Stance: The left TLU hits and raises the RSU. The left SLU extends forward until the left KJU is locked. At this point, support is shifted between the two TLU. The right KJU is unlocked by the trigger cable and a small knee flexion occurs.

5) Pre Swing: The left support leg starts to rotate about the left ankle on the FPU. The SU is again lowered with respect to the SFU to increase upward force. The left trigger cable begins to be stretched. The right TLU moves backward slightly, while the right KJU continues to flex. The RSU rests on the left TLU.

6) Initial Swing: The left support leg continues to rotate forward and reaches second upright position which translates to a second peak assistance of SU and EWU. The RSU rests on the left TLU and the left trigger cable is further stretched. The right TLU starts to move forward, while the right KJU reaches its peak swing flexion.

7) Mid Swing: The right TLU continues to progress forward eventually hitting and raising the RSU to take over support. The right SLU extends until the KJU locks. In this position, the SU and EWU provide lowest assistance. The left trigger cable is about to unlock the KJU.

8) Terminal Swing: The right support leg takes over support. The right KJU is locked and the RSU rests on the right TLU. The left KJU is unlocked and a small flexion occurs. The left TLU moves backward.

3.6.3 SEAT UNIT

The seat unit (SU) takes the function of a bicycle seat, where the user will constantly apply their weight. The SU rests on the wire rope of each EWU. Lowering the SU results in increasing tension in the EWU, which in turns increase upward force at the seat interface. Figure 3-6 and Table 3-3 reveal the SU assembly.

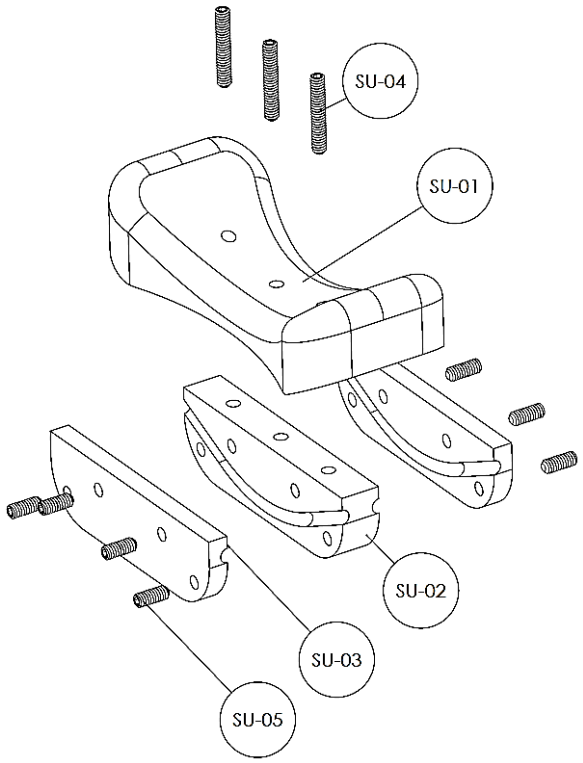

Figure 3-6: Exploded view of SU

Table 3-3: Part list description of SU.

Part ID	Description	Material	Qty.
SU-01	Seat hard shell	HDPE	1
SU-02	Middle bloc for holding wire ropes	HDPE	1
SU-03	Side bloc for holding wire ropes	HDPE	2
SU-04	Set screw for fixation – (¼”-20), (Length 1 ½”)	Alloy Steel	3
SU-05	Set screw - (¼”-20), (Length ½”)	Alloy Steel	8

The shape of the hard shell (SU-01) was design to wrap comfortably around the inner thighs of the user and to ensure that the SU remains under the groin region during gait. Note that, a medium density silicon padding, not shown in Figure 3-6, is placed over the seat hard shell. The middle (SU-02) and two side HDPE blocs (SU-03) hold the wire rope of each EWU. Grooves are created on all blocs so that the wire ropes are kept inside the SU. Note that, all grooves are made larger than the wire ropes so that the SU can freely slide forward and backward. Set screws (SU-04 and SU-05) are used to connect all parts together. Set screws were selected over bolts to have a flush surfaces.

3.6.4 SEAT FRAME UNIT

The seat frame unit (SFU) is the upper portion of the device and acts as an anchor unit for the two EWU, HJU and RSU. Figure 3-7 and Table 3-4 detail the unit's assembly

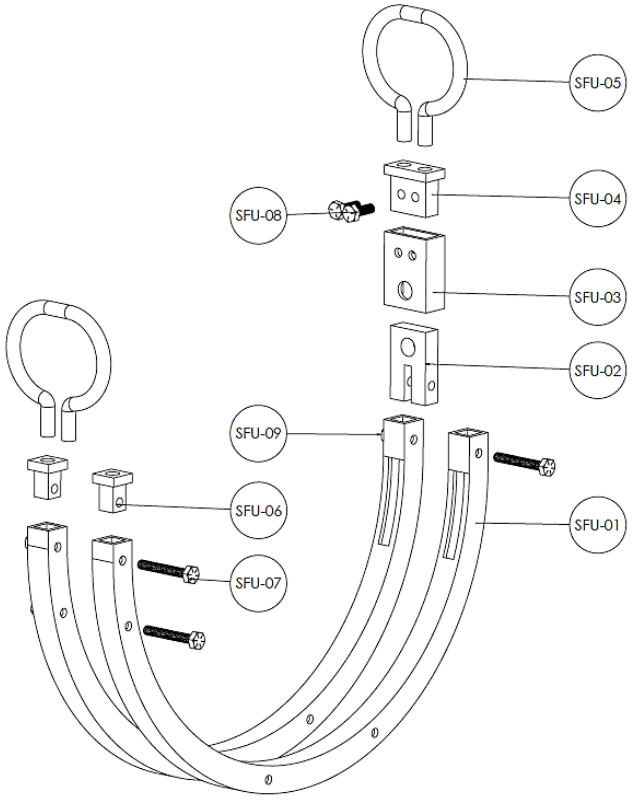

Figure 3-7: Exploded view of SFU

Table 3-4: Part list description of SFU.

Part ID	Description	Material	Qty.
SFU-01	Curved square tube - (⅛" thickness)	Aluminium 6061	2
SFU-02	Attachment bloc for hip joint unit	Aluminium 6061	1
SFU-03	Rectangular tube - (1 ½" × ¾"), (⅛" thickness)	Aluminium 6061	1
SFU-04	Back attachment bloc for handles	Aluminium 6061	1
SFU-05	Handle for exoskeleton fitting	Aluminium 6061	2
SFU-06	Front attachment bloc for handles	Aluminium 6061	2
SFU-07	Fixation hex bolt – (¼"-20), (Length – 1 ¾")	306 Stainless Steel	4
SFU-08	Fixation hex bolt - (¼"-20), (Length – 1")	306 Stainless Steel	2
SFU-09	Hex nut - (¼"-20)	306 Stainless Steel	4

The two main parts are the curved aluminium square tubes (SFU-01) held together by bolts (SFU-07). Two handles (SFU-05) are placed on the front and back of the SFU. These components are used in fitting the exoskeleton. The aluminium bloc inserted in the back portion of the SFU (SFU-02) is the attachment point for the HJU. Two slots are made on each square tube and are revealed in Figure 3-8.

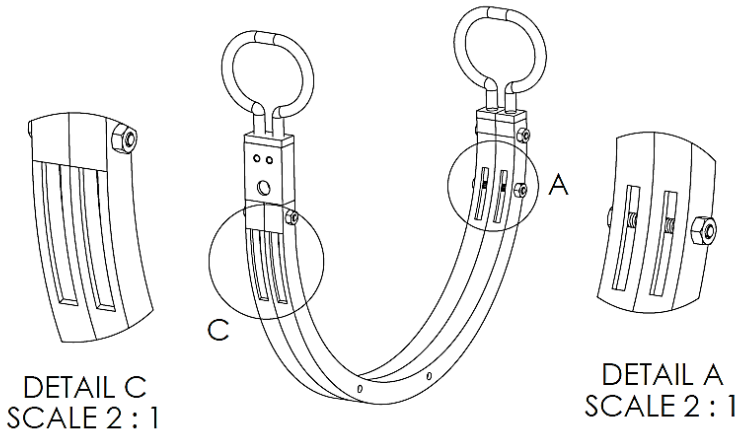

Figure 3-8: Detailed views of back slot (left) and front slot (right) of SFU.

In Figure 3-8, Detail A shows the front slot. The front slot is only made on the inside surface of each square tube. It is there that the EWU is connected. Detail C in Figure 3-8 shows the back slot. The back slot cuts through each square tube. The wire rope of each EWU will

pass through the back slot to loop over the pulleys on the HJU. Two holes are made on the bottom portion of the SFU. The two holes are the anchor points for the RSU.

3.6.5 HIP JOINT UNIT

The hip joint unit (HJU) is placed behind the SFU. The two bottom portions of the HJU connect to the TLU of each support leg. The major functions of the HJU are to provide sufficient hip motion and to guide the wire rope of each EWU. Figure 3-9 and Table 3-5 describe the unit.

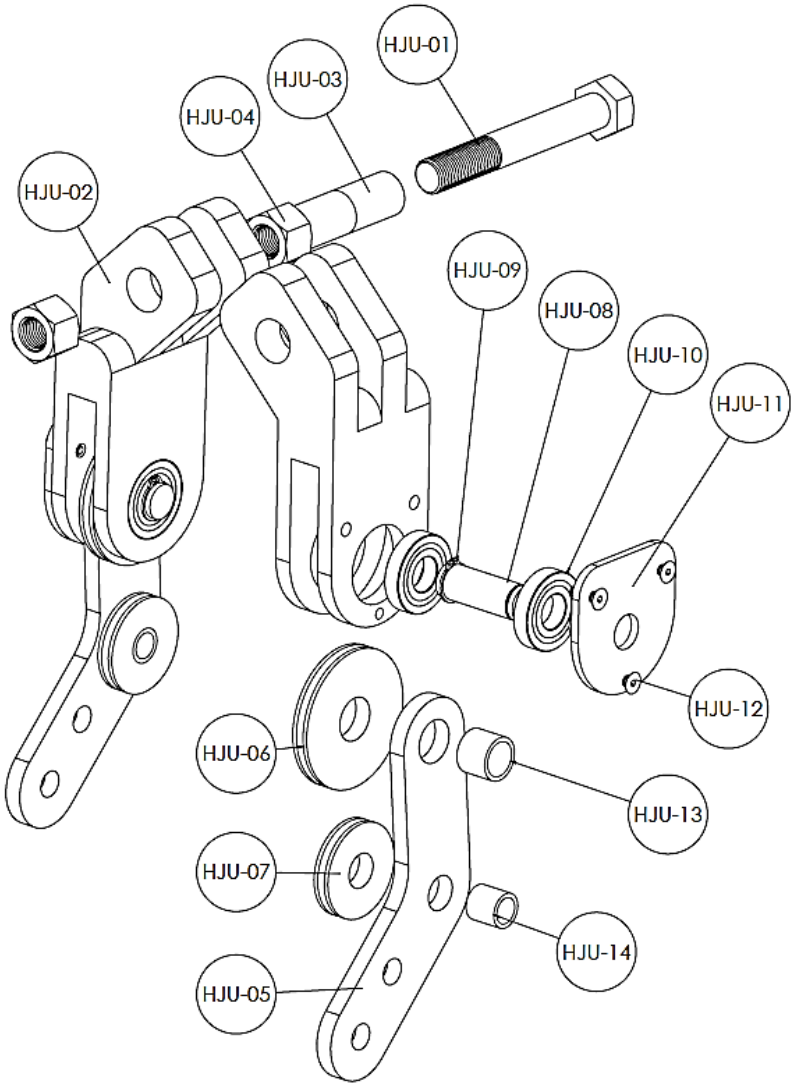

Figure 3-9: Exploded view of HJU.

Table 3-5: Part list description of HJU.

Part ID	Description	Material	Qty.
HJU-01	Hex bolt, - (½”-13), (Length 3 ½”)	Grade 9 Steel	1
HJU-02	Hinge bloc	Aluminium 6061	2
HJU-03	Sleeve bushing – (½” ID), (Length 1”)	Bronze	2
HJU-04	Hex nut – (½”-13)	Grade 9 Steel	2
HJU-05	Connection plate - (¼” thickness)	Aluminium 6061	2
HJU-06	Large pulley - (2 ½” OD), (¼” thickness)	Aluminium 6061	2
HJU-07	Small pulley - (1 ⅜” OD), (¼” thickness)	Aluminium 6061	2
HJU-08	Shaft – (½” OD), (Length 1 ¼”)	Aluminium 6061	2
HJU-09	External retaining ring	306 Stainless Steel	4
HJU-10	Ball bearing – (½” ID) ,(1 ⅛” OD), (¼” thickness)		4
HJU-11	Cover plate – (⅛” thickness)	Aluminium 6061	2
HJU-12	Fixation bolt - (6-32), (Length ⅜”)	306 Stainless Steel	6
HJU-13	Sleeve bushing – (½’ ID), (Length ½”)	Bronze	2
HJU-14	Sleeve bushing – (⅜” ID), (Length ½”)	Bronze	2

The two main parts of the HJU are the two aluminium hinge blocks (HJU-02). These blocs are connected to a partially threated bolt (HJU-01) to form a hinge. Thus, each bloc can perform a rotation about the frontal plane. The threaded portion of the hex bolt is connected to the aluminium bloc of the SFU (SFU-02). For each hinge bloc, a shaft (HJU-08) is found on which many components are mounted. First, a large pulley (HJU-06) is found on which each wire rope of the EWU wraps partially. Second, the aluminium connection plate (HJU-05) is placed next to the large pulley. The connection plate is the attachment point for each TLU. Being placed on a shaft, each connection plate can rotate about the sagittal plane. A small pulley (HJU-07) is mounted on each connection plate. The small pulley guides the wire rope of each EWU towards the TLU. Ball bearings (HJU-10) and sleeve bushings (HJU-03, HJU-13 and HJU-14) are used to provide smooth rotation. Aluminium covers (HJU-11) are placed on each side of the HJU to hide and protect all parts.

3.6.6 THIGH LINK UNIT

The thigh link unit (TLU) is the upper portion of each support leg. The TLU serves as an attachment point for the EWU and moves forward and backward during gait. It also hits

the RSU when the support leg is involved in reducing felt weight. Figure 3-10 and Table 3-6 detail the unit.

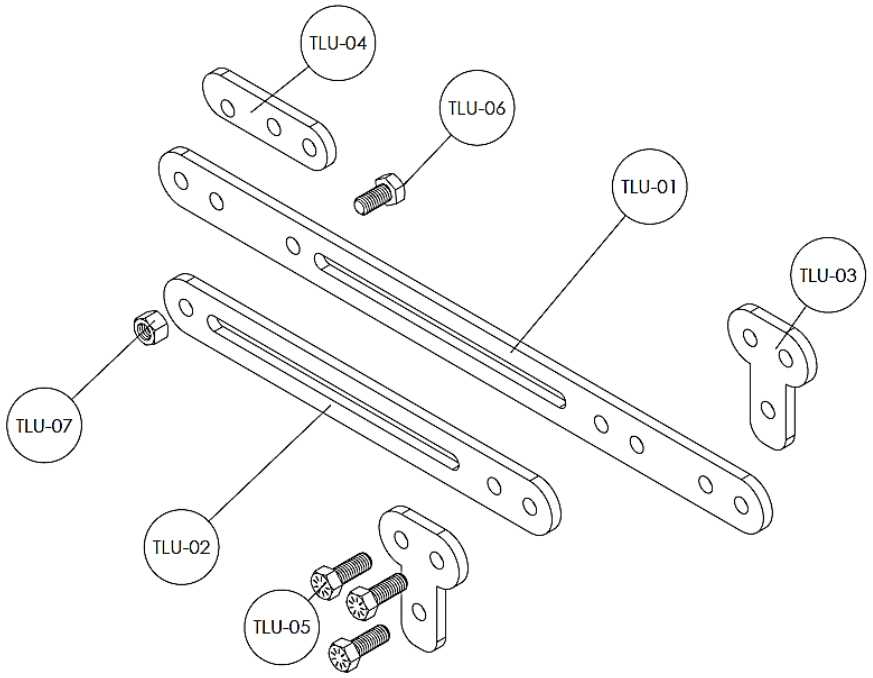

Figure 3-10: Exploded view of left TLU.

Table 3-6: Part list description of TLU.

Part ID	Description	Material	Qty.
TLU-01	Long plate – (Width-1”), (Thickness ¼”)	Aluminium 6061	1
TLU-02	Short plate - (Width-1”), (Thickness ¼”)	Aluminium 6061	1
TLU-03	Connection plate EWU – (Thickness ¼”)	Aluminium 6061	2
TLU-04	Cover plate pulley - (Thickness ¼”)	Aluminium 6061	1
TLU-05	Hex bolt – (⅜”-13), (Length-1’)	Grade 9 Steel	3
TLU-06	Hex bolt – (⅜”-13), (Length ¾”)	Grade 9 Steel	1
TLU-07	Hex nut – (⅜” -13)	Grade 9 Steel	1

The main parts of the TLU are two aluminium plates (TLU-01 and TLU-02). The reason why two plates were used over one is to provide sufficient space for connecting the EWU and to increase bending resistance. A linear slot is made along the length of both plates to reduce weight. Two smaller aluminium plates (TLU-03) are placed on the lower end of the TLU. The bottom hole of the two plates serves as the second anchor point of the EWU. Thus,

each EWU extends from the front slot of the SFU, wraps over the two pulleys in the HJU and ends on the TLU.

3.6.7 ELASTIC WIRE UNIT

The elastic wire unit (EWU) is the equivalent of the elastic cable in slacklining. Its role is to maintain a tension so that it constantly pushes the SU towards the pelvis of the user. In doing so, it provides the desired reduction of felt weight. Figure 3-11 and Table 3-7 detail the EWU.

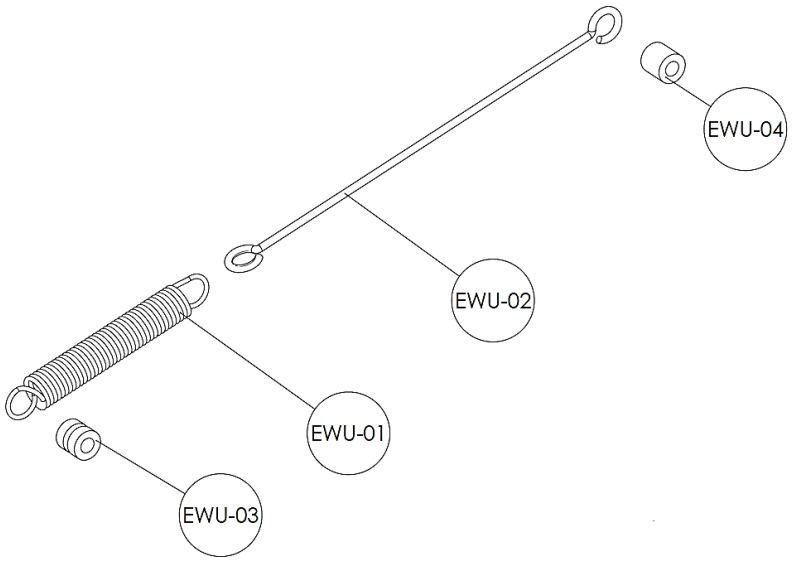

Figure 3-11: Exploded view of EWU.

Table 3-7: Part list description of EWU

Part ID	Description	Material	Qty.
EWU-01	Extension Spring – (Length 4”)	302 Stainless Steel	1
EWU-02	Wire rope – (3/32”- 7×7)	Galvanized Steel	1
EWU-03	Sleeve Bushing – (⅜” OD), (Length ½’)	Bronze	1
EWU-04	Sleeve Bushing – (⅜” OD), (Length ½’)	Bronze	1

The EWU is made of a wire rope (EWU-01) and an extension spring (EWU-02). In Figure 3-11, the left end is inserted in the front slot of the SFU. The right end is placed between two connection plates of the TLU (TLU-03). Sleeve bushing (EWU-03 and EWU-04) are used

on the two attachments ends so that the wire rope does not get damaged. Note that, the extension spring was placed on the lower end of the TLU to avoid any interference with other units and legs of the user.

3.6.8 RUBBER STOPPER UNIT

The rubber stopper unit (RSU) is placed under the SFU. During gait, the RSU is always in contact with one support leg. The RSU prevents forward collapse of the SFU. Figure 3-12 and Table 3-8 unveil and describe the RSU.

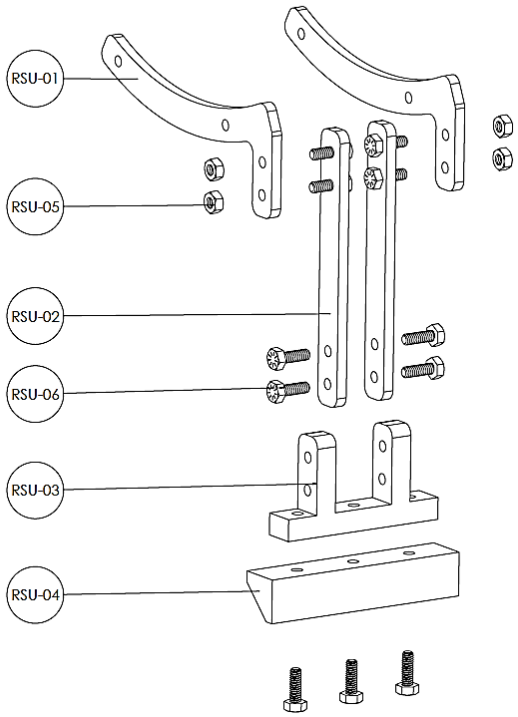

Figure 3-12: Exploded view of RSU.

Table 3-8: Part list description of RSU.

Part ID	Description	Material	Qty.
RSU-01	Side support plate	Aluminium 6061	2
RSU-02	Vertical support plate	Aluminium 6061	2
RSU-03	Bottom support bloc	Aluminium	1
RSU-04	Rubber stopper bloc	Polyurethane	1
RSU-05	Hex nut – (¼”-20)	Grade 9 Steel	4
RSU-06	Hex bolt – (¼”-20), (Length ¾”)	Grade 9 Steel	11

At the top, two side aluminium plates (RSU-01) connect to the SFU via bolts. Under them, two vertical aluminium plates (RSU-02) are attached. These components connect to the bottom support block (RSU-03) on which a polyurethane bloc (RSU-04) is fixed. The rubber bloc is the surface of contact between the RSU and the two TLU. When standing, both TLU rests on the rubber bloc. During gait, contact will alternate between the two TLU. Note that, the rubber stopper was sliced with the same angle as the TLU (θ_{TLU}). Bolts (RSU-05 and RSU-06) connect all parts together.

3.6.9 KNEE JOINT UNIT

The knee joint unit (KJU) is the bridge between each TLU and SLU. The unit employs a mechanical lock to block sagittal motion during stance. Figure 3-13 and Table 3-9 details the left KJU.

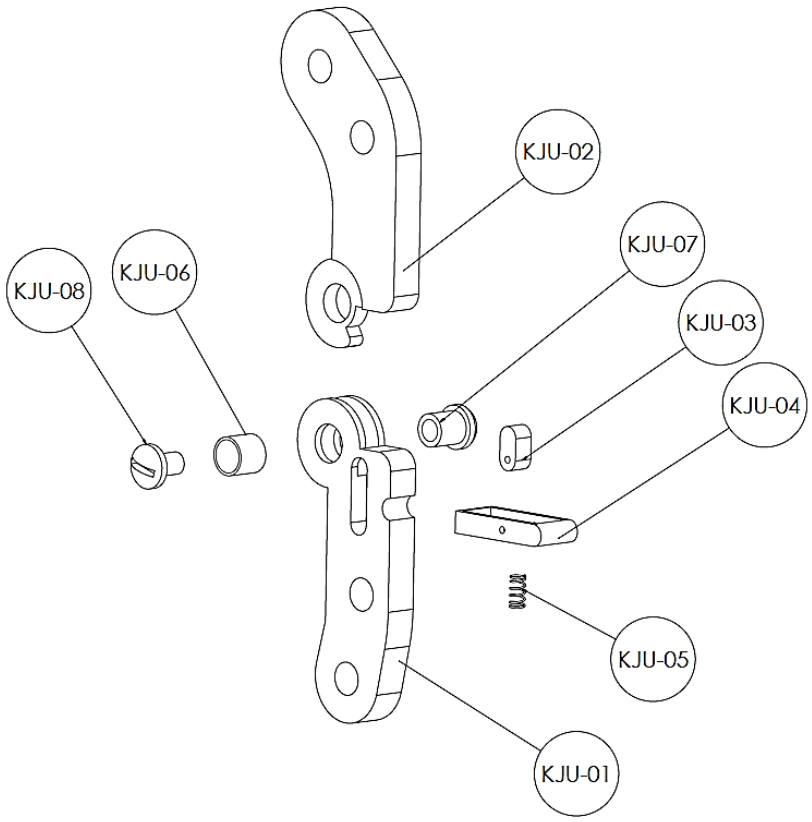

Figure 3-13: Exploded view of left KJU

Table 3-9: Part list description of left KJU.

Part ID	Description	Material	Qty.
KJU-01	Fork end joint plate – (Thickness ⅜”)	Stainless Steel 316	1
KJU-02	Eye end joint plate – (Thickness ⅜”)	Stainless Steel 316	1
KJU-03	Locking pin	Stainless Steel 316	1
KJU-04	Locking pin arm	Stainless Steel 316	1
KJU-05	Compression return spring	Stainless Steel 316	1
KJU-06	Sleeve bushing – (½” ID)	SAE 863 IC Bronze	1
KJU-07	Binding post barrel female – (½” OD)	Stainless Steel 316	1
KJU-08	Binding post barrel male – (¼” OD)	Stainless Steel 316	1

The KJU takes a knuckle joint arrangement with a fork end (KJU-01) and an eye end (KJU-02). The unit only offers sagittal rotation. Smooth rotation is provided by the binding post (KJU-07 and KJU-08) and sleeve bushing (KJU-06). The eye end connects to the top of the SLU, while the fork end connects to the bottom of the TLU. A locking pin (KJU-03) is inserted in the fork end. The locking pin is attached to the locking pin arm (KJU-04). A small compression spring (KJU-05) is placed under the locking pin in order to maintain the KJU locked. The trigger cable of the FPU is attached to the end of the locking pin arm. During stance, the trigger cable will gradually pull on the locking pin arm until a total disengagement of KJU is achieved during terminal stance.

3.6.10 SHANK LINK UNIT

The shank link unit (SLU) as shown by Figure 3-14, corresponds to an aluminium 6061 plate. The upper end of the plate connects to the KJU, while the lower end connects to the FPU.

Figure 3-14: Front view of the SLU.

3.6.11 FOOT PLATE UNIT

The foot plate unit (FPU) is the lower portion of each support leg. The two functions of the unit are to provide sufficient ROM to the ankle and maintain secure foot attachment. Figure 3-15 and Table 3-10 detail the assembly of the FPU. Note that the trigger cable is not shown in Figure 3-15.

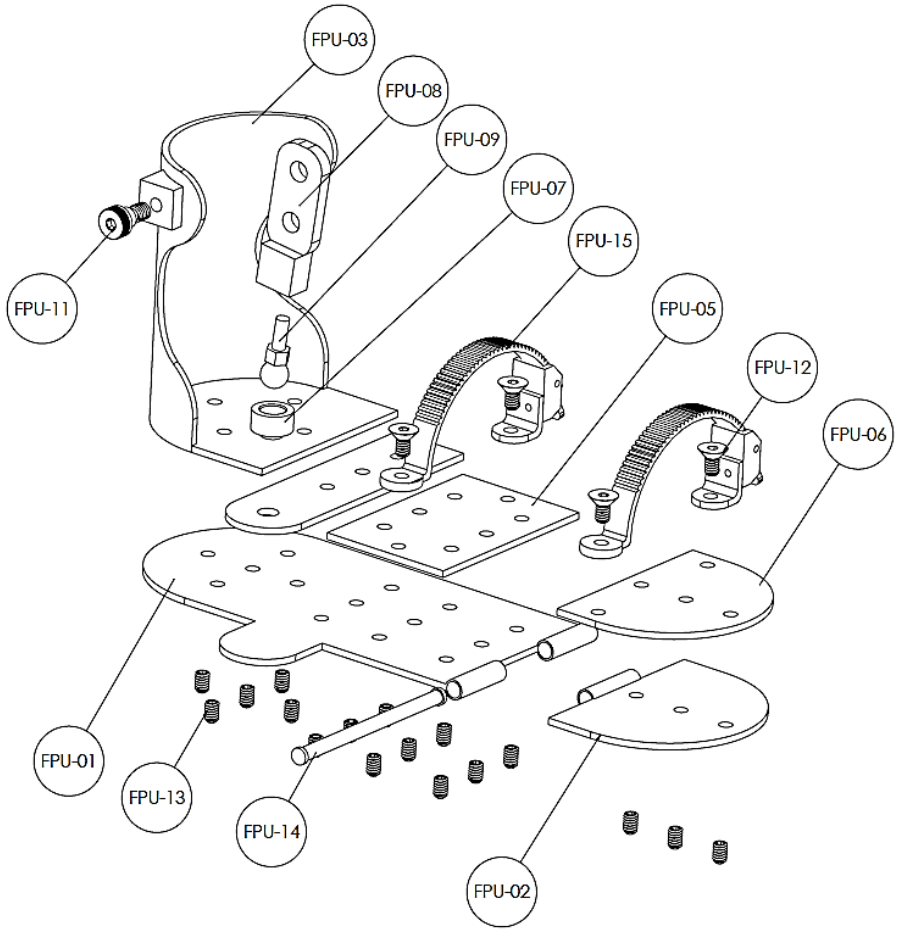

Figure 3-15: Exploded view of left FPU

Table 3-10: Part list description of FPU.

Part ID	Description	Material	Qty.
FPU-01	Bottom Back Sole Plate – (Thickness ⅛”)	Aluminium 6061	1
FPU-02	Bottom Front Sole Plate – (Thickness ⅛”)	Aluminium 6061	1
FPU-03	Top Back Resting Plate – (Thickness ⅛”)	Aluminium 6061	1
FPU-04	Top Middle Connection Plate – (Thickness ⅛”)	Aluminium 6061	1
FPU-05	Top Middle Plate – (Thickness ⅛”)	Aluminium 6061	1
FPU-06	Top Front Plate – (Thickness ⅛”)	Aluminium 6061	1
FPU-07	Spherical cup	Stainless Steel	1
FPU-08	Connection Plate with threaded end	Aluminium 6061	1
FPU-09	Spherical Ball with threated end	Stainless Steel	1
FPU-10	Ratchet Buckle – (½” Width)	LDPE	2
FPU-11	Shoulder Screw – (¼”-20), (Length ⅜”)	Stainless Steel	1
FPU-12	Flat Hex Screw – (¼”-20), (Length ⅜”)	Stainless Steel	4
FPU-13	Set Screw – (¼”-20), (Length ¼”)	Stainless Steel	16
FPU-14	Shaft – (¼” OD), (Length 4”)	Aluminium 6061	1
FPU-15	Ladder Strap	LDPE	2

The FPU is an assembly aluminium plates put together to form a support plate for the foot. Set screws (FPU-13) are used to hold the different plates together. The foot of the user is secured by two systems of ratchet buckle and ladder strap. A ball and socket joint is placed on the inner side of the FPU and connects to the SLU. The joint provide full ROM to the ankle. A hinge joint is found at the front of the FPU and it is intended to be aligned with the 2nd metatarsal joint of the user. The hinge joint promotes foot propulsion during late stance. A shoulder screw (FPU-11) is placed on the inner side of the back support plate (FPU-03). The trigger cable used to disengage the KJU is connected there. Figure 3-16 and Table 3-11 detail the trigger cable assembly.

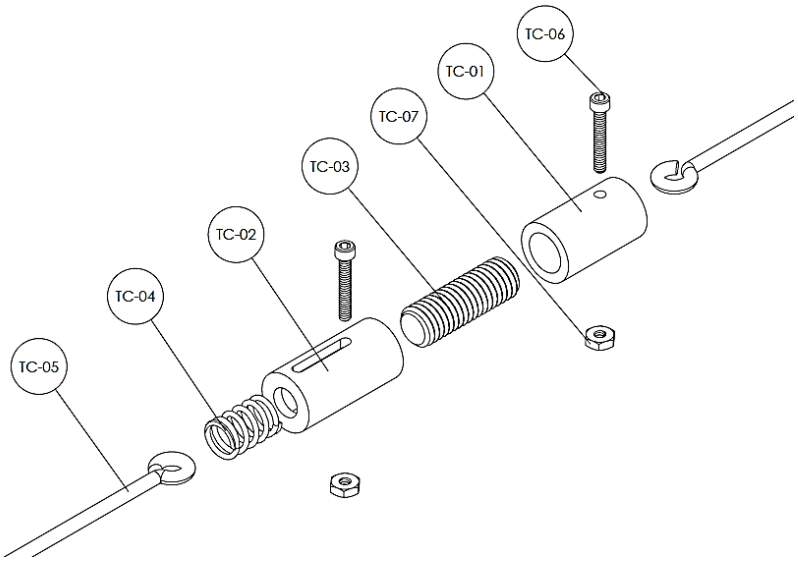

Figure 3-16: Exploded view of trigger cable.

Table 3-11: Part list description of trigger cable.

Part ID	Description	Material	Qty.
TC-01	Top adaptor.	Aluminium 6061	1
TC-02	Bottom adaptor.	Aluminium 6061	1
TC-03	Threaded rod – (½'-13), (Length 1').	Steel	1
TC-04	Compression Spring – (OD ½'), (Length ¾').	Stainless Steel 316	1
TC-05	Filament cable.	Polyamide	2
TC-06	Hex bolt – (6-32), (Length 3/4').	Steel Grade 9	2
TC-07	Hex nut – (6-32).	Steel Grade 9	2

The trigger cable is made of two adaptors (TC-01 and TC-02) connected together by a threaded rod (TC-03). The top adaptor holds one polyamide filament (TC-05). This filament attaches to the locking pin arm of the KJU (KJU-04). The bottom adaptor holds the second polyamide filament which wraps over the shoulder bolt of the FPU (FPU-11). A compression spring (TC-04) is placed inside the bottom adaptor so that the hex bolt holding the bottom polyamide filament can slide. During stance, the forward progression of the support leg will gradually pull on the trigger cable. In doing so, the spring gets compressed and tension in the polyamide filaments increases. The tension increases until reaching a sufficient value to unlock the KJU at terminal stance.

3.7 MODELLING OF FINAL PROTOTYPE

The final prototype was modelled for two motions: standing and walking. The first goal in modelling was to predict the amount of upward force provided by the SU and the EWU. The second goal of modelling was to determine load sharing on the device that would be later be used to discuss and interpret testing results.

Standing was considered due to its simplicity in analysis. A MATLAB script was built to compute the amount of upward force felt by the user based on the extension of the EWU, the vertical displacement of the SU and the stiffness of spring. The MATLAB script also computed the amount of load supported by each SLU when the user stands on the device.

The final design was also modelled for ground level walking. Gait data of the participant was combined with the dimensions of the final design to simulate how the device moves during gait. The simulation's results were used to plot the expected assistance provided by the SU and EWU. Finally, the loads acting on the SLU were computed when highest assistance is provided by the SU and EWU.

3.7.1 STANDING MODEL

Modelling the exoskeleton in a standing position consisted of two steps. First step; the position of the SU and the spring extension in the EWU is geometrically identified. Second step; the forces and moments acting on each unit were calculated. The following assumptions were made when modelling the exoskeleton for standing.

- Motion and loads in the sagittal plane were only considered.
- Standing on the device was considered as static.
- Friction was neglected for all pulleys and shafts.
- The SU is maintained horizontal when the user stands on the device.
- Both TLU rest on the RSU and distribute loads evenly.
- The position of COM and attachment points of all units were found from the final CAD model and the measuring tools in SolidWorks.

- The mass of each unit was found using the final CAD model and the mass properties options in SolidWorks.

Geometrically, standing can be divided into two distinct cases. Case 1 is when the exoskeleton stands by itself with no user and Case 2 is when the user is standing on the device. The two cases are depicted by Figure 3-17.

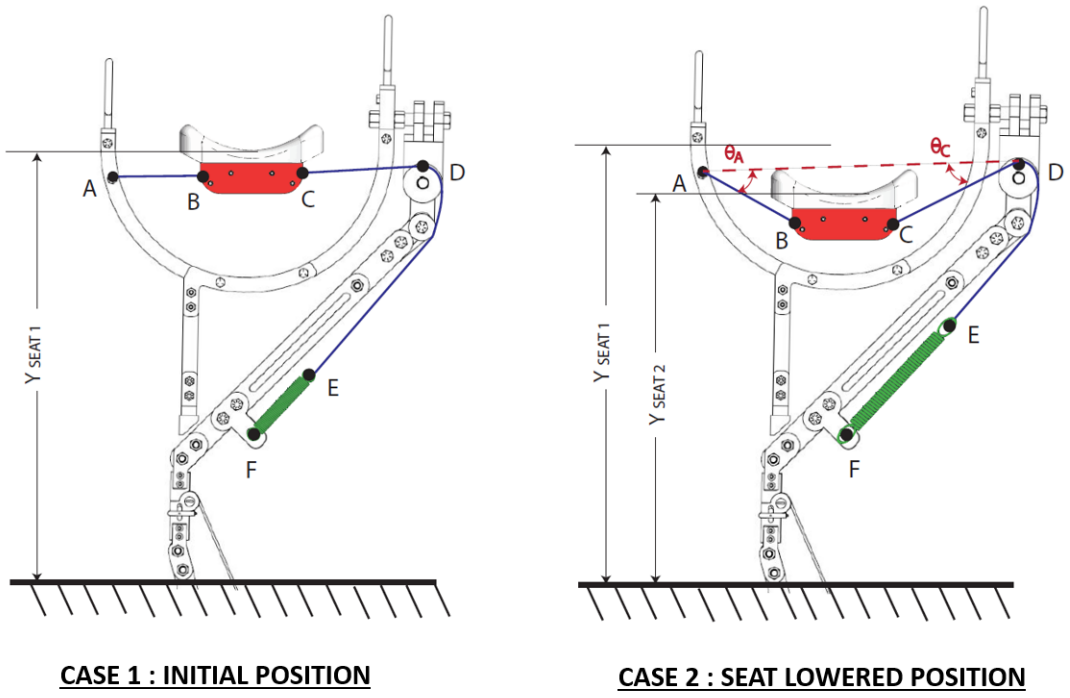

Figure 3-17: Schematic of standing position of exoskeleton when no user is sitting (left) and when the user is sitting (right).

For case 1 in Figure 3-17, the total length of the EWU ($L_{TOTAL\ 1}$) corresponds to the length of the wire rope (L_{AE}) and the length of the extension spring ($L_{EF\ 1}$) expressed by (3-1).

$$L_{TOTAL\ 1} = L_{AE} + L_{EF\ 1} \tag{3-1}$$

In case 1, the SU stays horizontal at its initial height ($Y_{SEAT\ 1}$). The spring in the EWU is initially preloaded in order to overcome the weight of the SU. The length of the extension spring in case 1 is given by the sum of the free length ($L_{SPRING\ FREE}$) and the initial extension ($\Delta L_{SPRING\ INITIAL}$) expressed by (3-2).

$$L_{EF\ 1} = L_{SPRING\ FREE} + \Delta L_{SPRING\ INITIAL} \tag{3-2}$$

For case 2 in Figure 3-17, the seat is lowered to a new height ($Y_{SEAT\ 2}$) by the user applying their weight. The height drop (ΔY_{SEAT}) is found by (3-3).

$$\Delta Y_{SEAT} = Y_{SEAT\ 1} - Y_{SEAT\ 2} \tag{3-3}$$

For the SU to reach $Y_{SEAT\ 2}$, the spring is stretched to a new length ($L_{EF\ 2}$). The spring extension between case 1 and case 2 (ΔL_{SPRING}) corresponds to the difference between $L_{EF\ 2}$ and $L_{EF\ 1.}$ It is expressed by (3-4).

$$\Delta L_{SPRING} = L_{EF\ 2} - L_{EF\ 1} \tag{3-4}$$

For case 2, the SU forms an angle for segment AB (θ_A). The value of θ_A is calculated by trigonometry and knowing the initial length of segment AB ($L_{AB\ 1}$) and ΔY_{SEAT}. The value of θ_A is found by (3-5).

$$\theta_A = \tan^{-1}\frac{\Delta Y_{SEAT}}{L_{AB\ 1}} \tag{3-5}$$

The length of segment AB for case 2 ($L_{AB\ 2}$) can also be computed using trigonometry and knowing $L_{AB\ 1}$ and θ_A. The value of $L_{AB\ 2}$ is found by (3-6).

$$L_{AB\ 2} = L_{AB\ 1} / \cos\theta_A \tag{3-6}$$

The length difference for segment AB between case 1 and case 2 (ΔL_{AB}) is expressed by (3-7).

$$\Delta L_{AB} = L_{AB\ 2} - L_{AB\ 1} \tag{3-7}$$

Similarly, the angle of segment CD (θ_C), the length of segment CD for case 2 ($L_{CD\ 2}$) and the difference between $L_{CD\ 1}$ and $L_{CD\ 2}$ can be computed. The value of ΔL_{SPRING} is directly equal to sum of ΔL_{AB} and ΔL_{CD}, since L_{AE} remains constant. The value of ΔL_{SPRING} is found by (3-8).

$$\Delta L_{SPRING} = \Delta L_{AB} + \Delta L_{CD} \tag{3-8}$$

The tension in the EWU (T_{EWU}) can be calculated by multiplying the stiffness of the spring (K_{SPRING}) and the total extension of the spring given by (3-9).

$$T_{EWU} = K_{SPRING}(\Delta L_{INITIAL\ SPRING} + \Delta L_{SPRING}) \tag{3-9}$$

The free body diagram (FBD) of the SU is drawn in order to determine the amount of upward assistive force felt by the user ($F_{USER\ Y}$). The FBD is unveiled by Figure 3-18.

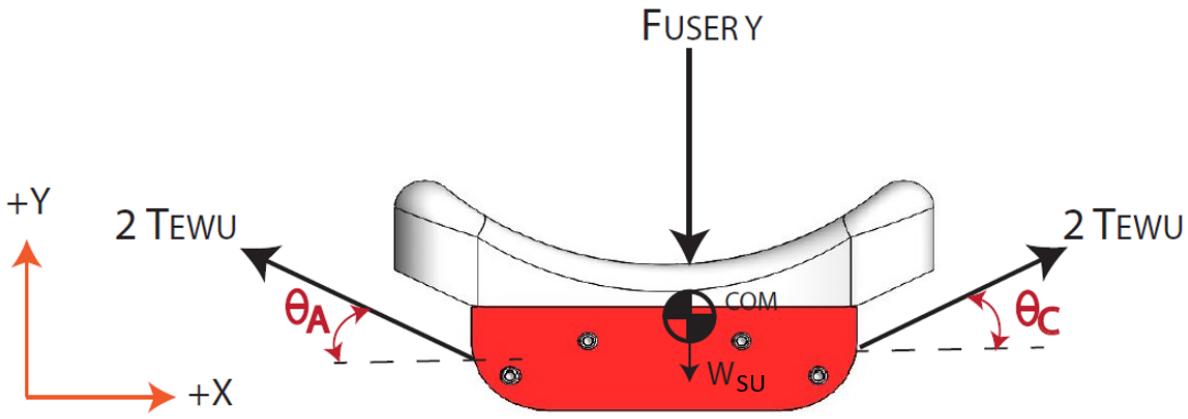

Figure 3-18: FBD of SU for standing position.

In Figure 3-18, the values of θ_A and θ_C are equal, since the SU stands midway inside the SFU. Thus, the horizontal component of T_{EWU} (left and right) cancel each other and no horizontal force is felt at the seat interface. Note that there are two EWU acting on the SU. Therefore, two values of T_{EWU} are found on each side. By Newton's force equilibrium, the value of $F_{USER\ Y}$ is found by adding the vertical contributions of T_{EWU} and subtracting the weight of the SU (W_{SU}). It is expressed by (3-10).

$$F_{USER\ Y} = 2 \times T_{EWU} \times \sin\theta_A + 2 \times T_{EWU} \times \sin\theta_C - W_{SU} \qquad (3\text{-}10)$$

An optimization script was built in MATLAB to calculate the value of $F_{USER\ Y}$ depending on values of K_{SPRING} and ΔY_{SEAT}. The optimization script can be found in APPENDIX B. Figure 3-19 presents the results of the optimization script when considering 6 springs that would later be used in human testing.

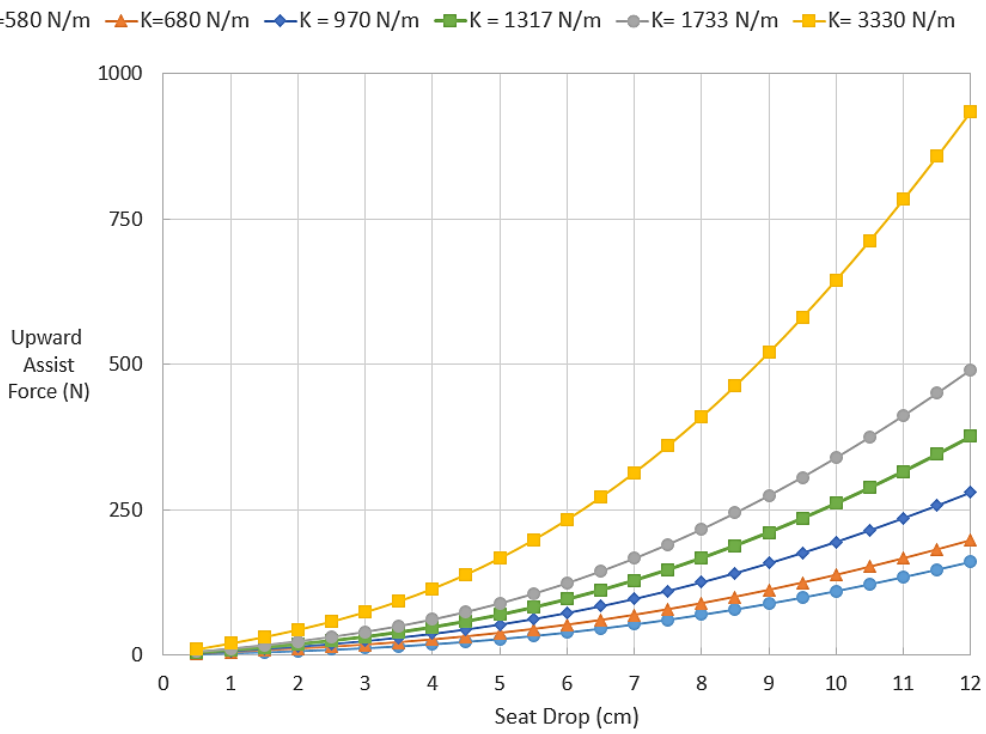

Figure 3-19: Results of optimization script for standing position.

Figure 3-19 reveals that a greater K_{SPRING} provides a higher $F_{USER\ Y}$ value for the same value of ΔY_{SEAT}. The optimization script was used to set the initial value of ΔY_{SEAT} for the standing condition which was set to be 9 cm. With such value, testing results should reveal a clear difference in assistance between the 6 springs. Note that, a higher initial value of ΔY_{SEAT} was not considered, because the maximum geometrical value of ΔY_{SEAT} offered is 13 cm. Table 3-12 presents the computed values of $F_{USER\ Y}$ for the intended initial value of ΔY_{SEAT}.

Table 3-12: Computed values of $F_{USER\ Y}$ for 6 springs when standing.

Spring ID	K_{SPRING} (N/m)	$F_{USER\ Y}$ (N)	$F_{USER\ Y}$ (% BW)
1	580	88	11
2	680	111	14
3	970	157	19
4	1317	211	26
5	1733	274	33
6	3300	520	63

In Table 3-12, $F_{USER\ Y}$ increases with higher K_{SPRING} value. The last column of Table 3-12 shows that by using a spring with a stiffness value of 970 N/m, a reduction of felt weight

of 19 % BW is achieved. Values of $F_{USER\ Y}$ of Table 3-12 were used to compute theoretical values of pressure at the seat interface (P_{SEAT}). P_{SEAT} was calculated by dividing $F_{USER\ Y}$ and the contact surface area of the SU (SA_{SU}). The value of SA_{SU} was found using the measuring tools in SolidWorks. The value of P_{SEAT} was computed by (3-13). Table 3-13 reveals the values of P_{SEAT} for the 6 different springs.

$$P_{SEAT} = \frac{F_{USER\ Y}}{SA_{\ SU}} \tag{3-11}$$

Table 3-13: Compute values of P_{SEAT} for 6 springs when standing.

Spring ID	K_{SPRING} (N/m)	P_{SEAT} (mmHg)
1	580	37
2	680	46
3	970	65
4	1317	88
5	1733	117
6	3300	216

Table 3-13 shows that only the use of spring #1 and spring #2 is below the pressure threshold of tissues (see Section 2.2.3). Table 3-13 predicts that the user is expected to feel discomfort when using the device for the last 4 springs.

Next, a kinetics analysis was conducted in order to determine the loads acting on each SLU when standing on the device. The kinetic analysis consisted in drawing the FBD of each unit and solving Newton's and Euler's Laws of Motion. Figure 3-20 shows the FBD of the SFU.

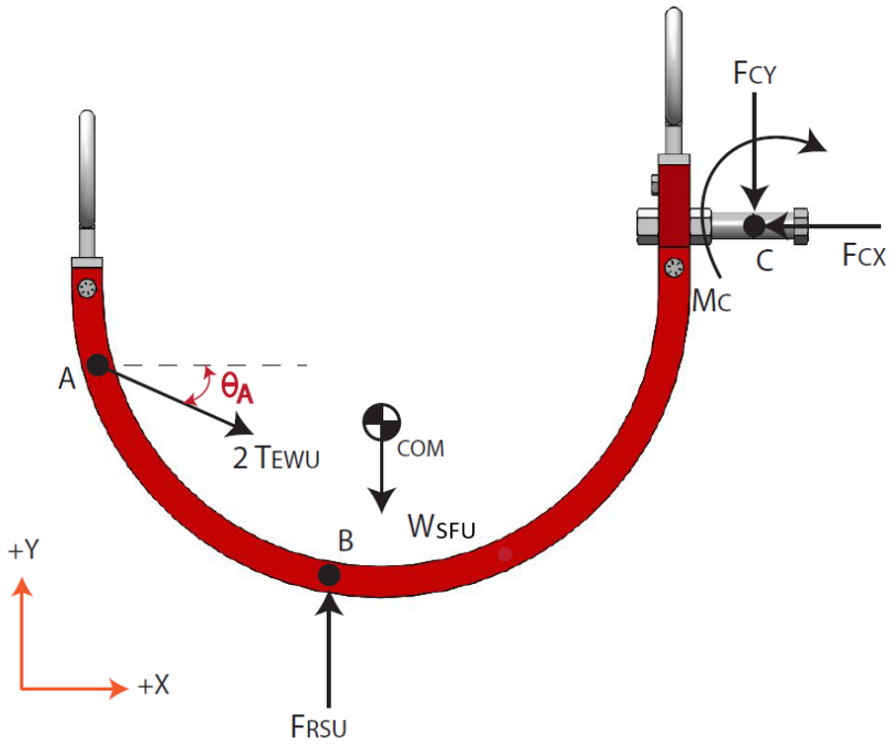

Figure 3-20: FBD of SFU for a standing condition.

In Figure 3-20, two T_{EWU} are placed on attachment point (A) and directed with an angle of θ_A. The force in the RSU (F_{RSU}) is a compression load, since the unit acts as a strut and no external load is applied on the unit. The weight of SFU (W_{SFU}) is placed at the COM. Point C corresponds to the attachment point of the HJU where reaction forces in both directions are found (F_{CX} and F_{CY}). The force balance about the x and y directions are given by (3-12) and (3-13).

$$\sum F_x = 2T_{EWU} \cos\theta_A - F_{CX} = 0 \tag{3-12}$$

$$\sum F_y = F_{RSU} - 2T_{EWU} \sin\theta_A - W_{SFU} + F_{CY} = 0 \tag{3-13}$$

At point C, a resulting moment (M_C) is found. The value of M_C can be computed by the summation of moment about point C given by 3-14.

$$\sum M_c = -F_{RSU}(Cx - Bx) + 2T_{EWU}\sin\theta_A + 2T_{EWU}\cos\theta_C(Cy - Ay) + W_{SFU}(Cx - COMx) - M_c = 0 \quad (3\text{-}14)$$

Figure 3-21 reveals the FBD of the HJU with two connection plates (HJU-05) disconnected.

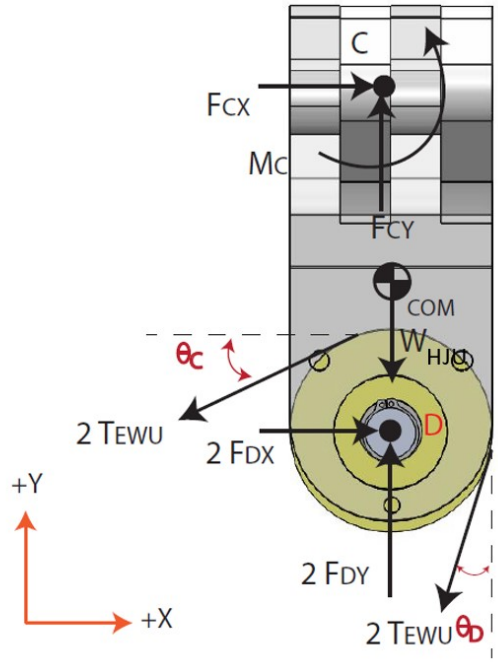

Figure 3-21: FBD of HJU without both connection plate of HJU for a standing condition.

In Figure 3-21, the wire ropes of each EWU wraps around the two large pulleys of known diameter (D_{PULLEY}). Each wire rope wraps about a quarter turn before being directed to the small pulley with an angle (θ_D). At point C, the opposite set of reaction forces and opposite moment are found. At point D, the TLU are connected to a shaft (TLU-08). Therefore, only two reaction forces are found (F_{DX} and F_{DY}). The weight of the HJU unit (W_{SLU}) is placed at the COM. The force equilibrium about the x axis and y axis are given by (3-15) and (3-16).

$$\sum F_x = F_{CX} - 2T_{EWU}\cos\theta_C - 2T_{EWU}\sin\theta_D + 2F_{DX} = 0 \quad (3\text{-}15)$$

$$\sum F_y = F_{CY} - W_{HJU} - 2T_{EWU}\sin\theta_C - 2T_{EWU}\cos\theta_D + 2F_{DY} = 0 \quad (3\text{-}16)$$

The moment equilibrium about point D is given by (3-17).

$$\sum M_D = M_C - F_{CX}(C_Y - D_Y) + 2T_{EWU}\cos\theta_C\left(\frac{D_{PULLEY}}{2}\right) - 2T_{EWU}\cos\theta_D\left(\frac{D_{PULLEY}}{2}\right) = 0 \quad (3\text{-}17)$$

Figure 3-22 presents the FBD for the small pulley disconnected from the connection plate of HJU (HJU-05).

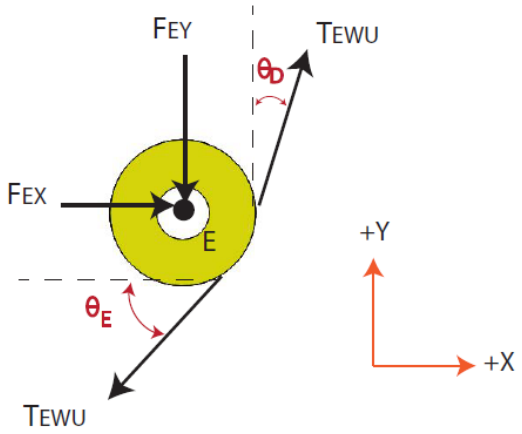

Figure 3-22: FBD of the small pulley for a standing position.

Figure 3-22 reveals that the wire rope of the EWU wraps with a small arc over the small pulley. The top part of the wire rope is directed towards the large pulley of the HJU with an angle of θ_D. The bottom part of the wire rope is directed towards the extension spring of the EWU with an angle of θ_E. The small pulley is mounted on the connection plate of the HJU (HJU-06) via a shaft and sleeve bushing at point E. Thus, only two reaction forces are found (F_{EX} and F_{EY}). The force equilibrium about the x and y direction are given by (3-18) and (3-19).

$$\sum F_X = F_{EX} + T_{EWU}\sin\theta_D - T_{EWU}\cos\theta_E = 0 \quad (3\text{-}18)$$

$$\sum F_Y = -F_{EY} + T_{EWU}\cos\theta_D - T_{EWU}\sin\theta_E = 0 \quad (3\text{-}19)$$

Figure 3-23 presents the FBD of the left TLU with the connection plate of the HJU (HJU-05) and top half of the left KJU.

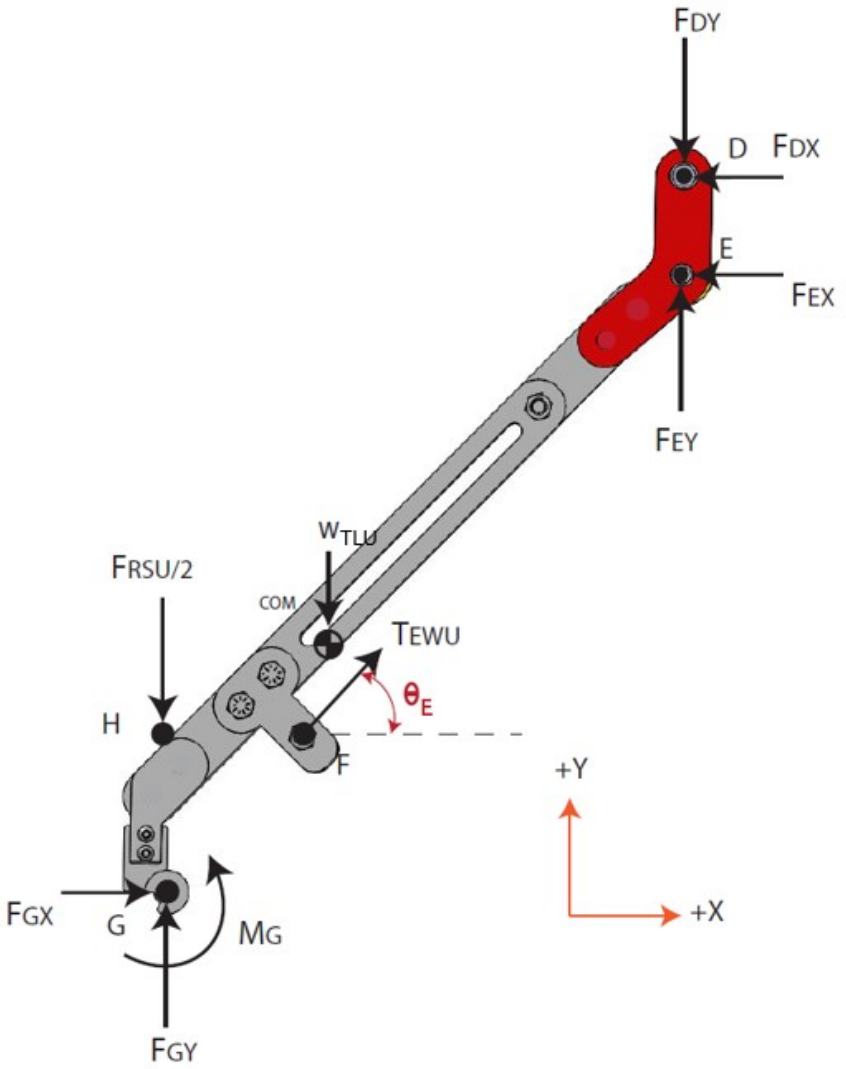

Figure 3-23: FBD of TLU with connection plate of HJU and top half of KJU for a standing position.

In Figure 3-23, the opposite set of forces are placed at points D and E. Point H marks the contact point of the RSU. Note that, the RSU rests on both support legs, thus the load is divided in half. Point F corresponds to the attachment point of the EWU, where T_{EWU} is directed with an angle of θ_E. At the COM, the weight of the TLU is placed (W_{TLU}). Point G corresponds to the center of rotation of the KJU. Since the KJU is locked, a set of reaction forces (F_{GX} and F_{GY}) are present. The force equilibrium equations about the x and y axis are given by (3-20) and (3-21).

$$\sum F_X = F_{GX} + T_{EWU}\cos\theta_E - F_{EX} - F_{DX} \tag{3-20}$$

$$\sum F_Y = F_{GY} + T_{EWU}\sin\theta_E - \frac{F_{RSU}}{2} - W_{TLU} + F_{EY} - F_{DY} \tag{3-21}$$

Due to fact the KJU is locked, a moment is also present at point G (M_G). The moment equilibrium about point G is given by (3-22).

$$\begin{aligned}\sum M_G = {} & -W_{TLU}(COM_X) + T_{EWU}\sin\theta_E\,(F_x - G_x) - T_{EWU}\cos\theta_E\,(F_y - G_y) \\ & + F_{EX}(E_y - G_y) + F_{EY}(E_x - G_x) - F_{DX}(D_y - G_y) \\ & - F_{DY}(D_x - G_x) + M_G\end{aligned} \tag{3-22}$$

Last FBD to draw is of the SLU in order to determine the amount of load sharing. Figure 3-24 presents the FBD of the SLU connected to the bottom half of KJU.

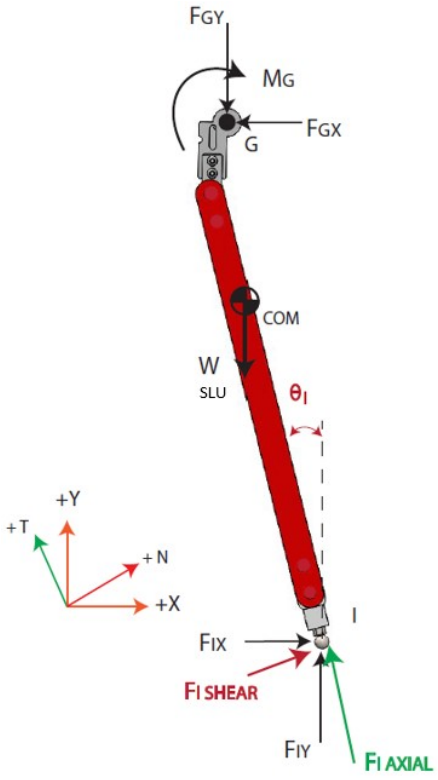

Figure 3-24: FBD of SLU connected to bottom half of KJU for a standing position.

In Figure 3-24, the SLU is inclined forward with an angle of θ_I. Note that the value of θ_I corresponds the value of θ_{SLU} (see Table 3-2). At point G, the opposite set of forces and

moment is placed. At the COM, the weight of the SLU is placed (W_{SLU}). Point I corresponds to the ball portion of the ankle joint in the FPU. Thus, only two reaction forces are found (F_{IX} and F_{IY}). The force equilibrium about the x and y directions are given by (3-23) and (3-24).

$$\sum F_X = F_{GX} - F_{IX} = 0 \tag{3-23}$$

$$\sum F_Y = -F_{GY} - W_{SLU} + F_{IY} = 0 \tag{3-24}$$

By rotating the system of coordinates by θ_I, the amount of compressive load (F_{AXIAL}) and shear load (F_{SHEAR}) in each SLU can be computed. The value of F_{AXIAL} is given by (3-25).

$$F_{AXIAL} = F_{IY} \cos\theta_I + F_{IX} \sin\theta_I = 0 \tag{3-25}$$

A MATLAB script was developed to solve the entire kinetic analysis based on the spring selected. The script can be found in the APPENDIX C. Table 3-14 presents the computed values of load sharing at each SLU for 6 spring later used in testing.

Table 3-14: Values of F_{AXIAL} and F_{SHEAR} for 6 different springs when standing.

Spring ID	K_{SPRING} (N/m)	F_{AXIAL} (N)	F_{SHEAR} (N)
1	580	100	27
2	680	119	32
3	970	162	43
4	1317	213	57
5	1733	273	73
6	3300	506	136

Table 3-14 reveals that a stiffer spring yields to an increase in values of F_{AXIAL} and F_{SHEAR}. During testing, the value of F_{AXIAL} will be measured and compared to values presented in Table 3-14.

3.7.2 WALKING MODEL

Modelling the device for walking is more complex due to the dynamic nature of the motion. The approach taken to model the device consisted of three steps. The first step was to

plot how the device is expected to move with respect to the legs of the user during gait. To provide an accurate model, a rapid gait trial was conducted on the participant in order to track how his legs moved. The gait model proposed by Winters was used as a reference in conducting the trial [17]. In such a gait model, each leg is modelled as an assembly of three rigid segments (thigh, shank and foot) connected to three joints (hip, knee and ankle). In the gait model, the femoral trochanter represents the hip, the medial femoral condyle represents the knee and the lateral malleolus represent the ankle. Reflective markers recorded the motion of those three anatomical landmarks as the participant walked. The data collected of reflective markers was plotted in MATLAB. Next, four points were spatially positioned in order to describe the motion of each support leg of the exoskeleton with respect to the legs of the user. Figure 3-25 depicts the four points used in modelling.

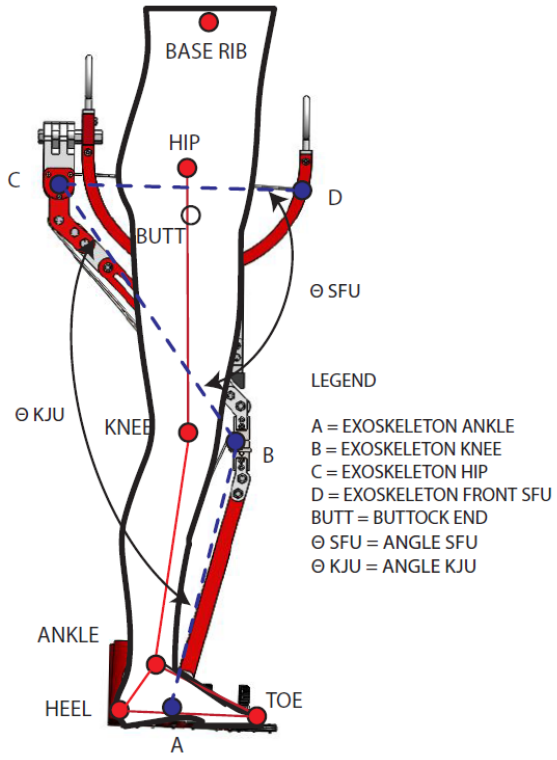

Figure 3-25: Schematic of walking modelling points with reflective markers (red) and calculated points (blue).

In Figure 3-25, the red points correspond to the reflective markers placed on the participant. The blue points depict the exoskeleton. Point A represents the center of rotation of the ankle joint in the FPU. Point B represents the center rotation of the KJU. Point C

represents the center of rotation of the HJU. Point D represents the attachment point of the EWU on the SFU. The distances between the four blue points were found in SolidWorks using the final CAD model. The locking angle between the TLU and SLU (θ_{KJU}) and the locking angle between the TLU and SFU (θ_{SFU}) were also found from the CAD model in SolidWorks. The four blue points were positioned in space in a way to match the expected behaviour of the device during gait (see Section 3.6.2). Point BUTT in Figure 3-25 represents the end of the buttock. It was assumed that the SU would follow point BUTT throughout gait. It was also assumed that Point BUTT moves in the same pattern as the COG. Given this assumption, the relative vertical and horizontal distances between the end of buttock and the COG of user would be maintained during gait. Anthropometry was used to compute the relative vertical and horizontal distances of point BUTT with the COG (see APPENDIX A for reference). MATLAB was used to add the four blue points and point BUTT on the gait trial of the participant in order to plot the progression of the proposed WAE during gait. The walking simulation is shown by Figure 3-26, while the MATLAB script can be found in APPENDIX B.

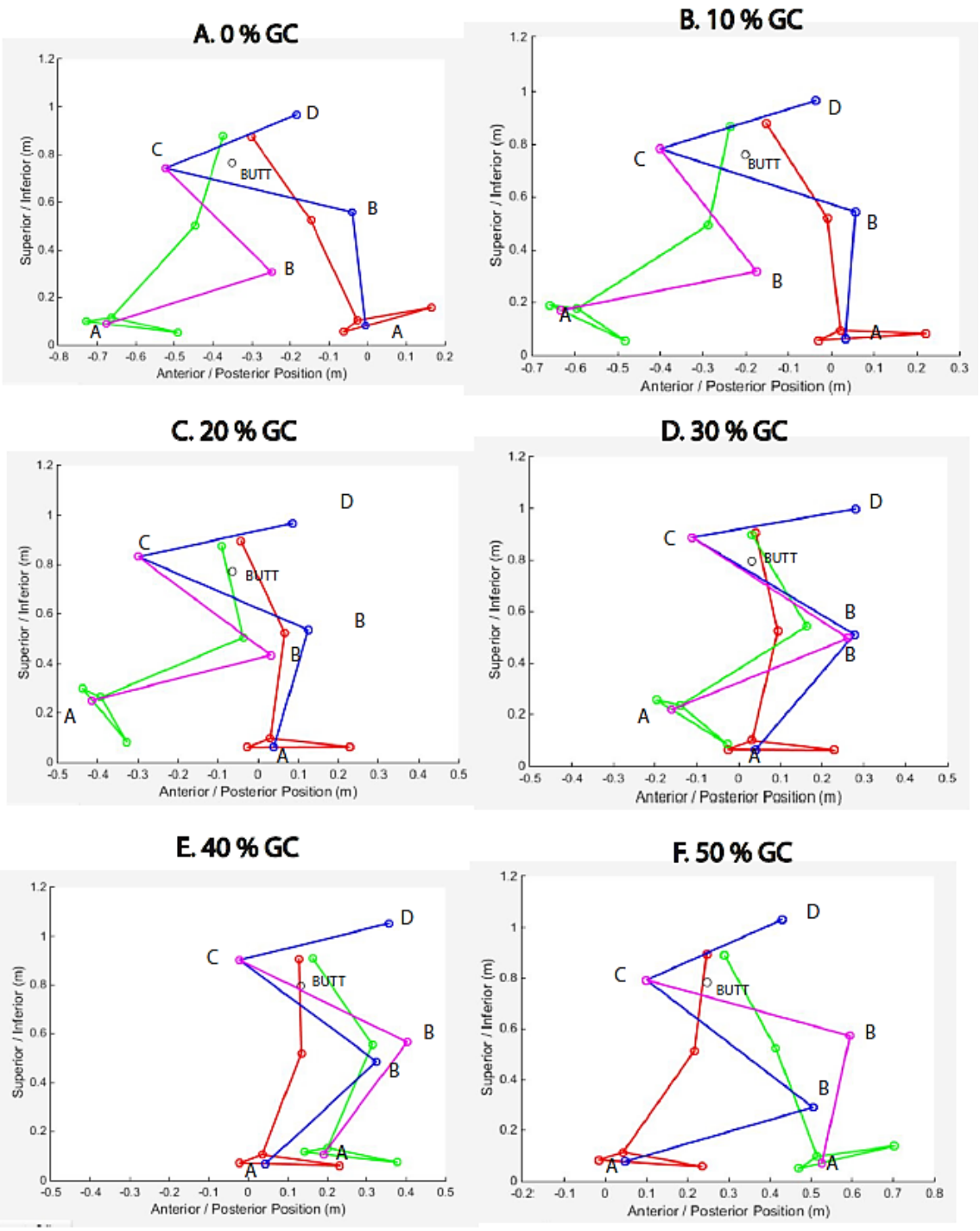

Figure 3-26: MATLAB simulation for walking with the proposed WAE.

In Figure 3-26, the red segments correspond to the right leg of the user, while the green segments depict the left leg of the user. The blue segments depict the right support leg of the exoskeleton, while the purple segments depict the left support leg of the exoskeleton. Note

that only half of the GC is shown by Figure 3-26. The reason of such choice is that motion of the right support leg during second half of GC corresponds to the motion of the left support leg during the first half of GC.

The second step in modelling the exoskeleton walking was to plot the assistance of the SU and EWU. The MATLAB simulation was used to approximate the spring extension of EWU (ΔL_{SPRING}) throughout the first half of GC. The value of ΔL_{SPRING} was approximated using the position of Point C, Point D and Point BUTT in the MATLAB simulation. Figure 3-27 depict how the device is positioned at 20 % GC based on the MATLAB simulation.

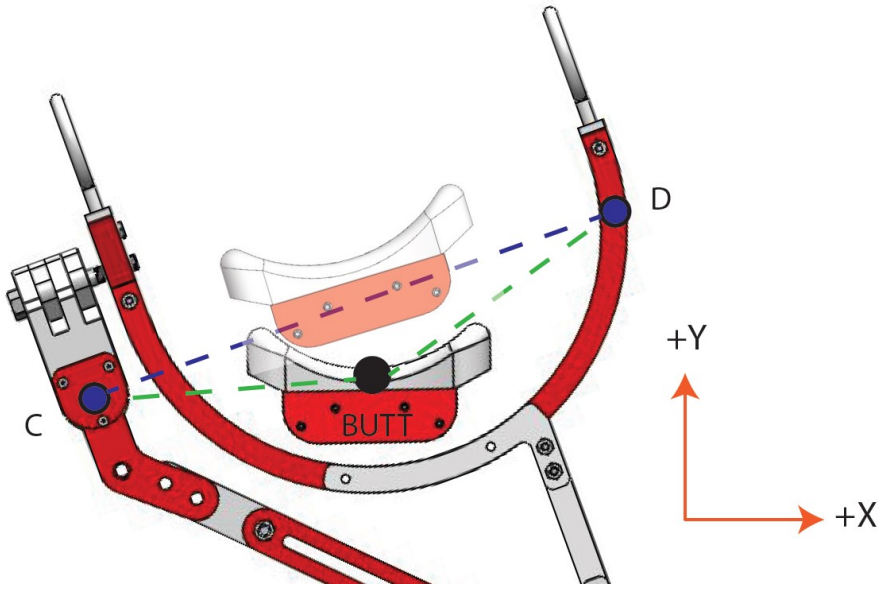

Figure 3-27: Illustration of top portion of WAE at 20 %GC.

In Figure 3-27, the position of Point C, Point D and Point BUTT are revealed. The value of ΔL_{SPRING} was calculated by finding the differences in distance between the three points. Segment CD was assumed to represent the initial length of the top portion of the wire rope when no user is using the device and no load is applied on the SU. At such a condition, Point BUTT is about midway along segment CD. Length CD (L_{CD}) was calculated by knowing the spatial position of Point C and Point D from the MATLAB simulation. The value of L_{CD} is expressed by (3-26).

$$L_{CD} = \sqrt{(y_D - y_c)^2 + (x_D - x_C)^2} \tag{3-26}$$

During gait, the SU is loaded and Point BUTT is lowered. The distance between Point C and Point BUTT ($L_{C/BUTT}$) as well as the distance between Point D and Point BUTT ($L_{D/BUTT}$) can be computed in the same way L_{CD} was computed. Then by geometry, the value of ΔL_{SPRING} corresponds to the different in lengths of segment CD between the unloaded and the loaded condition. It unveiled by (3-27).

$$\Delta L_{SPRING} = \left(L_{C/BUTT} + L_{D/BUTT}\right) - L_{CD} \tag{3-27}$$

Using MATLAB, a script was built to calculate the value of ΔL_{SPRING} throughout gait and plot the results shown by Figure 3-28.

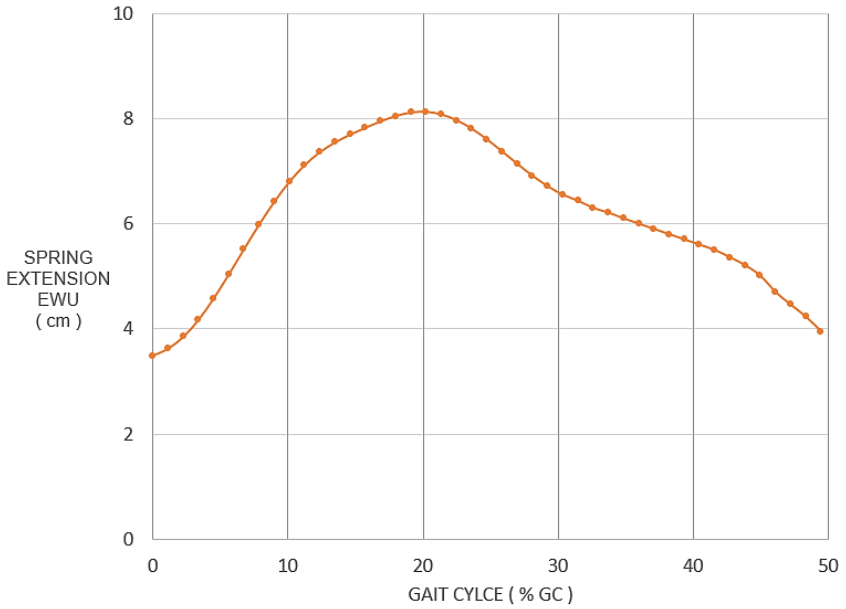

Figure 3-28: Plot of spring Extension in EWU (cm) versus gait cycle for walking condition.

Figure 3-28 reveals that ΔL_{SPRING} values increase during loading response and early midstance. At 20 % GC, a peak value of 8 cm for ΔL_{SPRING} is reached which corresponds to the moment where highest upward force is provided at the SU interface. Afterward, the value of ΔL_{SPRING} decreases during the remaining of stance. Next step in modelling the device for walking involved drawing the FBD of the SU to determine peak values of $F_{USER\ Y}$. Figure 3-29 depicts the FBD of the SU at 20 % GC.

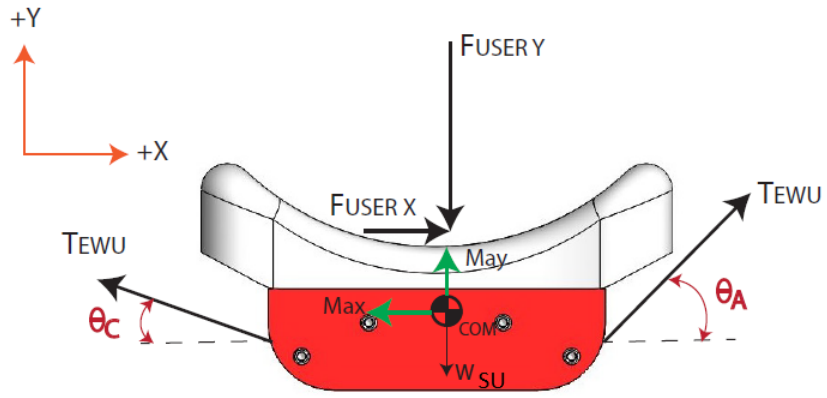

Figure 3-29: FBD of the SU at 20 % GC.

The FBD of the SU for the walking condition differentiates itself from the FBD for the standing condition (see Figure 3-18) by the addition of inertia components and by having different values of θ_A and θ_C. The new value of θ_A was approximated using the position of Point BUTT and Point D in the MATLAB simulation at 20 % GC. The value of θ_A is given by (3-28).

$$\theta_A = \tan^{-1}\frac{(y_D - y_{BUTT})}{(x_D - x_{BUTT})} \tag{3-28}$$

The value of θ_C was found using the same approach. It considers the position of Point C and Point BUTT in the MATLAB simulation at 20 % GC. The value of θ_C is given by (3-29).

$$\theta_C = \tan^{-1}\frac{(y_C - y_{BUTT})}{(x_C - x_{BUTT})} \tag{3-29}$$

The value of T_{EWU} was computed using the peak value of ΔL_{SPRING} in Figure 3-28, the value of $\Delta L_{INITIAL}$ and the value of K_{SPRING}. The value of T_{EWU} is given by (3-30).

$$T_{EWU} = K_{SPRING}(\Delta L_{INITIAL} + \Delta L_{SPRING}) \tag{3-30}$$

The horizontal and vertical accelerations of the SU (a_X, a_y) correspond to the accelerations of Point BUTT in the MATLAB simulation at 20 % GC. The dynamic force equilibrium about the x direction is expressed by (3-31).

$$\sum F_x = F_{USER\,X} + 2\,T_{EWU}\cos\theta_A - 2\,T_{EWU}\cos\theta_C = m_{SU}a_x \tag{3-31}$$

For walking, there exists a horizontal force felt by the user ($F_{USER\,X}$). The value of $F_{USER\,Y}$ is found by the dynamic force equilibrium about the y direction given by (3-32).

$$\sum F_y = 2\,T_{EWU}\sin\theta_A + 2\,T_{EWU}\sin\theta_C - F_{USER\,Y} - W_{SU} = m_{SU}a_y \tag{3-32}$$

A MATLAB script was developed to compute the values of $F_{USER\,Y}$ and $F_{USER\,X}$. The script can be found in APPENDIX B. Table 3-15 presents the computed values of $F_{USER\,Y}$ and $F_{USER\,X}$ at 20 % GC for the 6 springs to be later tested.

Table 3-15: Values of $F_{USER\,Y}$ and $F_{USER\,X}$ at 20 % GC for 6 springs.

Spring ID	K_{SPRING} (N/m)	$F_{USER\,X}$ (N)	$F_{USER\,Y}$ (N)	$F_{USER\,Y}$ (%BW)
1	580	38	111	13
2	680	48	139	17
3	970	69	199	24
4	1317	94	270	33
5	1733	124	353	43
6	3300	238	678	82

Table 3-15 shows that values of $F_{USER\,Y}$ and $F_{USER\,X}$ increase as K_{SPRING} value increases. The last column of Table 3-15 reveals that the amount of upward assistance surpasses the performance of the Honda Bodyweight Support Assist for last 4 springs. For walking, the value of P_{SEAT} was found by dividing the resulting force at the SU interface over SA_{SU} given by (3-33).

$$P_{SEAT} = \frac{\sqrt{(F_{USER\,X})^2 + (F_{USER\,Y})^2}}{SA_{SU}} \tag{3-33}$$

Table 3-16 presents the values of P_{SEAT} at 20 %GC.

Table 3-16: Values of P_{SEAT} at 20 % GC.

Spring ID	K_{SPRING} (N/m)	P_{SEAT} (mmHg)
1	580	49
2	680	61
3	970	88
4	1317	119
5	1733	156
6	3300	300

Table 3-16 reveals that only spring #1 yields to a value of P_{SEAT} below the threshold of pressure for tissues. Note that the values of P_{SEAT} in Table 3-16 occur for a very brief period of time.

The third step in modelling the WAE for walking was to conduct a kinetic analysis to determine the loads acting on the right SLU at peak assistance. Once again, the approach consisted in drawing the FBD and computing forces and moments. The following general assumptions were made in the process:

- The analysis studied forces and moments acting on each unit at 20 % GC which corresponds to the instance where highest value of ΔL_{SPRING} was found.
- Linear and angular accelerations of each unit were found using the MATLAB simulation.
- The mass and moment of inertia (I) values of each unit were found using the CAD model and the mass properties tools in SolidWorks.
- The positions of COM and attachment points were found using the CAD model and the measuring tools in SolidWorks.
- Friction was neglected for all pulleys and shafts.
- The analysis only considered the sagittal plane. Motion and loads in other planes were neglected.

- The positions of the SFU, TLU and SLU at 20 %GC were taken from the MATLAB simulation.
- The nomenclature used to describe forces, moments, angles and attachment points is identical to the standing model.
- The SU is assumed to be horizontal at 20 % GC.
- The left leg of the device was omitted from the analysis to simplify the analysis. It was later found that their addition varied final values by less than 5 %.

Figure 3-30 depicts the FBD of the SFU at 20 % GC.

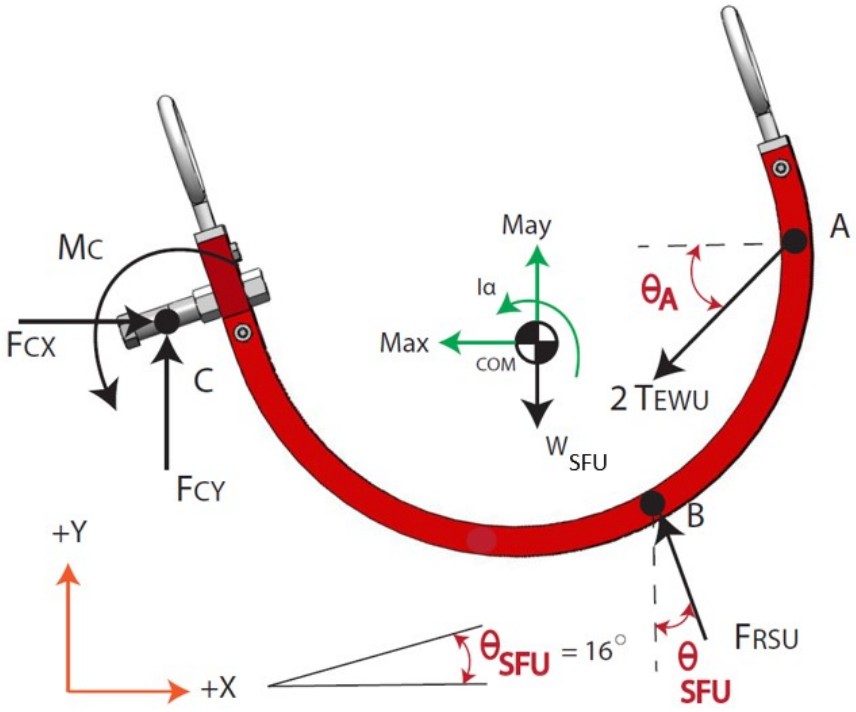

Figure 3-30: FBD of SFU at 20 % GC.

At 20 % GC, the MATLAB simulation indicated that the SFU is tilted with an angle (θ_{SFU}) of 16º. The horizontal and vertical accelerations of the SFU ($a_{COM\,X}$, $a_{COM\,Y}$) were found using direct kinematics. Their values relate to the acceleration of attachment point A (a_{AX} and a_{AY}) , the angular velocity of the SFU (ω_{SFU}) and angular acceleration of the SFU (α_{SFU}). Note that, the attachment point A in Figure 3-30 corresponds to Point A in the MATLAB simulation. The values $a_{COM\,X}$ and $a_{COM\,Y}$ are given by (3-34) and (3-35).

$$a_{COM\,X} = a_{AX} - {\omega_{SFU}}^2 L_{ACOM} \cos\theta - \alpha_{SFU} L_{ACOM} \sin\theta \tag{3-34}$$

$$a_{COM\,Y} = a_{AY} - {\omega_{SFU}}^2 L_{ACOM} \sin\theta + \alpha_{SFU} L_{ACOM} \cos\theta \tag{3-35}$$

The dynamic force equilibrium in the x and y directions are given by (3-36) and (3-37).

$$\sum F_x = F_{CX} - F_{RSU} \sin\theta_{SFU} - 2T_{EWU} \cos\theta_A = m_{SFU} a_{COM\,X} \tag{3-36}$$

$$\sum F_y = F_{CY} + F_{RSU} \cos\theta_{SFU} - 2T_{EWU} \sin\theta_A - W_{SFU} = m_{SFU} a_{COM\,Y} \tag{3-37}$$

The dynamic moment equilibrium about the attachment point C is given by (3-38).

$$\begin{aligned} \sum M_C = {} & F_{RSU} \cos\theta_{SFU}(B_x - C_x) \\ & - F_{RSU} \sin\theta_{SFU}(C_y - B_y) + 2T_{EWU} \cos\theta_A(A_x - C_x) \\ & - 2T_{EWU} \sin\theta_A(A_y - C_y) - W_{SFU}(COM_x - C_x) - M_c \\ & = I_{SFU}\alpha_{SFU} \end{aligned} \tag{3-38}$$

For the purpose of avoiding redundancy, only the detailed analysis of the SFU will be unveiled. It is apparent that the analysis of the HJU, TLU and SLU between the standing and walking condition are close to identical. The only two differences are the addition of inertia terms and modified angle values. The remaining FBD and equilibrium equations can be found in APPENDIX A and APPENDIX C. Figure 3-31 unveils the FBD of the right SLU and the bottom half of KJU at 20 % GC.

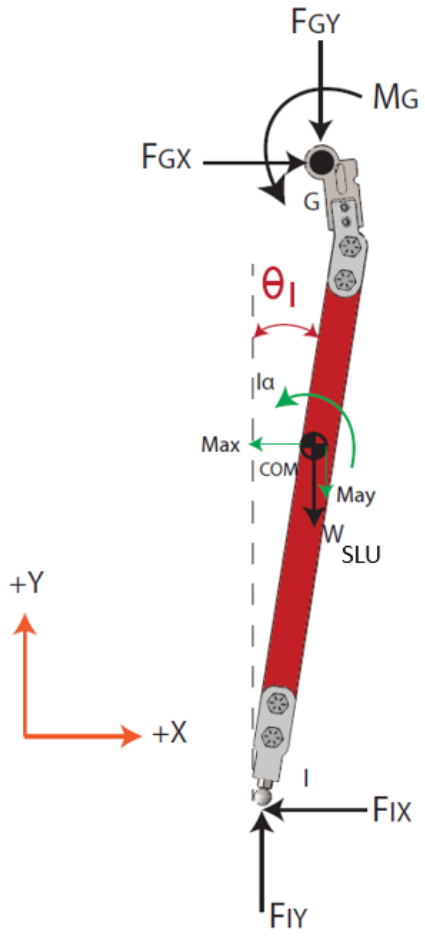

Figure 3-31: FBD of SLU with bottom half of KJU at 20 % GC.

Figure 3-31 reveals that the SLU is tilted slightly backward by 6º in comparison to the standing position. The value of θ_I corresponds to 81º. A compressive and shear load are acting at point I. A MATLAB script was developed to complete the kinetic analysis for the walking condition. The script can be found in APPENDIX B. Table 3-17 presents the values of F_{AXIAL} and F_{SHEAR} computed at 20 % GC.

Table 3-17: Values of F_{AXIAL} and F_{SHEAR} at 20 % GC for 6 springs.

Spring ID	K_{SPRING} (N/m)	F_{AXIAL} (N)	F_{SHEAR} (N)
1	580	206	47
2	680	251	59
3	970	347	83
4	1317	459	111
5	1733	592	145
6	3300	1103	277

Table 3-17 shows that values of F_{AXIAL} and F_{SHEAR} increase with a larger value of K_{SPRING}. Also, the values of F_{AXIAL} and F_{SHEAR} for the walking condition are higher than those computed for the standing condition. During testing, the values of F_{AXIAL} will be measured and compared to those presented in Table 3-17.

CHAPTER 4: PROTOTYPING, EXPERIMENTAL SETUP AND METHODOLOGY

Chapter 4 details the construction of multiple prototypes. The manufacturing steps for each prototype are described with a primary focus on the final prototype used during testing. Then, Chapter 4 describes the implementation and use of motion capture technologies and load cells to evaluate the mechanical performance of the final prototype. Next, the protocols followed during standing and walking trials are presented. The chapter ends on relevant preliminary results of manual tests conducted on the final prototype.

4.1 PROTOTYPING

A design project implies a process of continual revision of design concepts. At the start of the project, multiple design concepts were considered on how to implement the proposed seat mechanism. Numerous prototypes were built to study and validate each design concept. During the process, insights on the challenges of creating a WAE that reduces felt weight were gained. At the end of prototyping phase, a final device was created for the purpose of conducting tests and it corresponds to the design presented in Chapter 3.

4.1.1 PRELIMINARY PROTOTYPES

At the start of the thesis, small prototypes were built to experiment how the concept of slacklining could be applied on an exoskeleton. The use of 3D printers was solicited to create quick small sized prototypes. CAD models were created and exported from SolidWorks for part printing. Pulleys, bolts and springs used in the assemblies were acquired. Figure 4-1 unveils the last small sized prototype created.

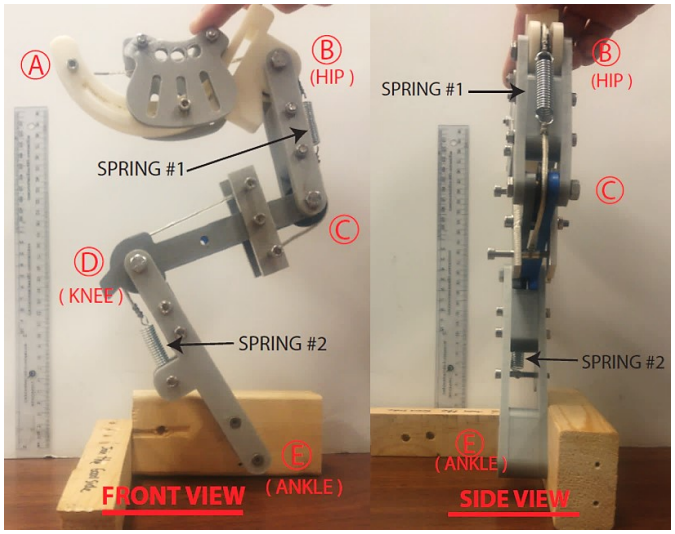

Figure 4-1: Photographs of small sized prototype: front view (left) and side view (right).

The prototype shown by Figure 4-1 is made of four links connected at 5 points. Pulleys are found at points B, C and D. Note that segment BC and segment CD are fixed with respect to each other. In this prototype, two extension springs were used. Spring #1 is stretched when the seat is lowered, while spring # 2 is stretched when the knee (Point D) is flexed. The major insights gained from this prototype are listed below.

- The option of using an arrangement of elastic strands (similar to a bungee cord) instead of a rigid cable and spring was studied. Such option was eliminated due to continue loosening of attachment knots.
- Use of elastic element only on the upper portion of the structure. The effect of adding an elastic element that loops over the knee (point D) results in a constant knee extension. To implement such idea on a full scale exoskeleton implies a structure that would constantly try to extend the knee of the user.
- Need to minimize friction at pulleys, otherwise undesirable moments would be created. At the hip (point B), high friction creates an extension moment. Such a moment was found to compromise the action of the spring and the seat unit.
- Need to lock motion of knee (point D) and hip (point B), otherwise structure height is not maintained and no assistance is gained at the seat by the elastic element.

The next series of prototypes created were full scale. The intention of creating larger prototypes was to further test insights gained from smaller prototypes and determine overall geometries. These prototypes were quickly built using available materials and parts at the University of Ottawa. Figure 4-2 unveils the first human scale prototype created that studied the mechanical response of the structure when standing.

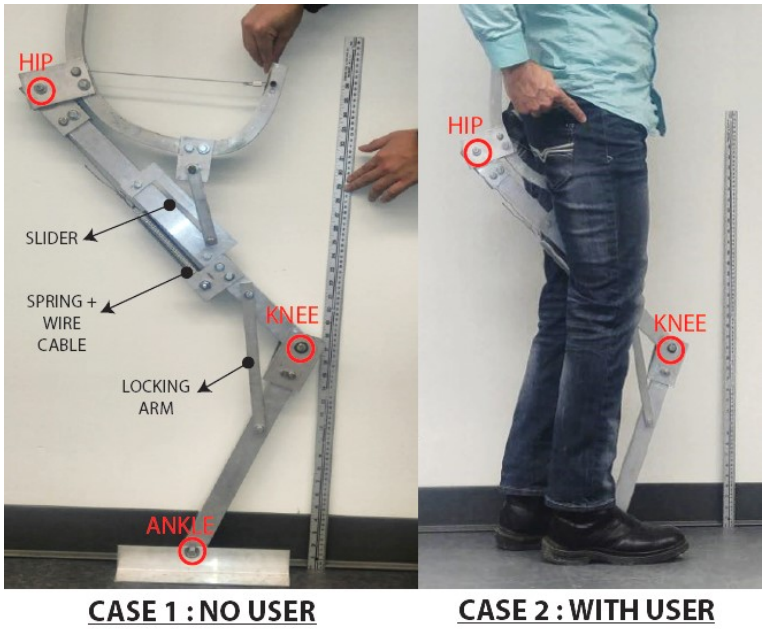

Figure 4-2: Photographs of first real scale prototype for no user (left) and with user (right).

The prototype in Figure 4-2 was primarily built of rectangular and square tubes. A bicycle seat, not shown in Figure 4-2, was placed over the wire rope at the center of the curved square tube. The extension spring was placed on the lower end of the thigh segment. The knee was locked by a locking arm. A linear slider mechanism was used to block hip rotation when weight was applied on the bicycle seat. Major findings from this prototype are listed below.

- Need to minimize the thickness of all segments in order to be able to place the exoskeleton comfortably between the legs of the user.
- The use of a linear slider mechanism for walking is expected to impose a kinematic constraint to the hip. Placing weight on the seat always maintains the slider at its lowest position, thus blocking a hip extension needed at terminal stance.
- By replicating the stance portion of gait with this prototype, it was found that the whole structure behaves as a rigid lever and follows the pelvis of the user. This is when both knee and hip motions are blocked.
- Attachments on the foot portion of the device need to be secure. When weight was placed on the seat, the whole structure showed a tendency to slide away from the feet of the user.

- The timing when the knee is locked and unlocked is crucial. There is a need to develop a mechanism that locks the knee before the foot hits the ground and unlocks it when the opposite foot reaches the ground.

4.1.2 FINAL PROTOTYPE

After a series of prototypes and many design revisions, the final prototype was built. The researcher decided to undertake the complete responsibility in creating such prototype. The University of Ottawa offers a student machine shop equipped with basic manufacturing machines. The researcher was already familiar with all the equipment offered and had the knowledge required to create most parts. Note that the precision of the researcher on all the machines does not come close to the precision achieved by technicians. Tolerances values were measured to vary between 5 mm. Thus fit between parts are not of highest quality. The following list unveils the manufacturing steps and modifications of the final CAD model taken to create the final prototype.

- All parts described as aluminium plates were created in three steps. First step, the outline of each part was printed on paper from the CAD model. Second step, the outlines were taped to a large plate of specific thickness and cut to the desired shape via a vertical band saw. Third step, all holes on the parts were drilled using a drill press.

- All parts described as aluminium or HDPE blocks were created in four steps. First step, larger blocks were cut into blocks of desired length, depth and width. Second step, the 3 standard views of each parts were printed and taped on the small block. Third step, a vertical mill and four flute mill end were used to shape the block into its final shape. Fourth step, drill bits were used on the milling machine to create all the holes needed.

- There are a few aluminium parts that needed to be bent. The two main ones are the two square tube of the SFU (SFU-01). The bending of these pieces was done under heating conditions and using a guide piece shown by Figure 4-3. The starting piece in the process was a 3 feet long square tube. The ends of the workpiece were closed with wood inserts. Beforehand, sand was compacted inside the square tube in order to preserve the structural shape of the workpiece when it is being bent. One end of the square tube was securely fixed on a bench vise. An aluminium tube of 12 inch outer

diameter was placed under the work piece and acted as the guide piece. The workpiece was continually heated using a propane torch. The workpiece was manually wrapped around the guide piece until reaching the desired curvature. The extra lengths of the workpiece were cut on the vertical band saw.

Figure 4-3: Photograph of curved square tube and guide piece.

- A Tungsten Inert Gas (TIG) welder was used to weld aluminium parts together. It was used to fix the two safety handles of the SFU (SFU-05) to their respective holding blocs. It was also used to fix the curved back support plate of the FPU (FPU-03).
- The KJU shown in Chapter 3 was directly inspired by an existing product: the Wedge Lock System Cable Knee Joint by Otto Bock (Duderstadt, Germany) as shown by Figure 4-4. A decision was made to simply acquire the product as used on the final prototype in order to save time. Two knee joints were received from the company with the direction of using them solely for research purposes.

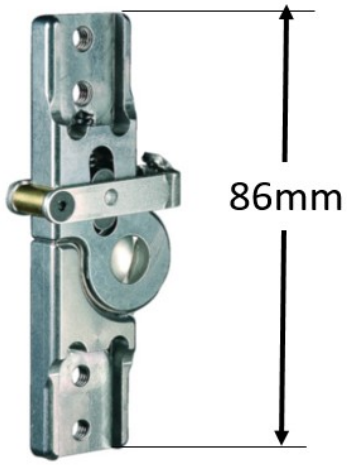

Figure 4-4: Otto Bock Wedge Lock System Cable Knee Joint (taken from Manufacturer's website).

- The trigger cable presented in Chapter 3 was removed from the final prototype. Instead, a rigid cable was connected to the locking arm of each Otto Bock product. Preliminary tests on the final prototype revealed the difficulty of selecting the proper length of polyamide filament and compression spring to disengage the knee joint. For testing purposes, it was much easier to achieve manually by pulling on a rigid cable.
- A ball joint linkage shown by Figure 4-5, was purchased and used to create the ankle joint at the FPU. Machining a ball and socket assembly represents a time consuming challenge. The part was welded to the FPU using a Metal Inert Gas (MIG) welder.

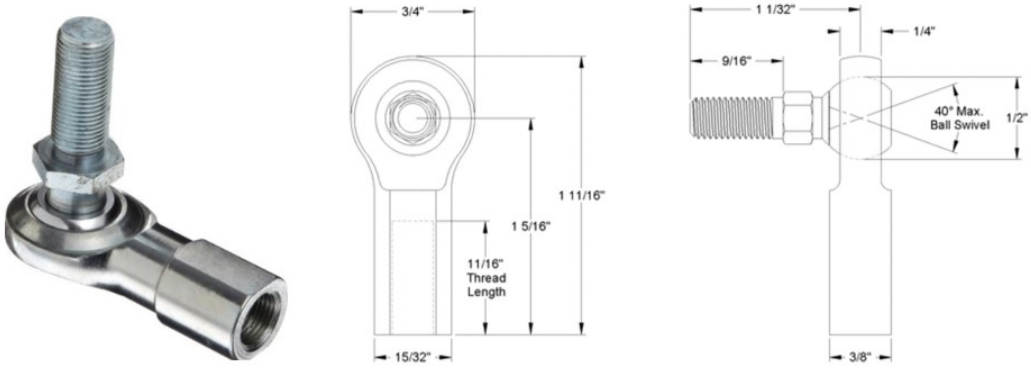

Figure 4-5: Ball Joint Linkage. Supplier: McMaster Carr.

- Pulleys of the HJU (HJU-06 and HJU-07) were made using a lathe. A large aluminium rod was reduced to the needed outer diameter using a cutting bit. Then, a 3 mm cut off blade was used to create the middle cavity and cut away the pulley from the initial stock rod.

- The wire rope in the EWU (EWU-02) was purchased and cut to its needed length using a cable cutter. Swage sleeves were used to create a loop on the ends of the wire rope as shown by Figure 4-6. One end loop was inserted in the front slot of the SFU and the second loop end was hooked to the extension spring end. A total of 6 hook type extension spring were purchased and used on the device.

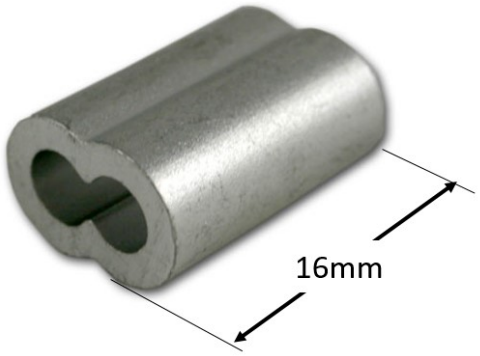

Figure 4-6: Photographs of swage sleeve on wire rope

- Snowshoe bindings were purchased in order to retrieve the ratchet buckles and ladder straps mechanisms. These parts were bolted to the two FPU.

- All the fasteners and bushings needed were acquired based on the specifications given in Chapter 3.

The final prototype has a total mass of 6.18 kg and is shown by Figure 4-7.

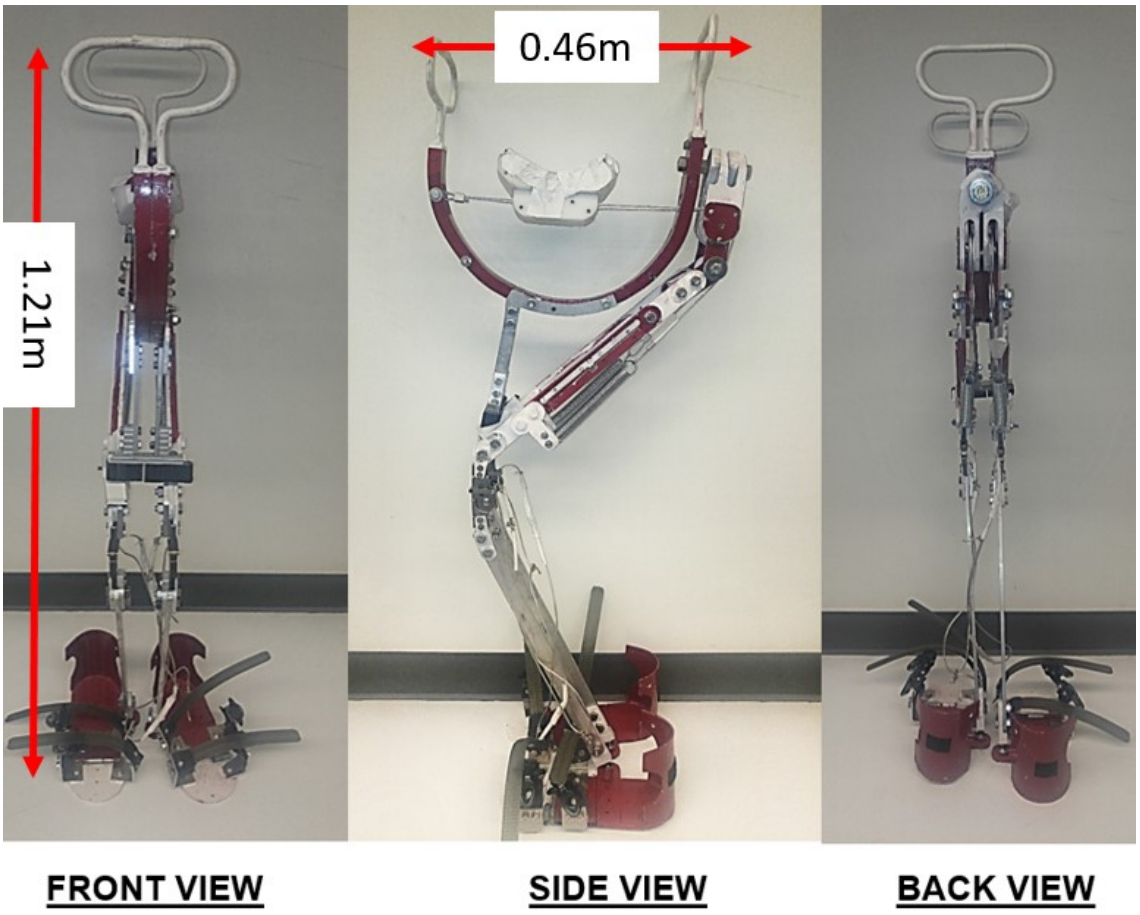

Figure 4-7: Photographs of final prototype. Front view shot (left), side view shot (center) and back view shot (right).

4.2 EXPERIMENTAL SETUP

The final prototype was built with the intention to test two specific parameters. First, the assistance at midstance provided by the seat mechanism needed to be measured in order to evaluate the performance of the exoskeleton. Second, the kinematics of someone using the device needed to be recorded in order to determine if their gait pattern is altered.

4.2.1 LOAD CELLS

Initially, there was a desire to use pressure sensors on the SU interface in order to directly measure upward force. Such approach was found to be very challenging due to the lack of appropriate surface required for sensors placement and wiring. Instead, an indirect measurement approach was considered. In the modelling sections of Chapter 3, it is revealed that the action of the EWU and SU would produce a specific set of loading conditions at the SLU. In order words, the values of F_{AXIAL} and F_{SHEAR} can be related to the action of the SU and EWU of producing $F_{USER\ Y}$ and $F_{USER\ X}$. By measuring loads at the SLU, recorded values can be compared with the computed values of F_{AXIAL} and F_{SHEAR} presented in Table 3-14 and Table 3-17.

Two RB-Phi-204 500 kg s-type load cell were purchased and used to measure the value of F_{AXIAL} on each SLU. One load cell was placed on each SLU near the ankle joint. Based on the FBD shown in Figure 3-24 and Figure 3-31, there is only a compressive and shear load at the ankle joint when standing and walking with the device. The RB-Phi-204 is a sensor based on the Wheatstone bridge sensor arrangement and that can only detect axial strain. Figure 4-8 and Table 4-1 reveal and detail the load cell used.

Figure 4-8:. Photograph of RB-Phi-204 500 kg s-type load cell.

Table 4-1: Specifications of RB-Phi-204 500 kg s-type load cell.

Description	Value (s)
Dimensions	H-76mm, W-51mm, t-26mm
Weight	603 g
Weight Capacity Max	500 kg
Output Impedance	350
Supply Voltage	5-12V
Material	Alloy Steel
Cable Length	3 m

Axial strain is detected by reading the voltage difference across strain gauges in the sensor. Since, those voltage differences are so small, their signals required amplification. An Arduino Uno 3 microcontroller was used to power and collect voltage readings from the two sensors. A RB-Onl-38 was connected to the Arduino Uno 3. The RB-On-38 is pre-assembled board intended for load cell reading using an Arduino. It incorporates an AD8426 amplifier and a low pass 2^{nd} order Bessel filter. After wiring everything according to the provided specification, a programming code is uploaded on the Arduino board via an integrated development environment (IDE). Values from 0 to 355 are displayed on the serial monitor of the Arduino IDE. Both load cells were calibrated using selected weights to convert numerical reading values to force values. The Arduino programming code, wiring documentation and calibration plots can be found in APPENDIX A.

The two SLU of the final design needed to be altered in order to accommodate the two load cells. Two adaptors were built and placed at the top and bottom part of each load cell via two threaded rod. The remaining length of the SLU were once again made of aluminum plate. The weight of new SLU corresponds to 793.17g. The CAD model of the modified SLU can be found in APPENDIX A. Figure 4-9 presents the modified SLU.

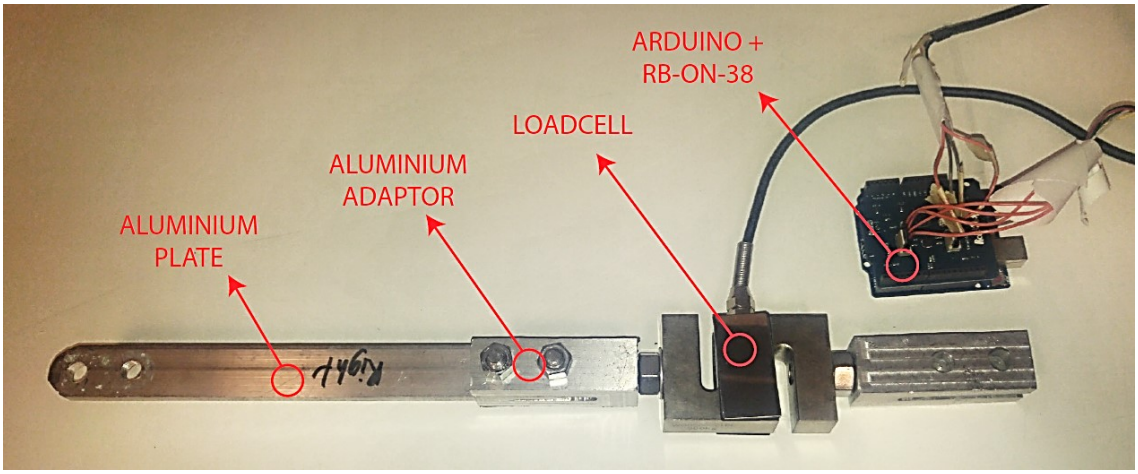

Figure 4-9: Photograph of modified SLU with loadcell along with identified parts.

4.2.2 MOTION CAPTURE

Motion capture system was used to record the motion of the user and final prototype when standing and walking. The Gait Laboratory at the Mechanical Engineering Department at the University of Ottawa is equipped with 16 OptiTrack V100:R2 infrared cameras that detect the motion of reflective markers through time. Table 4-2 details the general specifications of the infrared cameras.

Table 4-2: Specifications of OptiTrack V100:R2 infrared cameras.

Property	Value
Frame Rate	25 -100 Hz
Resolution	0.3 MP (640 × 480)
Shutter Speed	1 ms
Latency	10 ms
Operating range	15 cm – 6m
Input / Output	USB 2.0 Hi-speed
Accuracy	2D sub millimeter

During testing, the capture rate was set at 100 Hz. For each testing session, the cameras were calibrated using the calibration wand and L-shape position frame provided by the manufacturer. Motive (Natural Point Inc, USA) was the software package used to record and process data. The 14 mm X-base reflective marker by OptiTrack were used. A total of 10 reflective markers were placed on the user and on the device for each side (left and right). Marker placement matches what was presented in the walking modelling section, as shown in

Figure 3-25. Table 4-3 describes marker placement, while Figure 4-10 reveals the position of each reflective marker for the right side. Note that in Figure 4-10, marker BASERIB is hidden by the right arm of the user.

Table 4-3: Market set placement description.

Marker ID	Placement
BASERIB	On base of rib cage
HIP	On femoral trochanter
KNEE	On lateral femoral condyle
ANKLE	On lateral malleolus
HEEL	Placed on back support plate of FPU And aligned with calcaneus
TOE	Over 2nd meta-tarsal head
EXOSEAT	Above attachment bolt of SFU
EXOHIP	Over center of rotation of HJU
EXOKNEE	Over center of rotation of KJU
EXOANKLE	Align with ankle joint of FPU

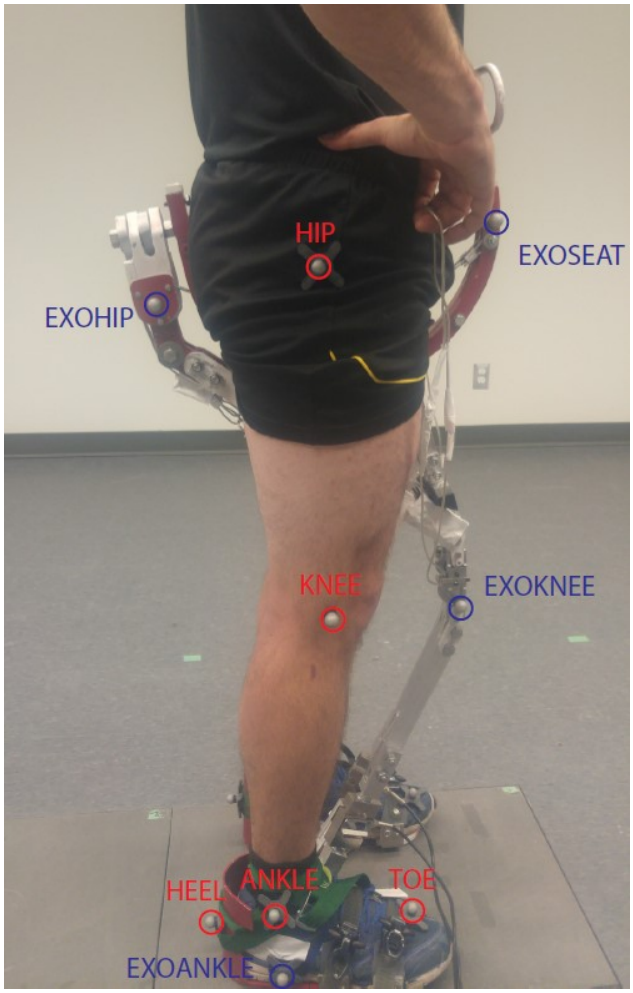

Figure 4-10: Photograph of user standing with exoskeleton with identified markers.

Hip, knee and ankle kinematics were found by analyzing the position of the red circled markers in Figure 4-10. The gait model proposed by D. A. Winters was again used as reference in the determination of gait kinematics. Note that, the HEEL marker is not placed directly on the shoe of the user. It was placed on the back support plate of the FPU (FPU-03). In terms of filtering, a 2nd order low pass Butterworth filter with a cut off frequency of 10 Hz was applied to every trial. Such filtering value corresponds to a medium level of filtering [69]. Recording and processing of data was done in Motive. Each trial was exported as a C3D file and imported in MATLAB to determine gait kinematics. The MATLAB script used to determine gait kinematics is found in APPENDIX B. The open source program Cool Term was used in order to sync the Arduino with Motive via start trigger.

4.2.3 FORCE PLATES

The Gait Laboratory is also equipped with two Bertec FP4060-07 forces plates. The two devices were used to measure GRF. The force plates are flush with the floor and placed next to each other. Each force plate is connected to an AM6800 amplifier and interacts directly with the Motive software. During trial, the participant was instructed to hit the force plates with their right leg. It is how the starting point (heel strike on force plate #1) and ending point (heel strike on force plate #2) of gait are identified. The values of GRF about the sagittal plane were plotted for each trial in order to determine if any differences between using and not using the final prototype. Note that GRF force readings were not normalized according to the weight of the user, because testing only considered a single participant. The sampling frequency was set to 1000 Hz. Figure 4-11 shows the two force plates and the L-frame. The L-frame sets the position of the origin and defines the system of coordinates.

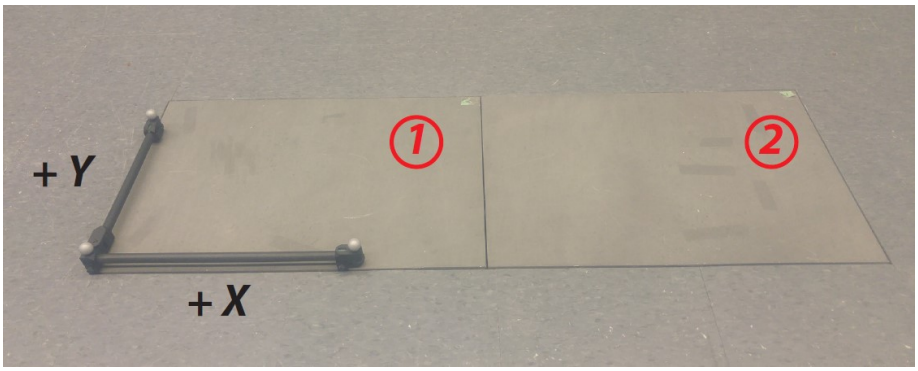

Figure 4-11. Photograph of two Bertec force plates with the L-frame.

4.2.4 EXTENSION SPRINGS

The sole variable that changed between trials was the extension spring of each EWU. From the modelling section, a stiffer spring implies a greater assistance to the user. A total of 6 hook type extension springs were used on the final prototype and are presented in Table 4-4. All springs were initially pre-tensioned when being placed on the exoskeleton in order to keep the SU stable. Such action corresponds to the value of $\Delta L_{INITIAL}$ in Table 4-4.

Table 4-4: Specifications of 6 extensions spring used for testing.

ID	Manufacturer	OD	Total Length	K_{SPRING}	$\Delta L_{INITIAL}$
	(Product Number)	(inch)	(inch)	(N/m)	(cm)
01	CAMPI SPRING, No 803	0.75	6.25	580	2.00
02	Century Spring, No C263	0.875	6.00	680	2.60
03	Gardner Spring	0.640	6.00	970	2.40
04	Gardner Spring	0.730	6.00	1317	2.40
05	CAMPI SPRINGS, No	0.75	6.00	1734	2.30
06	CAMPI SPRINGS, No	0.875	6.00	3327	1.40

4.3 METHODOLOGY

The University of Ottawa requires an applications form for ethics approval for all testing involving humans. The application form is reviewed and approved by the Office of Research Ethics and Integrity. The application form for this study is found in APPENDIX C. A total of 6 test sessions were conducted with the final prototype. At each test session, standing and walking were tested for two conditions: 1) no use of exoskeleton and 2) use of exoskeleton. For condition 2), the spring in the EWU was modified between each test session. The following methodology was developed in order to achieve uniformity among test session and to facilitate comparison.

1) Prepare Gait Laboratory
    a) Turn on computer and open Motive. Turn on force plate amplifier.
    b) Calibrate cameras using calibration wand.
    c) Set origin by placing L-frame on force plate.
2) Prepare Participant
    a) Participant changes into motion capture suit. Wear provided sneakers.
    b) Reflective markers are placed on anatomical landmarks.
3) Record Walking Condition
    a) Participant instructed to practice gait stride across the laboratory for 5 minutes at most comfortable speed.

b) Record walking stride of participant. Ensure that participant hits the two force plates with their right leg.

c) Repeat process two times.

d) Participant instructed to walk with slower speed in order to replicate elderly gait (15 min).

e) Record 3 trials.

4) Prepare Final Prototype

a) Select spring for testing. Attach one end of spring to the TLU via a bolt. Attach second end to the loop of the wire rope.

b) The KJU is unlocked and the prototype is placed between the participant's legs.

c) Participant's foot securely attached to FPU by ratchet buckles and ladder straps.

d) Participant lifts upper part of device using two safety handles on the SFU. Participant lifts device until the SU is placed under the groin region and both KJU's are locked.

e) Participant gets familiarized with the device by performing few gait strides. At any sign of discomfort, participant re-adjusts the SU for better comfort. The practice period is 20 minutes.

5) Prepare Load Cells

a) Open Arduino IDE and open Cool Term program.

b) Sync Motive and Arduino IDE.

c) Test if trigger works by pressing run.

6) Record Standing Condition

a) Participant stands on one force plate. Participant ensures both TLU's are in contact with the RSU and feet are evenly apart.

b) Record 3 standing trial for both legs.

c) Participant ask to unlock left KJU and stand only on right leg.

d) Record 3 standing trial for single leg.

7) Record Walking Condition

a) Participant instructed to practice walking stride in order to hit two force plates with right leg.

b) When ready, record 3 walking trials.

8) Data Processing

a) Performing filtering on motion capture and force plate data.

b) Export motion capture data as C3D and export load cell data as text file.

c) Run MATLAB script.

4.4 MANUAL TESTING

Prior to human testing, a few manual tests were conducted on the device alone. The first objective of such tests was to further validate that the combined action of the EWU and SU was directly related to the loading conditions at each SLU. By manually lowering the SU, it is expected that the tension in the EWU increases and that F_{AXIAL} at the SLU proportionally increases. The use of a stiffer spring should result in greater values of F_{AXIAL}. The second objective with manual testing was to ensure that all testing apparatus operated properly.

Figure 4-12 shows the researcher conducting a manual test on the final prototype. During a manual test, the final prototype was placed over one force plate. Both KJU were locked and the RSU was placed on both TLU. The device was maintained upright by holding on the SU. Two reflective markers were placed on the side of the SU. Two reflective markers were placed on each EWU. One marker was placed over the attachment point on the TLU. The other marker was taped to the extension spring end. When recording started, the researcher gradually applied a downward force on the SU in order to lower it. The researcher continued this action until reaching maximum vertical displacement possible. The applied downward force action is to mimic $F_{USER\ Y}$ and analyse system behaviour.

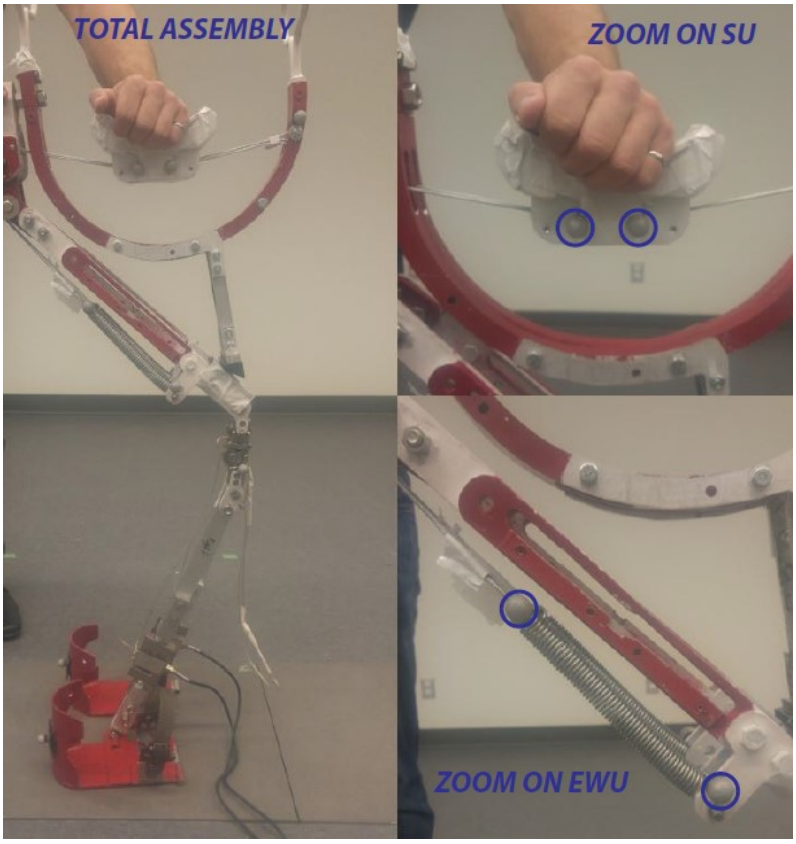

Figure 4-12: Photograph of manual test. View of total prototype (left). View on SU unit (top right) and view on right EWU (bottom right).

The value of ΔY_{SEAT} was computed by subtracting the vertical position of the reflective markers placed on the SU with their starting vertical position. The value of ΔL_{SPRING} was calculated by subtracting the distance between the two markers placed on each EWU with the initial distance. Figure 4-13 reveals the values of ΔY_{SEAT} and ΔL_{SPRING} for conducting a manual test on spring #1.

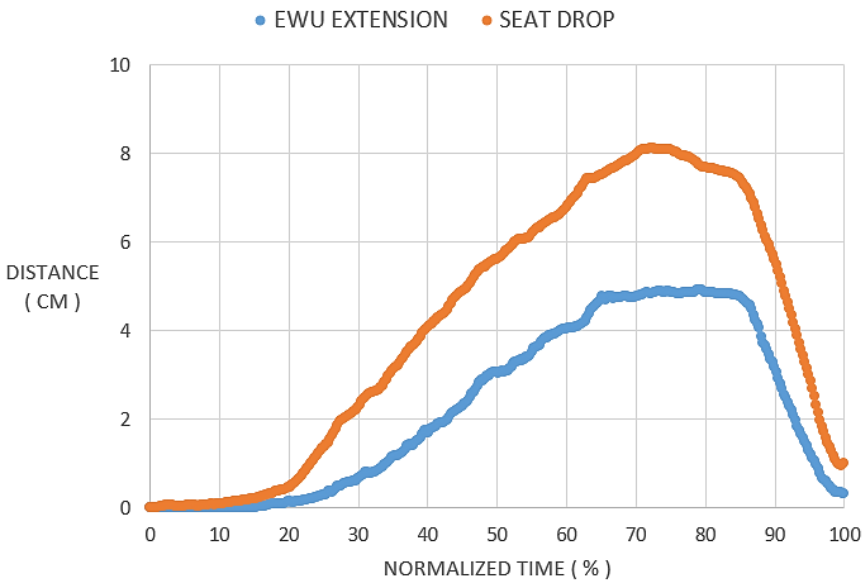

Figure 4-13: Values of ΔL_{SPRING} and ΔY_{SEAT} for manual test on final prototype using spring #1.

Figure 4-13 reveals that lowering the SU resulted in a direct increase of ΔL_{SPRING} values. For spring #1, the SU was lowered by 8 cm which resulted in a EWU extension of 5 cm. The value of ΔL_{SPRING} closely matches what the standing model predicts. Thus, the geometrical relationship between ΔL_{SPRING} and ΔY_{SEAT} is valid. A similar profile was found for the remaining 5 springs. Their results can be found in APPENDIX C. There is one significant difference observed for spring #5 and spring #6. The SU was only lowered by 2.5 cm due to the very high resistance provided by their EWU. While the SU was lowered, the two load cells measured F_{AXIAL} on each support leg. The force plate measured the vertical component of GRF. Figure 4-14 reveals load cells and force plate readings for the manual test using spring #1.

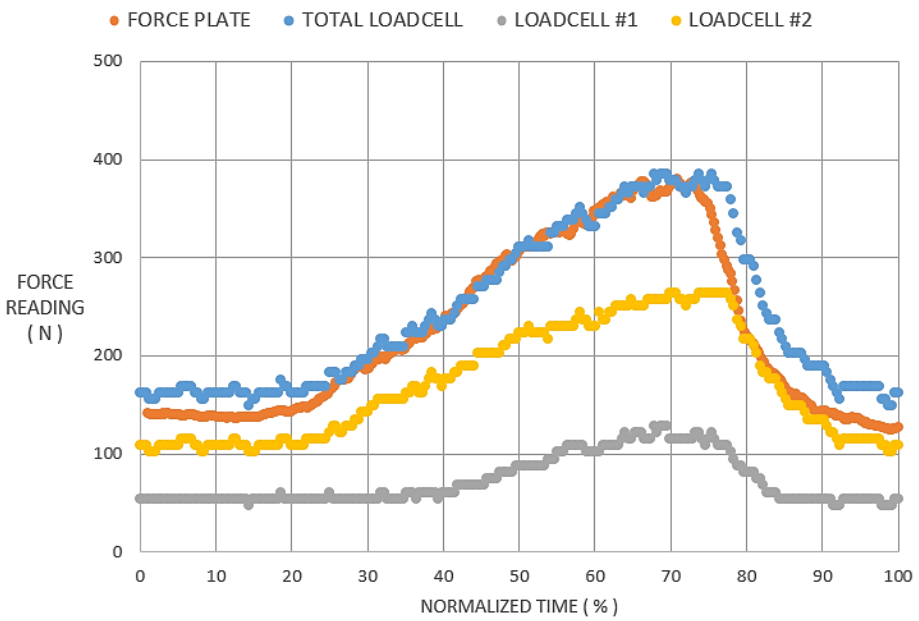

Figure 4-14: Force reading of lodcells and force plate versus normalized time for manual test using spring #1.

In Figure 4-14, the force readings of the load cell placed on the right SLU correspond to the LOADCELL #1 entry. The force readings for the left SLU correspond to the LOADCELL #2 entry. The TOTAL LOADCELL entry is the sum of the two load cell readings. Figure 4-14 shows that lowering the SU increased both values of F_{AXIAL}. At maximum ΔY_{SEAT}, the combined value of F_{AXIAL} corresponds to 390 N. Note that the value of LOADCELL #1 and LOADCELL #2 are not identical. During the manual test, it was observed that the left support leg was longer in length. Thus, the RSU rested mostly on the left TLU which implies more load was transferred to the left support leg. The profile of vertical GRF (FORCE PLATE entry in Figure 4-14) matches TOTAL LOADCELL which is expected. Similar plots were acquired for the remaining springs with a trend that a stiffer spring yield a higher value of total load sharing (see APPENDIX C for plots). All the data collected from manual trials was compiled on two plots to show the relationship between the total value of F_{AXIAL} (both left and right load cells) versus the recorded value of ΔY_{SEAT} and ΔL_{SPRING}. Figure 4-15 and Figure 4-16 represent the outcomes of such compilation process.

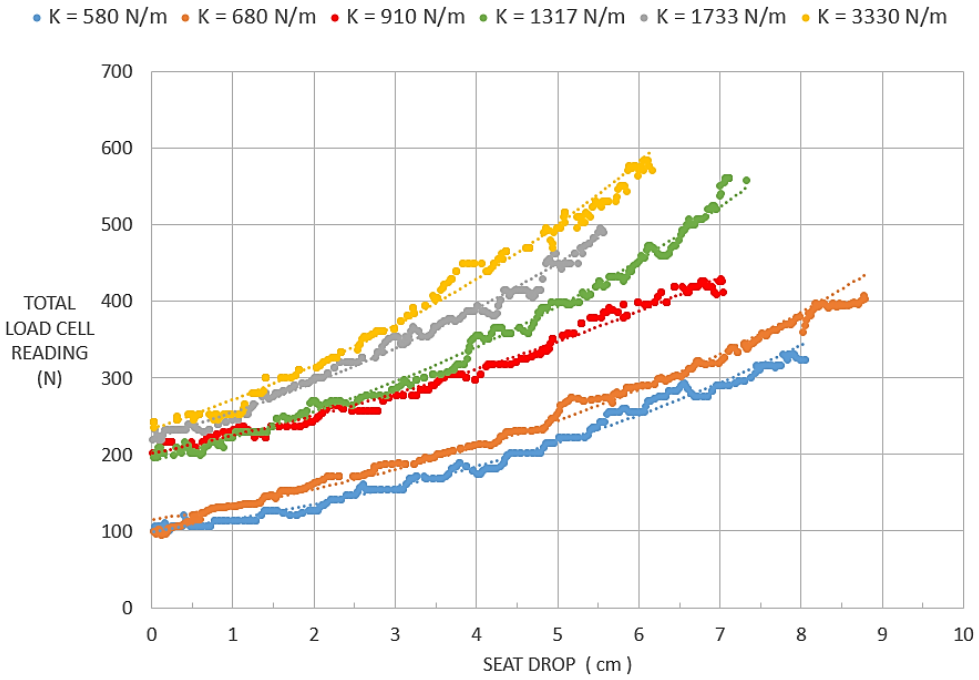

Figure 4-15: Total value of F_{AXIAL} versus ΔY_{SEAT} for manual tests using 6 different springs.

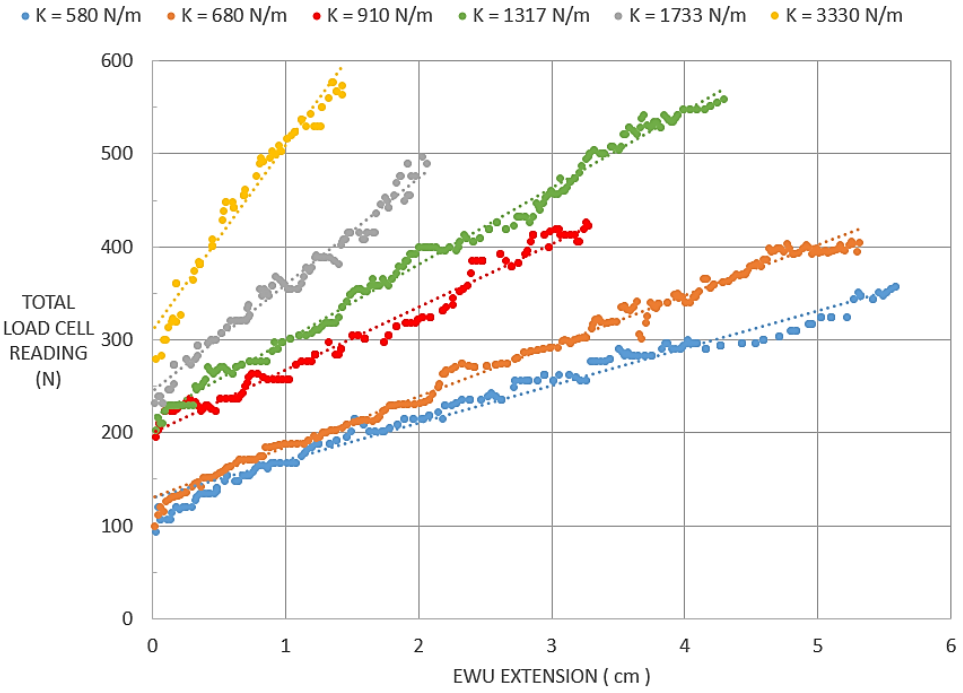

Figure 4-16: Total value of F_{AXIAL} versus ΔL_{SPRING} for manual tests using 6 different springs

Figure 4-15 shows that for the same value of $\Delta Y_{SEAT,}$ a stiffer spring yields to a higher a value of total F_{AXIAL}. Such relationship was expected and correlates well with the results from

modelling the device in standing (see Figure 3-19). Note that values of F_{AXIAL} for use of spring #5 and spring #6 were found to be lower than their expected values. With those springs, the researcher had a difficulty lowering the SU, because the resistance of the two EWU's was much greater than with using the first 4 springs.

Figure 4-16 reveals that there is a linear relationship between ΔL_{SPRING} and F_{AXIAL} which was expected from modelling the seat mechanism. For the same value of ΔL_{SPRING}, a stiffer spring generates a greater value of F_{AXIAL}. Therefore, the approach of assessing the assistance provided by the seat mechanism via the measurement of F_{AXIAL} is valid. In short, if a stiffer spring yields to a greater value of F_{AXIAL}, then one can conclude that a greater upward force is felt at the SU interface.

During manual test, friction was felt at three locations when lowering the SU. First location of friction was at the pulleys which did not act as frictionless when the SU was lowered. Second location of friction identified was on the back slot of the SFU (see Figure 3-8) where both wire ropes rubbed when the SU was lowered. The third location of friction was in the inner grooves of the SU where the two wire ropes pass through. The SU did not slide smoothly forward and backward when the SU was lowered. Friction effects were more noticeable for higher stiffness springs.

CHAPTER 5: TESTING RESULTS AND DISCUSSION

Chapter 5 presents testing results of standing and walking with the exoskeleton. For both conditions, the results acquired by load cells and motion capture technologies are illustrated. Also, experimental results are compared to analytical model in order to discuss if the WAE behaved as predicted. All observations and comments made by the participant when using the device are also stated as they help in qualitatively characterising the final prototype.

5.1 STANDING RESULTS

During standing trials, for each spring three values of F_{AXIAL} were measured by each load cell. The value of F_{AXIAL} corresponds to the axial load acting on the ankle joint of the exoskeleton. The value was computed in both standing and walking model. The values of F_{AXIAL} among the three trials were very close to each other. Therefore, all the data presented in this section was averaged over the three trials. Table 5-1 reveals the experimental values of F_{AXIAL} recorded by the two load cells when standing on the device.

Table 5-1: Average values of F_{AXIAL} recorded during standing trials.

Spring ID	K_{SPRING} (N/m)	**Right** F_{AXIAL} (N)	**Left** F_{AXIAL} (N)s	**Total** F_{AXIAL} (N)	F_{AXIAL} **% error** (%)
1	580	87	166	253	9
2	680	94	206	300	10
3	970	95	264	359	3
4	1317	100	355	455	2
5	1734	82	412	494	11
6	3327	199	371	571	43

In Table 5-1, the value of total F_{AXIAL} is the sum of the two load cell readings. The value of F_{AXIAL} % error was computed by comparing experimental value of F_{AXIAL} with value of modelling section Table 3-17. In Table 5-1, value of total F_{AXIAL} increases as a stiffer spring is used which was expected. A greater value of F_{AXIAL} implies that a greater upward force is expected at the SU interface. A distinguishable increasing upward force was felt by the participant when using a stiffer spring. Similarly, to the results of manual tests, greater values of F_{AXIAL} were recorded on the left SLU versus on the right SLU. Again, such result reveals that the compressive load at the RSU is not equally distributed on the two TLU's. The values of total F_{AXIAL} for the first four spring are above their modelling values. Thus, the values of upward assistance at the SU should also be in close range of what the standing model predicts. The use of spring #5 and spring #6 yielded values of F_{AXIAL} below what was predicted. Such a result may be explained by major discomfort felt by the participant. The pressure felt at the SU interface when standing on the device could not be tolerated for more than 10 minutes without a readjustment or removal of the device. Standing on the device with spring #5 and spring #6 gave pressure levels well above the participant tolerance. Such a result was predicted

by the expected value of P_{SEAT} in the standing model (see Table 3-13). In contrast, the user was able to stand on the device for more than 15 minutes without the need of readjustment when using the first 4 springs.

In the standing model, the angle of each SLU about the sagittal plane (θ_{SLU}) was 75º. During testing, it was visually apparent that the final prototype appeared to be tilted forward meaning that values of θ_{SLU} were lower. Motion capture was used to acquire the values of θ_{SLU} for both SLU when standing on the device, the values are presented in Table 5-2.

Table 5-2: Average θ_{SLU} values for standing trials.

Spring ID	K_{SPRING} (N/m)	**Right** θ_{SLU} (º)	**Left** θ_{SLU} (º)
1	580	68	70
2	680	68	69
3	970	70	71
4	1317	70	72
5	1734	65	65
6	3327	60	61

Table 5-2 reveals that the final prototype position was tilted forward compared to the model. Thus, the actual value of ΔY_{SEAT} and F_{AXIAL} are expected to be lowered. To adjust the standing model for a different value of θ_{SLU} implies to repeat a geometrical analysis and kinetic analysis. The use of the first 4 springs yielded a forward tilt of the exoskeleton of about 5º. Note that, variation among the first 4 θ_{SLU} values can be attributed to a different fit of the device. During testing, it was measured that the horizontal position of the SU with respect to the remaining units on the exoskeleton varied ±5 cm. For springs #5 and #6, θ_{SLU} values are higher than for the first 4 springs which implies that the exoskeleton was further tilted forward. Consequently, the theoretical values of F_{AXIAL} are expected to be much lower than to those presented in Table 5-1. The final measurement considered for standing trials was the value of $\Delta Y_{SEAT.}$ This value was found by measuring the position of the SU with the floor before and after standing on the device. The average values of ΔY_{SEAT} for standing trials are presented in Table 5-3.

Table 5-3: Average values of ΔY_{SEAT} for standing trials.

Spring ID	K_{SPRING} (N/m)	ΔY_{SEAT} (mm)	% Error ΔY_{SEAT} (%)
1	580	87	3
2	680	89	1
3	970	89	1
4	1317	87	3
5	1734	53	41
6	3327	56	38

When the device was modelled, the expected value of ΔY_{SEAT} was 9 cm. Table 5-3 shows that the first 4 springs are in close range of the expected value. Such result further supports that the standing model provided good estimates of F_{AXIAL} values for the first 4 springs. Interestingly, values of ΔY_{SEAT} were much lowered than 9 cm for spring #5 and spring #6. Based on the behaviour of the seat mechanism, a smaller value of ΔY_{SEAT} implies a smaller value of F_{AXIAL}.

In short, the results of standing trials revealed that the standing model help predict the amount of F_{AXIAL} for the first four springs. The values of θ_{SLU} and the value of ΔY_{SEAT} were both in close range of what was predicted by the model. Thus, the results of the standing model can be used to assess the upward assistance at the SU interface. Another positive outcome for the first springs is that the participant was able to stand comfortably on the device. For the last two springs, an opposite set of conclusion is drawn. All recorded values were lowered than their theoretical values. The participant could not stand comfortably on the device. Such result foresees difficulties using the device when walking. One recurrent observation from the participant was that the FPU needed to be securely attached, otherwise slippage was felt between the feet of the user and the FPU. For all springs, the ratchet buckles and ladder straps on the FPU needed to be highly tightened reaching levels where pressure points were felt by the user.

The following list unveils the source of errors exclusive to the standing condition.

- The vertical position of the SU was measured using a measuring tape as it was difficult to place a reflective marker that would be detected by motion capture cameras. Such way of measuring vertical position implies a reading imprecision.

- The value of θ_{SLU} was computed using the sagittal position of markers EXOKNEE and EXOANKLE. The marker EXOANKLE is not placed directly over the ankle joint of the device due to the small size and position of the ankle joint. Instead, the marker was placed on the lateral side of the shoe and align as best as possible with the ankle joint. Such approach implies that recorded values of θ_{SLU} may slightly be off from their actual values.

- The position of the SU may not have been exactly at the midpoint of the SFU. The participant placed the device at the most comfortable position and did not look to have it centered. By the SU not being centered, it implies that the two wire cables were not tilted with the same angles (θ_A and θ_B) which will change values in the kinetic analysis portion of the standing model.

5.2 WALKING RESULTS

Similar to the standing condition, a total of three trials were recorded when walking with the device for a given spring. It was difficult to average the three trials due to the fact that the user would never walk in the exact same gait pattern. Repeatability of motion when using a WAE is always an issue. To ease data interpretation among springs, only one trial was selected to be presented in the following section. For each spring, the participant was asked to identify the trial where lowest amount of pressure was felt at the SU interface. Spring #6 was omitted from the walking trial given its high stiffness which led to painful discomfort to the user.

5.2.1 LOAD CELLS RESULTS

Throughout the walking trials, both load cells measured the value of F_{AXIAL} in each SLU. Figure 5-1 shows the readings of both load cell versus the GC when walking with the device with spring #3. Note that data points were jointed by lines to illustrate the profile of F_{AXIAL} for a GC.

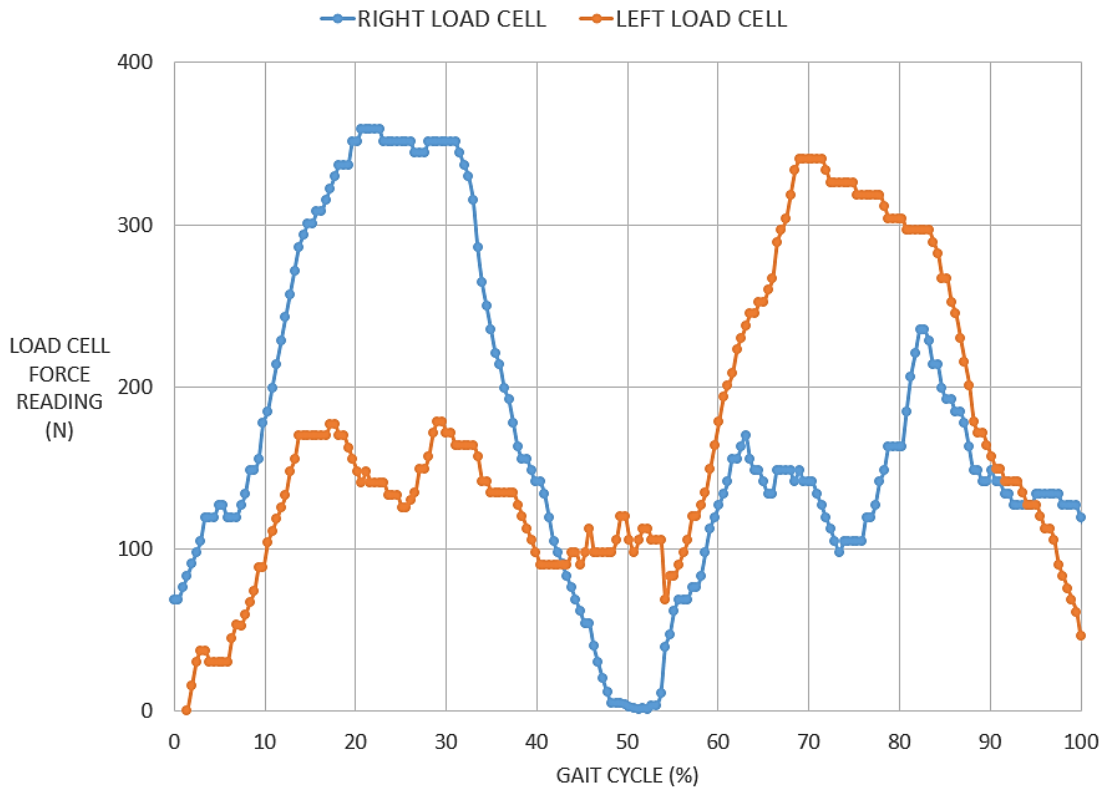

Figure 5-1: Values of right F_{AXIAL} (in blue) and left F_{AXIAL} (in orange) for walking trial with spring #3.

In Figure 5-1, the blue entry corresponds to the value of F_{AXIAL} for the right SLU, while the orange entry corresponds to the value of F_{AXIAL} for the left SLU. During gait, two distinct peaks were recorded. The first peak at 22 % GC for the right load cell and a second peak at 70 % GC for the left load cell. Such behaviour was predicted by the walking model. However, the walking model predicted that those peaks would be found at 20 % and 70 % GC. In case of spring #3, the two peak assistances are close to where they were expected. By comparing the profile of right F_{AXIAL} with the expected plot of the walking model (see Figure 3-28), it is clear that the device did not behave in the predicted manner. The walking model predicted a gradual increase in F_{AXIAL} during loading response until early midstance. A peak value would be reached at 20 % GC followed by a close to linear gradual decrease throughout the remaining of stance. For the second half of the GC, the same profile is repeated, but for the opposite support leg.

In Figure 5-1, there is a linear increase up to 20 %GC before reaching the first high peak value. Next, F_{AXIAL} values remain high and decrease slowly between 20 %GC and 30

%GC. Such behaviour is different than what the model predicted. Afterwards, F_{AXIAL} values decrease more rapidly for the remaining of stance. The slow decrease of F_{AXIAL} values can be attributed to the difficulty in switching support on the RSU between the two TLU's. It is between 20 and 30 % GC that change of support at the RSU between the two TLU's occurred. During testing, it was noticed that such change of support was never done in a rapid manner. The participant would need to load the right support leg to be able to raise the RSU with the left TLU, before changing support. It was also noted that unlocking the KJU rapidly was difficult to achieve. The process took more than few milliseconds. The walking model predicted that the assistance of the device would alternate between the two support legs. Such behaviour is shown in Figure 5-1. The profile of the right load cell for the first half of gait is similar to the profile of the left load cell for the second half of gait. The plots of F_{AXIAL} versus GC for the remaining 4 springs had many similarities. Figure 5-2 reveals the value of right F_{AXIAL} for the 5 different springs.

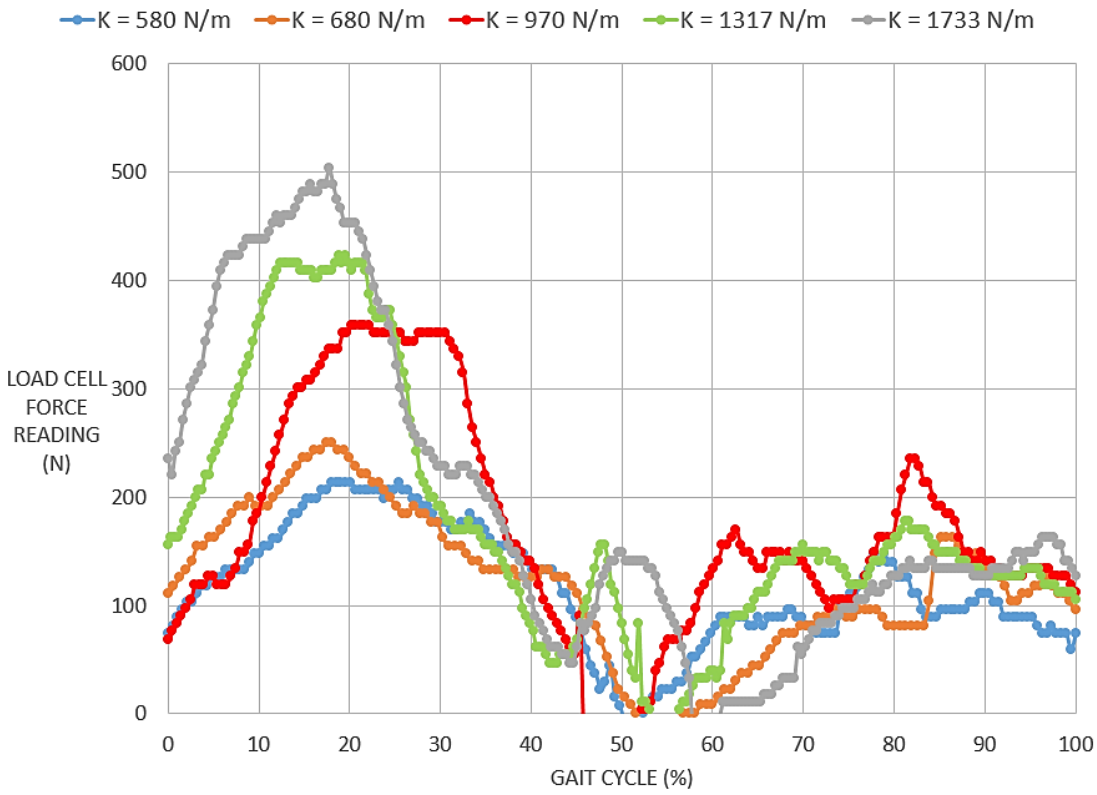

Figure 5-2: Values of right F_{AXIAL} for walking with 5 different springs.

Figure 5-2 reveals the F_{AXIAL} profile varied among the 5 different springs. Such result reflects the fact that the user never walked with the same gait pattern when using the device. In Figure 5-2, there is a peak value of F_{AXIAL} value reached by all springs during midstance. For all springs, F_{AXIAL} value rises in early stance and reaches a peak in midstance. The value of F_{AXIAL} would then slowly decrease for few milliseconds, before decreasing during late stance. For spring #2 and spring #5, values of F_{AXIAL} would rapidly decrease after reaching their peak value. The time at which a peak F_{AXIAL} value was recorded varied between all springs, but that value was always found in midstance. In Figure 5-2, the peak value of F_{AXIAL} increases with the stiffness of spring which was expected. From Figure 5-2, peak value of F_{AXIAL} were found along with their time of occurrence in the GC. The findings are presented in Table 5-4.

Table 5-4: Peak value of F_{AXIAL} for walking trials using 5 different springs.

ID	K_{SPRING}	Peak time	Peak F_{AXIAL}	% Error F_{AXIAL}
	(N/m)	(% GC)	(N)	(N)
1	580	18	229	8
2	680	19	257	1
3	970	21	358	4
4	1317	20	434	9
5	1733	18	503	16

The walking model predicted the peak value of F_{AXIAL} to occur at 20 % GC. Table 5-4 reveals that only spring #3 and spring #4 recorded peak F_{AXIAL} values at 20 % GC. When the value of K_{SPRING} is increased, value of F_{AXIAL} also increases. By comparing last two columns of Table 5-4, one can notice that peak values of F_{AXIAL} are within range of their theoretical values for first 3 springs. Such results reveal that the walking model provided good approximation of the F_{AXIAL} value. Note that the use of spring #5 has the greatest difference between its experimental and theoretical value of F_{AXIAL}. During testing, the participant repeatedly reported high levels of pressure at the SU interface that required constant re-adjustment and/or removal of the exoskeleton. The walking model predicted that the value of θ_{SLU} would be 81º at 20 % GC meaning that the exoskeleton is slightly tilted backwards in comparison to its standing position. Motion capture recorded the value of right θ_{SLU} at their peak time and the results are presented in Table 5-5.

Table 5-5: Values of right θ_{SLU} for walking trials using 5 different springs at peak value of F_{AXIAL}.

ID	K_{SPRING}	Peak time	Right θ_{SLU}
	(N/m)	(% GC)	(º)
1	580	18	71
2	680	19	69
3	970	21	72
4	1317	20	67
5	1733	18	66

The walking model predicted that the expected value of θ_{SLU} at peak assistance is 81º. Table 5-5 reveals that the device was tilted forward instead of being tilted backward as predicted. The value of right θ_{SLU} was different among all 5 springs. For the first 3 springs, the

difference between theoretical and experimental value of θ_{SLU} is about 10º. The difference is about 15º for last two springs.

5.2.2 GAIT KINEMATICS RESULTS

The motion with exoskeleton during walking was recorded in order to observe if the device hindered the original gait. The leg motion of the user when using the device was compared to two baseline conditions measured using motion capture. The first baseline condition is referred to 'healthy' and corresponds to the natural gait of user when asked to walk at his most comfortable speed. The second baseline condition is referred to 'elderly' and corresponds to the gait of user when asked to replicate an elderly gait (shorter stride and slower walking speed). Table 5-6 presents gait parameters of the walking trials.

Table 5-6: Gait parameters of walking trials.

ID	K_{SPRING} (N/m)	GC Duration (s)	Step Length (m)
Health	-	1.07	1.25
Elderly	-	1.57	0.97
1	580	3.20	0.95
2	680	3.44	0.99
3	970	2.99	0.98
4	1317	3.35	0.89
5	1733	4.85	0.73

In Table 5-6, gait duration was determined by calculating the time between two heel strikes. Step length was calculated by subtracting the position of the HEEL marker at start and end of gait. Table 5-6 reveals that the use of the device reduced step length when compared to the healthy condition. The step length recorded by the first 4 springs is comparable to the elderly condition. For the last spring, stride length is much smaller, which reflects the difficulty experienced by the participant to walk with the device. Gait duration was close to double that of the elderly condition. Such a longer gait duration is attributed to the difficulties of quickly and smoothly transferring support on the RSU and of unlocking both KJU's. Table 5-6 reveals that the gait when using the device is expected to be more similar to the elderly condition. During testing, it was visually apparent that stride length was reduced, ROM for all

joints have decreased and time of double support was increased in comparison to the healthy condition.

The data of reflective markers placed on the participant were processed to determine hip, knee and ankle kinematics about the sagittal plane. After processing all the data, it was quickly noticed that kinematics varied among trials when the device was used, but overall the pattern was similar. For this reason, gait kinematics presented in the following section only show the results for spring #1 and spring #3. This decision was made in order to ease interpretation of plots, otherwise it became hard to discern all trials on the same plot. Kinematics results are presented as curves in order to ease comparison between the two baseline conditions and two spring conditions. Figure 5-3 unveils the results of hip kinematics for spring #1, spring #3 and the two baseline conditions.

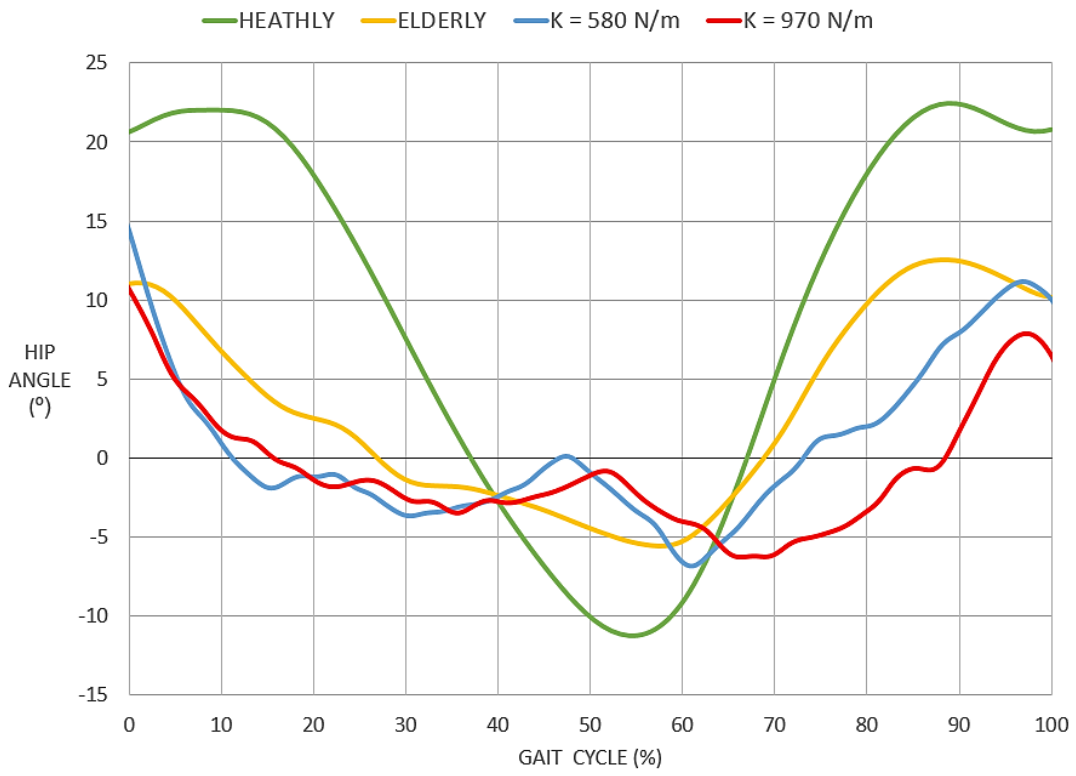

Figure 5-3: Hip angle vs. gait cycle for walking trials with spring #1, spring #3 and for two baseline conditions.

Figure 5-3 reveals that hip motion was obstructed when using the device. Both springs show similar motion during gait. For first 30 % GC, the hip flexes. From 30 to 60 % GC, the hip extends before flexing again until reaching its furthest posterior position. During swing,

the hip mostly extends. Such motion does not match the healthy condition. The ROM of hip for the two spring conditions is about 15 º, while ROM for the healthy condition is 34º. The peak posterior position corresponds to about -6º for the two spring condition versus -12º for the healthy condition. When comparing the two spring conditions with the elderly condition, ROM is about the same, but motion during gait is not the same. For the remaining three springs not shown in Figure 5-3, the same conclusion can be made. The results of hip kinematics for the remaining springs can be found in APPENDIX C. During testing, the participant frequently noticed how the presence of the RSU limited motion at the hip. Since the RSU is always loaded, it is constantly forced to rest on at least one TLU. It created a problem every time the user needed to change support on the RSU. To change support, the user voluntarily needed to lift the RSU in order to switch support which corresponds to the small extension in terminal stance. The results of hip kinematics point to the need to modify the design of the RSU. Instead of having a rigid link stopper, it would be ideal to have a stopper with a varying length to enable the hip to continue flexing during terminal stance. Figure 5-4 unveils the results of knee kinematics for spring #1, spring #3 and two baseline conditions.

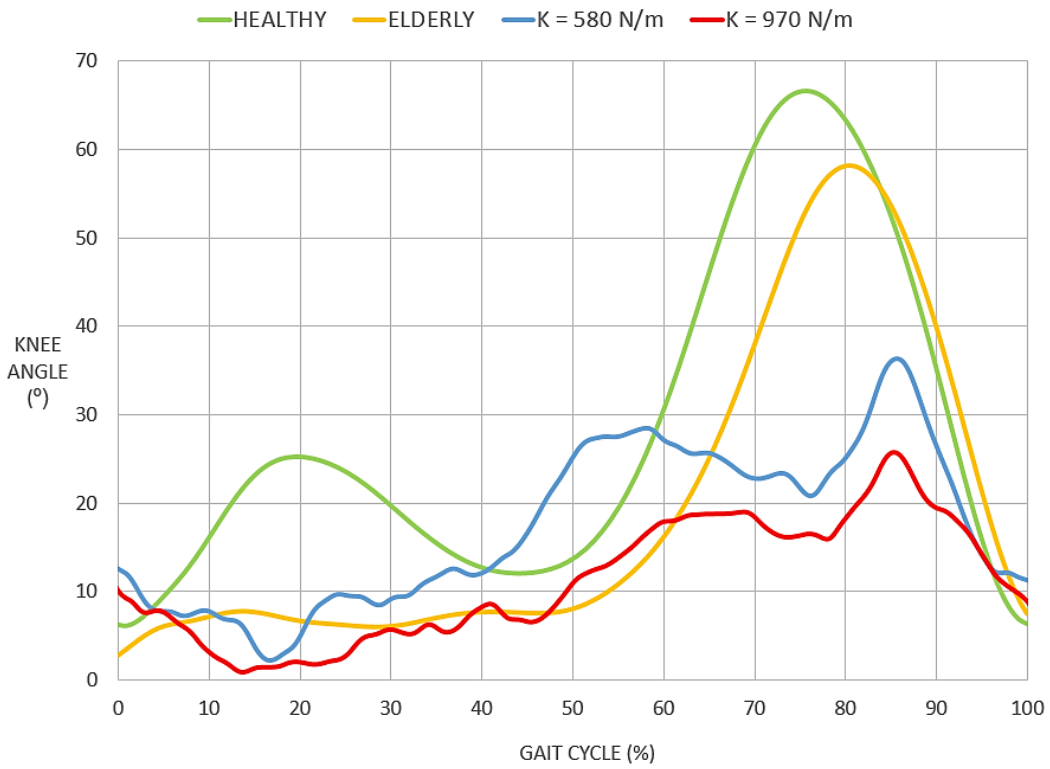

Figure 5-4: Knee angle vs. gait cycle for walking trials with spring #1, spring #3 and for two baseline conditions.

Figure 5-4 shows that the use of the device impeded knee motion. For both spring conditions, knee motion does not match the healthy and elderly condition. When using the device, the knee extends slightly during loading response. For the reminder of stance, the knee is flexing. It is followed by a period where knee angle slightly varies. At the end of mid swing, the knee further flexes and the angle reaches its peak value. In terminal swing, the knee extends. By comparing the condition of spring #1 versus the condition of spring #3, the only observable difference is that ROM is greater for a lower K_{SPRING}. However, such an observation does not hold when considering the remaining three springs, where the knee motion for spring #4 resembles the knee motion of spring #1. The ROM for all spring conditions is well below both healthy and elderly conditions. Figure 5-4 reveals that the KJU design needs to be revised and modified. The implementation of a rigid locking mechanism severely obstructs knee motion. Another relevant observation concerning the KJU is the difficulty of quickly unlocking the KJU manually. Figure 5-5 reveals the ankle kinematics for spring #1, spring #3 and two baseline conditions.

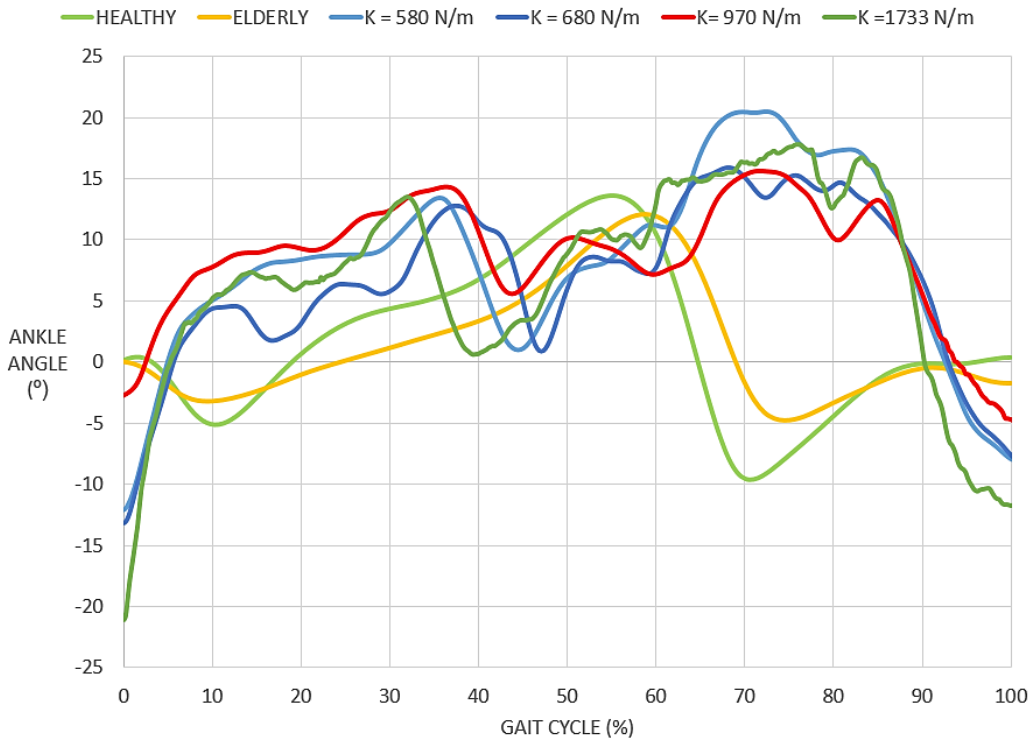

Figure 5-5: Ankle joint vs. gait cycle for walking trials using spring #1, spring #3 and for two baseline conditions.

Figure 5-5 reveals that the user did not move his ankle in the same pattern as the two baseline conditions even though the ankle of the exoskeleton offers full ROM. The most obvious difference between two baseline conditions and two spring conditions is that there is not a clear toe push off near the end of stance. In other words, the user is propelling his foot with less motion. It is expected that power at push off would be much lower. During loading response and midstance, the ankle is mostly dorsiflexing. Next, the ankle reaches a peak angle before producing a plantarflexion. It is at this precise moment that support transfer at the RSU occurs. The participant explained that in order to shift support, he needed to lift his whole body. After such motion, the ankle dorsiflexes again until reaching a second peak value at about 70 % GC when maximum assistance is provided by left support leg of the device. For the reminder of the swing, the ankle is predominantly plantarflexing. Ankle kinematics were observed to have the most variance among all springs in terms of ROM and peak values. One common characteristics for all spring conditions is that they showed the plantarflexing action at about 30 % GC. The remaining results of ankle kinematics can be found in APPENDIX C. Ankle ROM for the two spring conditions surpasses both baseline conditions. Two comments

were noted down during testing. The first comment is that the ladder straps and ratchet buckles on each FPU needed to be tightened with high levels of tensions. The participant felt pressure points on his feet. The second comment is that the ankle joint used on the prototype was too small in size, which created interference between the load cell bracket and the FPU during gait.

5.2.3 GAIT KINETICS RESULTS

The readings of GRF of all walking trials were also processed to plot their distribution. At first, GRF values were not intended to be studied, since their values could not directly assess the mechanical performance of the exoskeleton. After uncovering that gait kinematics were altered from using the device, it was decided to briefly study GRF values to uncover other problems with the current design. The device was modelled assuming that the profile of GRF did not change from using the device. After processing GRF data, it was found that the profile of GRF was altered due to using the device. To ease interpretation, only GRF values for spring #3 are compared to the two baseline conditions. Note that GRF data for the remaining four springs can be found in the APPENDIX C. Figure 5-6 reveals the profile of vertical GRF for spring #3 and the two baseline conditions.

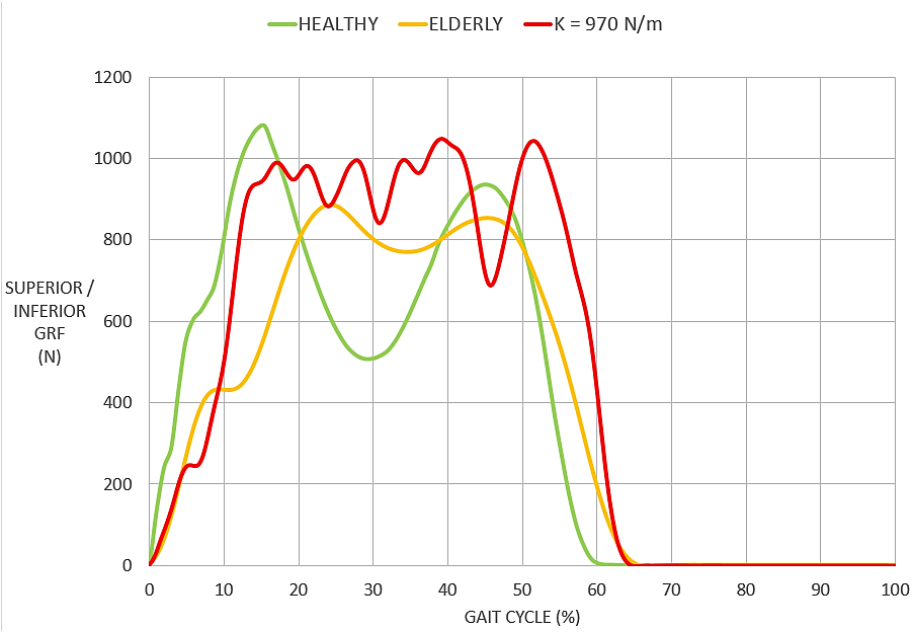

Figure 5-6: Value of vertical GRF vs. gait cycle of walking trial for spring #3 and two baseline conditions.

Figure 5-6 reveals that the vertical GRF profile for spring #3 does not show the butterfly profile of the healthy and elderly condition. There are no clear positive peaks in the GRF at early midstance and end of terminal stance. At loading response, vertical GRF ramps up as expected. During midstance, the value oscillates slightly but without showing a clear peak. During terminal stance at about 40 % GC, there is a downward peak. The same peak is also noticeable for all the remaining springs. The drop in GRF values varies among the 5 spring conditions. It does not increase with values of K_{SPRING}. The drop in vertical GRF matches the instance when the user would raise their body and to complete transfer of support on the RSU. Figure 5-7 presents the values of horizontal GRF for spring #3 and two baseline conditions.

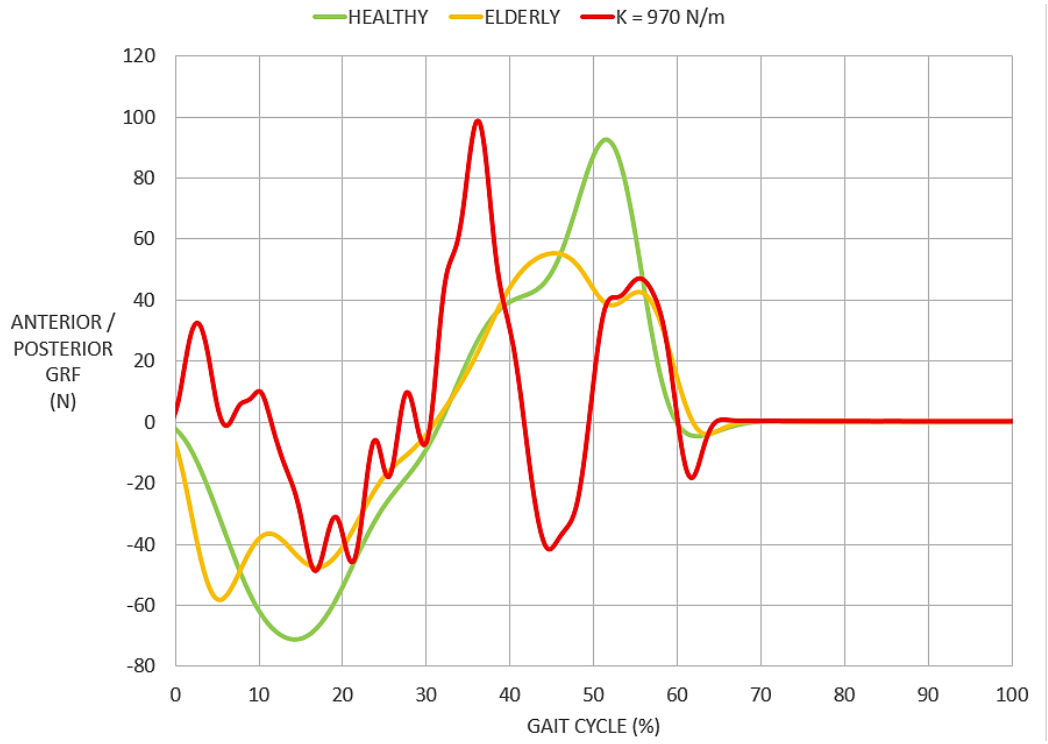

Figure 5-7: Values of horizontal GRF vs. gait cycle of walking trials for spring #3 and for two baseline conditions.

Figure 5-7 shows that the profile of horizontal GRF did not match the two baseline conditions. The healthy and elderly conditions show clearly a braking (negative) action of the foot during the first half of stance and a propulsive (positive) action of the foot for the remaining of stance. For the spring #3 condition, a positive value is found in early part of loading response. It correlates with the excessive dorsiflexion of ankle at beginning of stance. During midstance, there is a shift between a negative and positive value of GRF. At 40 % GC, there is a sudden burst of propulsive force. Such instances matches the plantarflexion action of ankle to raise the whole body and change support on the RSU. For the remaining of terminal stance, the foot creates a second propulsion on the ground in order to propel the right support leg forward. The described profile of horizontal GRF was also observed for the remaining springs. The result of vertical and horizontal GRF reveal the need to redesign the RSU.

5.3 SOURCE OF ERRORS FOR WALKING RESULTS

The following list uncovers the many sources of errors for walking condition.

- Friction was felt at three specific positions on the device which might impede on the spatial displacement of the SU and extension of the EWU. The three zones of friction are shown in Figure 5-8. First, friction was found on the back slots of the SFU where the wire cables of each EWU pass through. The wire ropes rubbed against the outer edge of the slot. Such friction negatively affects the extension of the EWU. Second, friction was felt at the inner slots of the SU where the two wire ropes of the EWU pass through. For last two springs, friction prevented smooth forward and backward motion of the SU. Third, friction appeared to exist at the pulleys of the HJU. A small moment could be noticed when using spring #5. Note that, a lubrication grease was used to minimize friction effects.

Figure 5-8: Photographs of three zones of friction. Friction at back slot (detail A), friction on SU (detail B) and friction on pulleys (detail C).

- The load cells communicated to the Arduino Uno and RB-Onl-38 via 2 wire cables measuring 3 m. A research colleague was asked to stand in front of the participant when walking in order to lift the cables off the ground to avoid tripping. In future works, it would be beneficial to convert all wiring to a portable system.

- The load cells were placed close to each ankle joint. The reason for such a position is that the FBD reveal that only an axial and shear load are present. It was not physically

possible to place the load cells directly on the ankle joint. Instead, they were placed slightly above. The offset implies that each loadcell also read the strain contribution from the moment. In future works, one may consider using a number of strain gauges that can differentiate between axial and bending strain. Use of stain gauges can also be used to measure the shear strain acting near the ankle joint.

- The configuration of the two force plates may have influenced the gait of the participant. The two force plates are collinear and next to each other. In such a configuration, the participant needed to hit the bottom end of the first force plate in order to be able to hit the second force plate with his foot. In short, the user needed to consciously match his stepping pattern to the position of the two force plates.
- Reflective markers were placed on the participant using Velcro and double sided tape. Such method of fixation involves the risk of reflective marker moving with the surface of adherence. For example, the participant wore shorts on which a marker was placed on the femoral trochanter. Between trials, the shorts may have moved which affects hip kinematics.
- Gait Kinematics were computed according to the marker set proposed by D. A. Winter. Such a marker set was considered due to its simplicity in data interpretation. However, the marker set does not offer the highest accuracy for the position of joint centers due to the fact that it only considers motion in the sagittal plane.
- Fitting of the device remains an important source of errors in the comparison of trial results. The initial position of the SU with respect to the participant pelvis was measured to vary by 5 cm. Note that an accelerometer was initially used to track the spatial progression of the SU during gait. However, recurrent wiring problems and difficulties in converting acceleration values to displacement values forced one to abandon the measuring approach. There would be great benefit in completing the development of such measurement approach as it would allow the possibility to set the initial position of the SU.
- The thesis only considered the sagittal plane. During testing, it was noticed that motion about the frontal plane was increased and probably compensated for disrupted motion

about the sagittal plane. For all springs, the participant would walk with a ‘hip hiking’ pattern meaning he would excessively raise his pelvis to the side. Such motion would occur when the user needed to accomplish change of support on the RSU.

CHAPTER 6: CONCLUSIONS AND RECOMMENDATIONS

Chapter 6 concludes the thesis by summarizing the major achievements. It is followed by a list of suggestions on potential future work such to improve the design of the device, walking model and future use in testing trials.

6.1 CONCLUSION

In conclusion, four major accomplishments emerged.

First, the major goal of designing an entirely passive WAE was achieved. The design only employs mechanical components, making it a simple, light and cost effective assistive system. The proposed design structurally resembles the Honda Bodyweight Support Assist, but weights less than 6.5 kg. The device has the potential to offer a valuable assistance to the user during midstance.

Second, the development of a seat mechanism aimed to reduce felt weight was achieved. The combined action of the SU and EWU acts to produce an upward force when the user is standing and when the user is walking. Two analytical models were developed upon the mechanism to determine the assistance provided according to the spring selection, extension of spring and seat displacement. The walking model help predict the amount of maximum assistance provided to the user.

Third, a human scale prototype was fabricated by the researcher to match the anatomical needs of a single participant. The final prototype was built using affordable building materials and using common manufacturing techniques. A few modifications were brought to the final prototype, but overall it resembles the proposed design in terms of shape, composition and mechanical function.

Fourth, the final prototype was successfully tested throughout a standing and walking trial. Testing reveals that the intended upward force was created by the EWU and SU. Also, results clearly showed that the use of a stiffer spring yields a greater assistance. However, there is a range of stiffness where the device can be worn comfortably by the user. For most springs used, the values recorded by load cells matched closely the predicted values of the two models. For walking, the kinematics results revealed that the device interferes with gait of user. More importantly, kinematic results reveal a few design issues that need to be revised in order to further improve the design.

6.2 FUTURE WORK

Although much work was accomplished in the development of a passive WAE, many issues and problems emerged while modelling and testing the proposed design. In the process, many potential improvements were elaborated as to how fix these issues and problems. They are categorized in three sections: design improvements, model improvements and testing improvements.

6.2.1 DESIGN IMPROVEMENTS

- The RSU needs to be redesigned because it restricts hip motion. The unit needs to be converted from a rigid link to a variable length unit. One idea was to implement two pneumatic cylinders. Each cylinder would connect to each TLU. A manual valve would be used to block air flow in the right cylinder at start of gait. During midstance, the valve would gradually open to provide compliance and enable the other cylinder to take over the load.

- The KJU can be redesigned to provide quicker locking and unlocking. The use of rigid cable for unlocking proved to require a large effort. One solution venue proposed is to consider a weight activated knee joint. Such device uses a friction drum to block motion about the knee. Such design provides quick blocking action.

- The size of the SU should be increased in order to increase the contact area between the SU and the pelvis of the user. By comparison to the seat of the Honda Bodyweight Support Assist, the SU is much smaller. A larger SU implies a better load distribution of the upward force which in turns is expected to improve comfort.

- The SFU can be enlarged to provide more room for the SU to move forward and backward as well as moving upward and downward. The back portion of the SFU needs to be modified to eliminate friction with wire ropes. One solution is to create wider slots.

- The fabrication of future prototypes should be delegated to machinists such as to achieve higher quality of assembly.

- The FPU's can be improved by placing a form of padding on their attachment system to reduce the pressure points felt during use. The ankle joint can be enlarged in order to provide smoother motion.

6.2.2 MODEL IMPROVEMENTS

- The standing model can be improved by including a correction factor that considers the actual device position. The user can input the actual value of θ_{SLU} which is then considered in computing the value of F_{AXIAL}.
- The walking model can be redeveloped using the data of an elderly gait. It was found that using the device forced the user to walk with a short stride. Therefore, the motion of the exoskeleton was much lower than expected. By considering an elderly gait, it is expected that a better assessment on the performance of the device can be reached.
- Consider completing a 3D analysis for both standing and walking models. In doing so, both models would provide more accurate estimate of motion and load values.
- There would be great benefit to perform an Inverse Dynamics analysis. The data of markers combined with the data of force plates can be used to determine and produce moment and power plots. These plots would help in determining if the effect of upward force at the SU interface offsets the negative effect of additional weight.
- The final design can be used to construct a parametric model. The process involves creating a MATLAB script based on a geometrical and structural analysis to find the optimal geometry for a user of certain height and mass.

6.2.3 TESTING IMPROVEMENTS

- Develop a pressure sensing apparatus to be placed directly under the SU. Such apparatus would be used to measure directly the upward assistance at the SU interface.
- Use of several strain gauges to measure strain at the SLU instead of a load cell. By placing strain gauges closer to the ankle joint, an accurate assessment of loads can be achieved. Also, there is benefit in creating a wireless sensing apparatus to avoid distraction and tripping issues found with long cables.

- Complete the development of an accelerometer to track the displacement of the SU in time. Complete analysis script to properly interpret acceleration data.
- Use of 3D marker set such as Helen Hayes when using motion capture. The laboratory recently purchased Visual 3D, a biomechanical analysis software, that processes and analyses gait data. The software can rapidly compute gait kinematics when using market set such as the Helen Hayes.
- There is a need to test the device on more participants in order to draw better conclusions on if the device provides assistance to its user. It would be ideal to have a larger pool of male and female participants.

REFERENCES:

[1] P. Newman and A. Matan, "Human mobility and human health," *Curr. Opin. Environ. Sustain.*, vol. 4, no. 4, pp. 420–426, Oct. 2012.

[2] S. C. Government of Canada, "The Daily — Population projections: Canada, the provinces and territories, 2013 to 2063," 17-Sep-2014. [Online]. Available: http://www.statcan.gc.ca/daily-quotidien/140917/dq140917a-eng.htm. [Accessed: 14-Apr-2016].

[3] U. C. Bureau, "An Aging Nation: The Older Population in the United States." [Online]. Available: https://www.census.gov/library/publications/2014/demo/p25-1140.html. [Accessed: 18-Apr-2016].

[4] R. C. Browning and R. Kram, "Energetic Cost and Preferred Speed of Walking in Obese vs. Normal Weight Women," *Obes. Res.*, vol. 13, no. 5, pp. 891–899, May 2005.

[5] J. P. DeLany, D. E. Kelley, K. C. Hames, J. M. Jakicic, and B. H. Goodpaster, "High energy expenditure masks low physical activity in obesity," *Int. J. Obes.*, vol. 37, no. 7, pp. 1006–1011, Jul. 2013.

[6] L. K. Twells, D. M. Gregory, J. Reddigan, and W. K. Midodzi, "Current and predicted prevalence of obesity in Canada: a trend analysis," *CMAJ Open*, vol. 2, no. 1, pp. E18–E26, Jan. 2014.

[7] E. A. Finkelstein *et al.*, "Obesity and severe obesity forecasts through 2030," *Am. J. Prev. Med.*, vol. 42, no. 6, pp. 563–570, Jun. 2012.

[8] C. M. McDonough and A. M. Jette, "The contribution of osteoarthritis to functional limitations and disability," *Clin. Geriatr. Med.*, vol. 26, no. 3, pp. 387–399, Aug. 2010.

[9] S. C. Government of Canada, "Arthritis, by sex, and by province and territory (Number)," 07-Mar-2016.[Online].Available:http://www.statcan.gc.ca/tables-tableaux/sumsom/l01/cst01/health52a-eng.htm. [Accessed: 24-Apr-2016].

[10] J. M. Hootman, C. G. Helmick, K. E. Barbour, K. A. Theis, and M. A. Boring, "Updated projected prevalence of self-reported doctor-diagnosed arthritis and arthritis-attributable activity limitation among US adults, 2015-2040," *Arthritis Rheumatol. Hoboken NJ*, Mar. 2016.

[11] E. W. Gregg, M. M. Engelgau, and V. Narayan, "Complications of diabetes in elderly people," *BMJ*, vol. 325, no. 7370, pp. 916–917, Oct. 2002.

[12] R. Mendes, N. Sousa, J. Themudo-Barata, and V. Reis, "Impact of a community-based exercise programme on physical fitness in middle-aged and older patients with type 2 diabetes," *Gac. Sanit.*, vol. 30, no. 3, pp. 215–220, May 2016.

[13] S. C. Government of Canada, "Diabetes, by age group and sex (Number of persons)," 07-Mar-2016.[Online].Available:http://www.statcan.gc.ca/tables-tableaux/sumsom/l01/cst01/health53a-eng.htm. [Accessed: 30-Apr-2016].

[14] S. H. Collins, M. B. Wiggin, and G. S. Sawicki, "Reducing the energy cost of human walking using an unpowered exoskeleton," *Nature*, vol. 522, no. 7555, pp. 212–215, Jun. 2015.

[15] J. Rose and J. G. Gamble, *Human Walking*. Williams & Wilkins, 1994.

[16] J. Perry, *Gait Analysis: Normal and Pathological Function*. SLACK, 1992.

[17] D. A. Winter, *Biomechanics and Motor Control of Human Movement*. John Wiley & Sons, 2009.

[18] M. W. Whittle, *Gait Analysis: An Introduction*. Butterworth-Heinemann, 2014.

[19] T. M. Cook, K. P. Farrell, I. A. Carey, J. M. Gibbs, and G. E. Wiger, "Effects of restricted knee flexion and walking speed on the vertical ground reaction force during gait," *J. Orthop. Sports Phys. Ther.*, vol. 25, no. 4, pp. 236–244, Apr. 1997.

[20] G. A. Cavagna and M. Kaneko, "Mechanical work and efficiency in level walking and running," *J. Physiol.*, vol. 268, no. 2, pp. 467–481, Jun. 1977.

[21] R. C. Browning, J. R. Modica, R. Kram, and A. Goswami, "The effects of adding mass to the legs on the energetics and biomechanics of walking," *Med. Sci. Sports Exerc.*, vol. 39, no. 3, pp. 515–525, Mar. 2007.

[22] T. P. Huang and A. D. Kuo, "Mechanics and energetics of load carriage during human walking," *J. Exp. Biol.*, vol. 217, no. 4, pp. 605–613, Feb. 2014.

[23] M. Y. Zarrugh, F. N. Todd, and H. J. Ralston, "Optimization of energy expenditure during level walking," *Eur. J. Appl. Physiol.*, vol. 33, no. 4, pp. 293–306, 1974.
[24] J. Booyens and R. A. Mccance, "Individual variations in expenditure of energy" *The Lancet*, vol. 269, no. 6962, pp. 225–229, Feb. 1957.
[25] R. L. Waters and S. Mulroy, "The energy expenditure of normal and pathologic gait," *Gait Posture*, vol. 9, no. 3, pp. 207–231, Jul. 1999.
[26] N. Sekiya, H. Nagasaki, H. Ito, and T. Furuna, "Optimal walking in terms of variability in step length," *J. Orthop. Sports Phys. Ther.*, vol. 26, no. 5, pp. 266–272, Nov. 1997.
[27] S. M. O'Connor, H. Z. Xu, and A. D. Kuo, "Energetic cost of walking with increased step variability," *Gait Posture*, vol. 36, no. 1, pp. 102–107, May 2012.
[28] J. S. Gottschall and R. Kram, "Energy cost and muscular activity required for propulsion during walking," *J. Appl. Physiol.*, vol. 94, no. 5, pp. 1766–1772, May 2003.
[29] C. T. Farley and T. A. McMahon, "Energetics of walking and running: insights from simulated reduced-gravity experiments," *J. Appl. Physiol.*, vol. 73, no. 6, pp. 2709–2712, Dec. 1992.
[30] C. Kirtley, "Chapter 3 - Three-dimensional gait analysis," in *Clinical Gait Analysis*, Edinburgh: Churchill Livingstone, 2006, pp. 53–71.
[31] R. L. Waters, B. R. Lunsford, J. Perry, and R. Byrd, "Energy-speed relationship of walking: standard tables," *J. Orthop. Res. Off. Publ. Orthop. Res. Soc.*, vol. 6, no. 2, pp. 215–222, 1988.
[32] M. P. Steultjens, J. Dekker, M. E. van Baar, R. A. Oostendorp, and J. W. Bijlsma, "Range of joint motion and disability in patients with osteoarthritis of the knee or hip," *Rheumatol. Oxf. Engl.*, vol. 39, no. 9, pp. 955–961, Sep. 2000.
[33] R. J. Elble, S. S. Thomas, C. Higgins, and J. Colliver, "Stride-dependent changes in gait of older people," *J. Neurol.*, vol. 238, no. 1, pp. 1–5, Feb. 1991.
[34] D. J. Blanke and P. A. Hageman, "Comparison of gait of young men and elderly men," *Phys. Ther.*, vol. 69, no. 2, pp. 144–148, Feb. 1989.
[35] F. J. Imms and O. G. Edholm, "Studies of gait and mobility in the elderly," *Age Ageing*, vol. 10, no. 3, pp. 147–156, Aug. 1981.
[36] J. E. Himann, D. A. Cunningham, P. A. Rechnitzer, and D. H. Paterson, "Age-related changes in speed of walking," *Med. Sci. Sports Exerc.*, vol. 20, no. 2, pp. 161–166, Apr. 1988.
[37] P. A. Hageman and D. J. Blanke, "Comparison of gait of young women and elderly women," *Phys. Ther.*, vol. 66, no. 9, pp. 1382–1387, Sep. 1986.
[38] D. D. Larish, P. E. Martin, and M. Mungiole, "Characteristic patterns of gait in the healthy old," *Ann. N. Y. Acad. Sci.*, vol. 515, pp. 18–32, 1988.
[39] D. A. Winter, A. E. Patla, J. S. Frank, and S. E. Walt, "Biomechanical walking pattern changes in the fit and healthy elderly," *Phys. Ther.*, vol. 70, no. 6, pp. 340–347, Jun. 1990.
[40] A. M. Ferrandez, J. Pailhous, and M. Durup, "Slowness in elderly gait," *Exp. Aging Res.*, vol. 16, no. 1–2, pp. 79–89, Spring-Summer 1990.
[41] T. Oberg, A. Karsznia, and K. Oberg, "Basic gait parameters: reference data for normal subjects, 10-79 years of age," *J. Rehabil. Res. Dev.*, vol. 30, no. 2, pp. 210–223, 1993.
[42] J. O. Judge, R. B. Davis, and S. Ounpuu, "Step length reductions in advanced age: the role of ankle and hip kinetics," *J. Gerontol. A. Biol. Sci. Med. Sci.*, vol. 51, no. 6, pp. M303-312, Nov. 1996.
[43] P. R. Trueblood and L. Z. Rubenstein, "Assessment of instability and gait in elderly persons," *Compr. Ther.*, vol. 17, no. 8, pp. 20–29, Aug. 1991.
[44] V. Monaco, A. Ghionzoli, P. Dario, and S. Micera, "Muscle synergies during walking: comparison between young and elderly people. Preliminary results," *Conf. Proc. Annu. Int. Conf. IEEE Eng. Med. Biol. Soc. IEEE Eng. Med. Biol. Soc. Annu. Conf.*, vol. 2008, pp. 5370–5373, 2008.
[45] J. J. Eng and D. A. Winter, "Kinetic analysis of the lower limbs during walking: what information can be gained from a three-dimensional model?," *J. Biomech.*, vol. 28, no. 6, pp. 753–758, Jun. 1995.

[46] N. Stergiou, G. Giakas, J. B. Byrne, and V. Pomeroy, “Frequency domain characteristics of ground reaction forces during walking of young and elderly females,” *Clin. Biomech. Bristol Avon*, vol. 17, no. 8, pp. 615–617, Oct. 2002.
[47] Z. Lovrenovic and M. Doumit, “Review and analysis of recent development of lower extremity exoskeletons for walking assist,” in *2016 IEEE EMBS International Student Conference (ISC)*, 2016, pp. 1–4.
[48] H. Kazerooni, N. H. Harding, and R. Angold, “Lower extremity exoskeleton,” US7947004 B2, 24-May-2011.
[49] B. Chen *et al.*, “Recent developments and challenges of lower extremity exoskeletons,” *J. Orthop. Transl.*, vol. 5, pp. 26–37, Apr. 2016.
[50] H. Kazerooni, “A Review of the Exoskeleton and Human Augmentation Technology,” pp. 1539–1547, Jan. 2008.
[51] J. Ashihara *et al.*, “Walking assist device,” US8118763 B2, 21-Feb-2012.
[52] Y. Ikeuchi, J. Ashihara, Y. Hiki, H. Kudoh, and T. Noda, “Walking assist device with bodyweight support system,” in *IEEE/RSJ International Conference on Intelligent Robots and Systems, 2009. IROS 2009*, 2009, pp. 4073–4079.
[53] C. Buesing *et al.*, “Effects of a wearable exoskeleton stride management assist system (SMA®) on spatiotemporal gait characteristics in individuals after stroke: a randomized controlled trial,” *J. NeuroEngineering Rehabil.*, vol. 12, p. 69, 2015.
[54] R. Kitatani, K. Ohata, H. Takahashi, S. Shibuta, Y. Hashiguchi, and N. Yamakami, “Reduction in Energy Expenditure During Walking Using an Automated Stride Assistance Device in Healthy Young Adults,” *Arch. Phys. Med. Rehabil.*, vol. 95, no. 11, pp. 2128–2133, Nov. 2014.
[55] M. Ishikawa, P. V. Komi, M. J. Grey, V. Lepola, and G.-P. Bruggemann, “Muscle-tendon interaction and elastic energy usage in human walking,” *J. Appl. Physiol. Bethesda Md 1985*, vol. 99, no. 2, pp. 603–608, Aug. 2005.
[56] W. van Dijk and H. V. der Kooij, “XPED2: A Passive Exoskeleton with Artificial Tendons,” *IEEE Robot. Autom. Mag.*, vol. 21, no. 4, pp. 56–61, Dec. 2014.
[57] A. J. van den Bogert, “Exotendons for assistance of human locomotion,” *Biomed. Eng. OnLine*, vol. 2, p. 17, 2003.
[58] S. Krut, M. Benoit, E. Dombre, and F. Pierrot, “MoonWalker, a lower limb exoskeleton able to sustain bodyweight using a passive force balancer,” in *2010 IEEE International Conference on Robotics and Automation (ICRA)*, 2010, pp. 2215–2220.
[59] M. Kohei, *MoonWalker, a Lower Limb Exoskeleton able to Sustain Bodyweight using a Passive Force Balancer*. 2010.
[60] K. M. Lee and D. Wang, “Design analysis of a passive weight-support lower-extremity-exoskeleton with compliant knee-joint,” in *2015 IEEE International Conference on Robotics and Automation (ICRA)*, 2015, pp. 5572–5577.
[61] M. Doumit, A. Fahim, and M. Munro, “Analytical Modeling and Experimental Validation of the Braided Pneumatic Muscle,” *IEEE Trans. Robot.*, vol. 25, no. 6, pp. 1282–1291, Dec. 2009.
[62] J. Leclair, M. Doumit, and G. McAllister, “Analytical Stiffness Modeling and Experimental Validation for a Pneumatic Artificial Muscle,” p. V009T12A089, Nov. 2014.
[63] A. M. Dollar and H. Herr, “Lower Extremity Exoskeletons and Active Orthoses: Challenges and State-of-the-Art,” *IEEE Trans. Robot.*, vol. 24, no. 1, pp. 144–158, Feb. 2008.
[64] D. P. Ferris, G. S. Sawicki, and M. A. Daley, “A physiologist's perspective on robotic exoskeletons for human locomotion” *Int. J. HR Humanoid Robot.*, vol. 4, no. 3, pp. 507–528, Sep. 2007.
[65] Y.-H. Lu and X.-Q. Dai, “Effect of External Pressure on Skin Blood Flow at Lower Limb in Different Postures,” *J. Fiber Bioeng. Inform.*, vol. 3, no. 1, pp. 22–26, Jun. 2010.
[66] S. Sabri, V. C. Roberts, and L. T. Cotton, “Effects of Externally Applied Pressure on the Haemodynamics of the Lower Limb,” *Br. Med. J.*, vol. 3, no. 5773, pp. 503–508, Aug. 1971.

[67] J. M. Hidler and A. E. Wall, “Alterations in muscle activation patterns during robotic-assisted walking,” *Clin. Biomech. Bristol Avon*, vol. 20, no. 2, pp. 184–193, Feb. 2005.
[68] P. Paoletti and L. Mahadevan, “Balancing on tightropes and slacklines,” *J. R. Soc. Interface*, vol. 9, no. 74, pp. 2097–2108, Sep. 2012.
[69] D. G. E. R. Whittlesey Graham E.Caldwell, Joseph Hamill, Gary Kamen and Saunders N., *Research Methods In Biomechanics 2nd Edition*. Human Kinetics, 2013.

APPENDIX A: ADDITIONAL INFORMATIONS

The following section presents all the additional information mentioned in the main body and placed in the according order.

- Table A-1 provides a thorough description of the moment and power plots.

Table A-1: Interpretation of moment and power plots for GC.

ID	%	DESCRIPTION
IC	0	Moment: - Extensor moment at hip by contraction of extensors. - Flexor moment at knee by contraction of hamstrings. - Little moment at ankle. Power: - Generation of power at hip due to concentric contraction. - Generation of power at knee due to concentric contraction. - Little power at ankle.
LR	0-10	Moment: - Extensor moment at hip by contraction of extensors. - Flexor moment at knee by contraction of hamstrings. - Dorsiflexor moment to resist external plantarflexor moment. Power: - Generation of power at hip due to concentric contraction. - Generation of power at knee due to concentric contraction. - Absorption power by eccentric contraction of tibialis anterior.
OT	10	Moment: - Extensor moment at hip by contraction of extensors. - Extensor moment by quadriceps to opposed external extensor moment. - At ankle,GRF line move forward, dorsiflexor moment swift to plantarflexor moment. Power: - Hip continues to generate power. - Knee absorbs power by eccentric contraction of quadriceps. - Ankle shows little changes in power.
MS	10-30	Moment: - At hip, extensor moment declines and disappears to be replaced by opposite moment. - Internal moment at knee - At ankle, increasing plantarflexion moment. Power: -Gradual decrease of power at hip. - The knee moves from flexion to extension, power generation takes place by quadriceps contraction. - At ankle, eccentric contraction of triceps surae to absorb power.
HR	30	Moment: - At hip, increasing flexor moment by contraction of adductor longus and rectus femoris. - At knee, extensor shifted to flexor moment by contraction of quadriceps. - At ankle, internal flexor moment to oppose external extensor moment by triceps surae. Power: - At hip, power absorption.

		- At knee, small and variable power exchange. - At ankle, eccentric contraction generates power absorption.
OI	50	Moment: - At hip, peak flexor moment from adductor longus contraction, passive tension ligaments and gravity. - At knee, knee joint in front of GRF to reverse moment from flexor to extensor. - At ankle, force vector in front foot creates a plantarflexor moment to oppose dorisflexor moment. Power: - At hip, power generation. - At knee, power absorption to limit rate of knee flexion by eccentric contraction of rectus femoris. - At ankle, largest power generation to accelerate limb forward in swing by concentric contraction of triceps surae.
TO	60	Moment: - At hip, internal flexor moment from gravity, ligaments elasticity and contraction of adductor longus and iliopsoas. - At knee, internal extensor moment to oppose external moment. - At ankle, internal plantarflexor moment reduces rapidly. Power: - At hip, power generation. - At knee, eccentric contraction of rectus femoris to limit speed of knee flexion. - At ankle, generation falls to around zero.
FA	73	Moment: - At hip, internal flexor moment by gravity, ligaments elasticity and rectus femoris and adductors. - At knee, small extensor moment. - At ankle, very small moment at ankle only the weight of foot is involved. Power: - At hip, highest peak of power generation, - At knee, eccentric contraction result in power absorption to prevent knee flexing too rapidly.
TV	87	Moment: - At hip, increasing extensor moment by contraction of hamstrings and gluteus maximus. - At knee, increasing flexor moment to prevent hyperextension knee. - At ankle, moment remains close to zero. Power: - At hip, very little power exchange since hip is relatively static. - At knee, power absorption due to eccentric contraction of hamstrings. - At ankle, very little power exchange.

- Figure A-1 reveals the four initial concepts that were considered in the evaluation process.

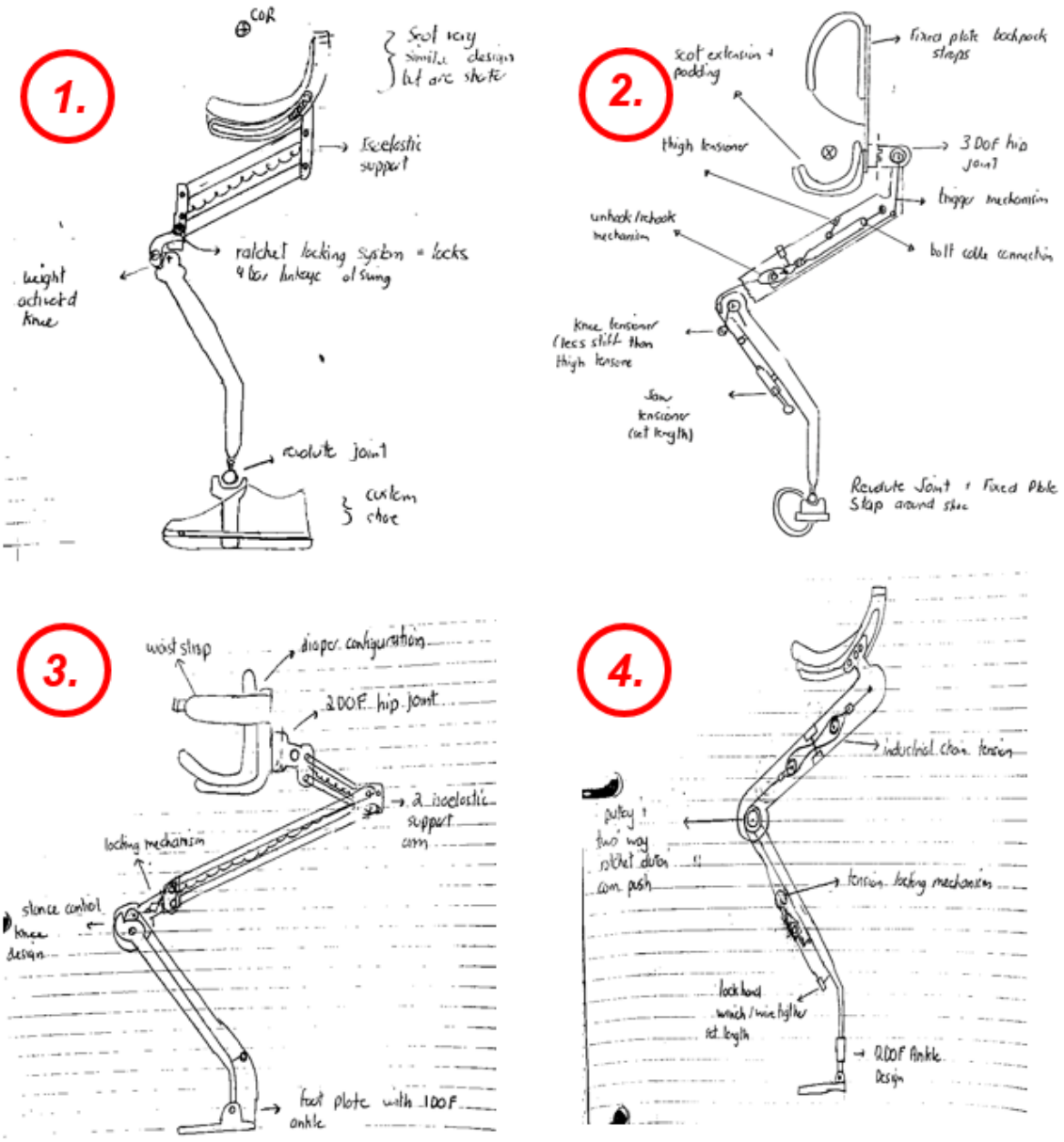

Figure A-1: Sketch of 4 design concepts for passive WAE.

- Table A-2 unveils the evaluation table produced in evaluating the 4 proposed design concepts.

Table A-2: Design Evaluation Table

Criteria	Weight	S1		S2		S3		S4	
		Score	W.S	Score	W.S.	Score	W.S.	Score	W.S.
1	10	80	8	72	7	63	8	72	10
2	8	64	8	64	6	48	8	64	8
3	9	63	6	42	7	49	9	63	9
4	6	36	4	24	9	54	6	36	6
5	7	42	7	42	9	54	7	42	7
6	8	72	6	54	6	54	8	72	8
7	8	48	6	48	6	72	9	64	8
TOTAL		367		298		322		349	

- Table A-3 and Figure A-2 presents the anthropometric data considered for the single participant.

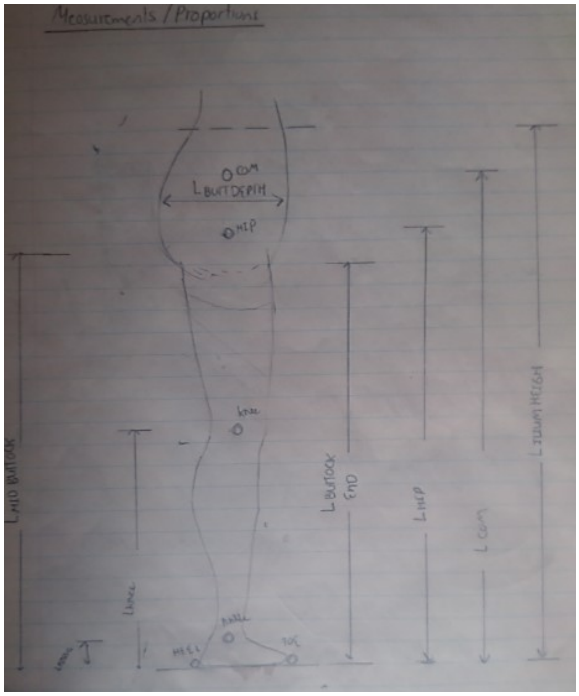

Figure A-2: Anthropometric schematic of human body.

Table A-3: Anthropometric data for participant (H=1.78 m)

Variable	Anthropometric relationship/ H	Value
L_{ILIUM}	0.602 H	107.3 cm
L_{COM}	0.551 H	98.3 cm
L_{HIP}	0.530 H	94.6 cm
$L_{BUTTOCK}$	0.458 H	81.7 cm
L_{KNEE}	0.283 H	50.5 cm
L_{ANKLE}	0.037 H	6.5 cm
$L_{BUTTOCK\ DEPTH}$	0.137 H	24.4 cm

- Figure A-3, Figure A-4 and Figure A-5 presents the remaining FBD of walking condition study. The force and moment equations can be found in the MATLAB script in APPENDIX B.

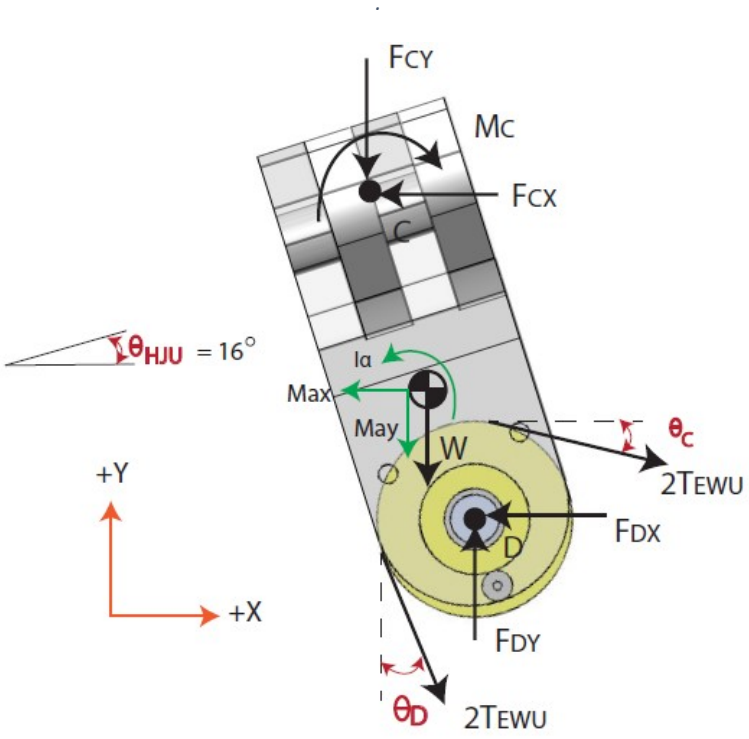

Figure A-3: FBD of HJU without connection plates at 20 % GC.

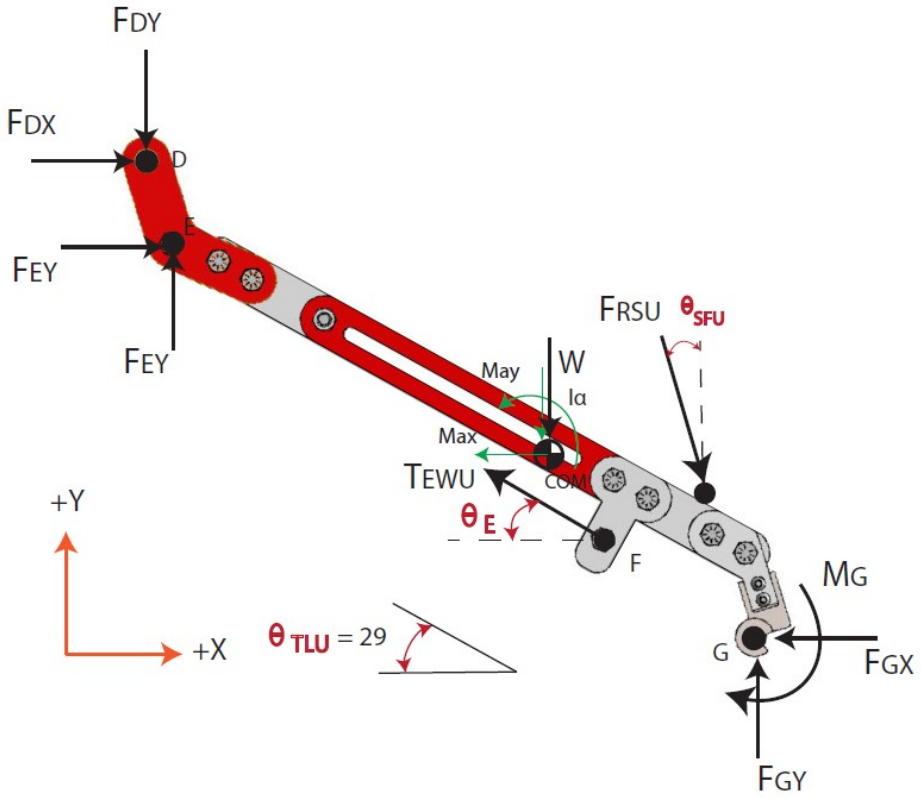

Figure A-4: FBD of TLU with connection plate and top half of KJU at 20 % GC.

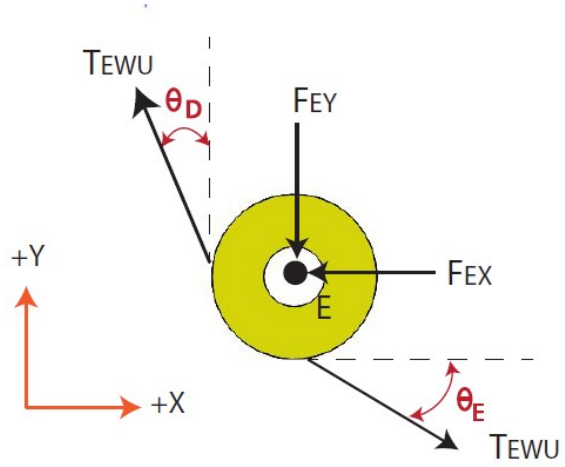

Figure A-5: FBD of small pulley at 20 % GC.

- Figure A-6 presents the Arduino programming code used to function the two load cells.

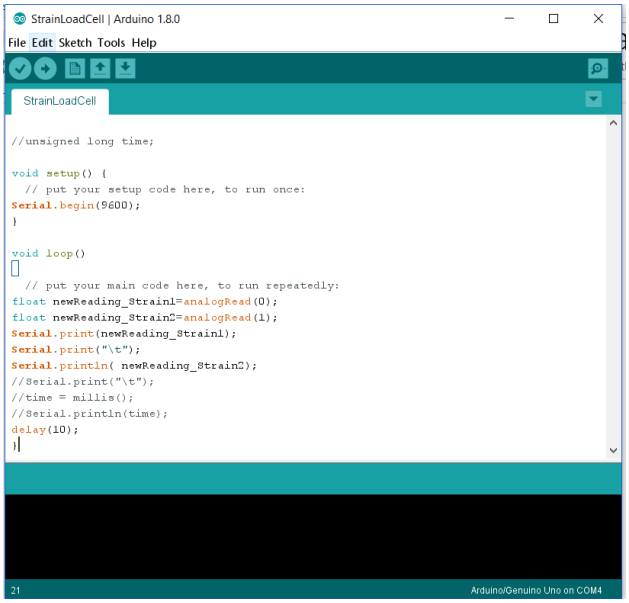

Figure A-6: Screen shot of MATLAB code for load cell use.

- Figure A-7 and Figure A-8 unveil the calibration plots generated for load cell #1 (right support leg) and load cell #2 (left support leg).

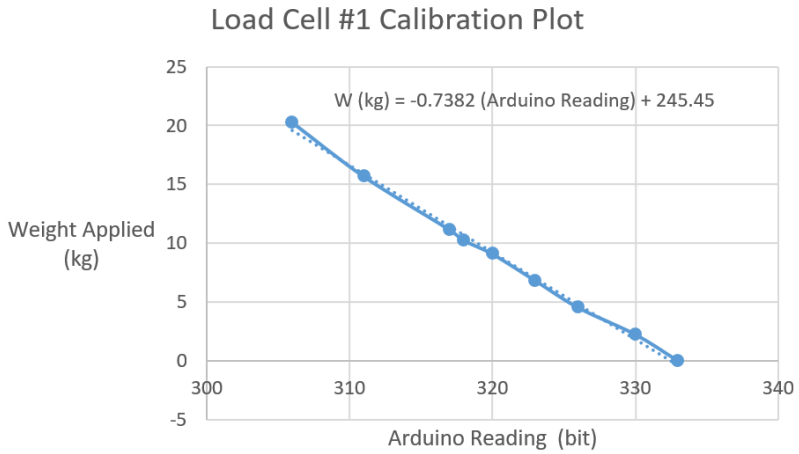

Figure A-7: Plot of calibration for load cell #1.

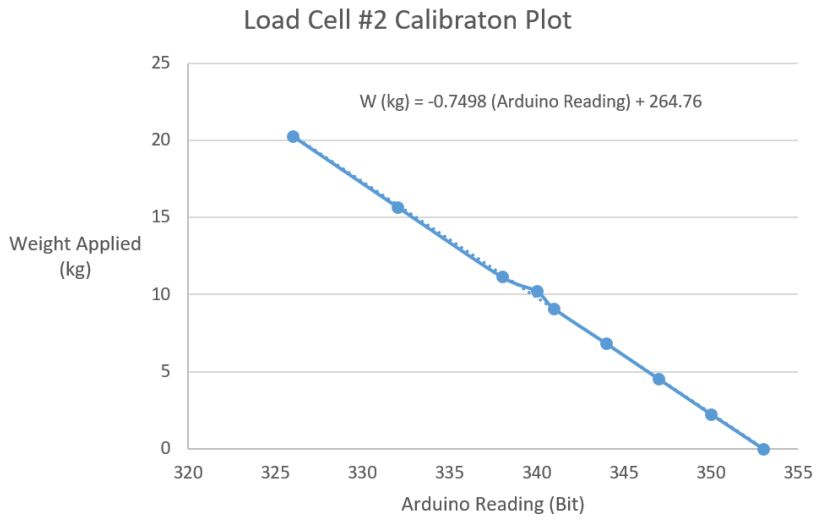

Figure A-8: Plot of calibration for load cell #2.

- Figure A-9 presents the CAD model of modified SLU.

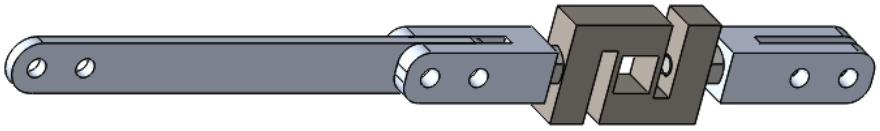

Figure A-9: CAD model of SLU with load cell.

APPENDIX B: MATLAB CODES

The following section unveils all the MATLAB script build and used in the thesis project.

01/05/17 10:54 PM E:\Masters Codin...\SeatDropSimulation.m 1 of 2

```
function [Seatdrop,forcespring,forceassist] = SeatDropSimulation()
%The function determine the amount of tension generated in the EWU and the
%assisitve force created at the seat.

%Define the initial length of segment AB
Lab1=14.125/100;

%Define the initial length of segment CD
Lcd1=14.125/100;

% Ask user to define the spring free length
Lspringzero=('Enter the free length of spring in cm')/100;

%Ask user to define the spring initial length
Lef1=input('Enter initial lenght of spring in cm')/100;

%Ask user for  the spring constant
Kspring=input('Enter the stiffness of spring in N/m');

%Determine the initial extension
initialdelta=Lef1-Lspringzero;


%Create a matrix for height drop of seat
Seatdrop=zeros(30,1);

for i=1:30
   Seatdrop(i,1)=(0.5*i)/100;
end

%Determine the tetha A and tetha C
tethaA=zeros(30,1);
tethaC=zeros(30,1);

for i=1:30
tethaA(i,1)=atand(Seatdrop(i,1)/Lab1);
tethaC(i,1)=atand(Seatdrop(i,1)/Lcd1);

end

%Determine the extension of segment AB and CD
Lab2=zeros(30,1);
Lcd2=zeros(30,1);
delthaLab=zeros(30,1);
delthaLcd=zeros(30,1);
for i=1:30
   Lab2(i,1)=Lab1/cos(tethaA(i,1)*pi/180);
   delthaLab(i,1)=Lab2(i,1)-Lab1;
   Lcd2(i,1)=Lcd1/cos(tethaC(i,1)*pi/180);
   delthaLcd(i,1)=Lcd2(i,1)-Lcd1;
end
```

```
%Determine the extension of spring
delthaLef=delthaLab+delthaLcd;

%Determine the force in EWU
forcespring=zeros(30,1);
for i=1:30
forcespring(i,1)=Kspring*(delthaLef(i,1)+initialdelta);
end

%Determine the amount of BW taken by the EWU
forceassist=zeros(30,1);
for i=1:30
   forceassist(i,1)=(2*(forcespring(i,1)*sin(tethaA(i,1)*pi/180)+forcespring(i,1)*sin↙
(tethaC(i,1)*pi/180)))/9.81;
end

end
```

```
function [Fiaxial,Fishear,Loadsharingleg,Faxialloadcell,Fshearloadcell,Mloadcell] =↙
StandingKinetics()
%The function determine the load sharing in each leg structure
%Define the initial length of segment AB
Lab1=14.125/100;

%Define the initial length of segment CD
Lcd1=14.125/100;

% Ask user to define the spring free length
Lspringzero=input('Enter the free length spring in cm')/100;

%Ask user to define the spring initial length
Lef1=input('Enter the initial spring length in cm')/100;

%Ask user to define the spring constant
Kspring=input('Enter the spring constant in N/m');

%Determine the initial extension
initialdelta=Lef1-Lspringzero;

%Define the expected seat drop
Seatdrop=12.50/100;

%Calculate tetha A
tethaA=atand(Seatdrop/Lab1);

%Calculate Lab2
Lab2=Lab1/cos(tethaA*pi/180);

%Calculate deltha Lab
delthaLab=Lab2-Lab1;

%Calculate tetha C
tethaC=atand(Seatdrop/Lcd1);

%Calculate Lcd2
Lcd2=Lcd1/cos(tethaC*pi/180);

%Calculate deltha Lcd
delthaLcd=Lcd2-Lcd1;

%Determine the extension of spring
delthaLef=delthaLab+delthaLcd;

%Determime tension in EWU
Tewu=Kspring*(delthaLef+initialdelta);

%Determine Fcx
Fcx=Tewu*cos(tethaA*pi/180)*2;
```

```
%Define the diameter of large pulley
Dpulley=50.80/1000;

%Define position of points C and D
pointC = [0,0.03585];
pointD = [0,-0.05228];

%Define tetha D
tethaD=7;

% Determine Mc
Mc=Fcx*(pointC(1,2)-pointD(1,2))-2*Tewu*cos(tethaC*pi/180)*Dpulley/2+2*Tewu*cos↙
(tethaD*pi/180)*Dpulley/2;

%Define position of points A, B and C
pointA = [-0.19719,0.00939];
pointB = [-0.05450,-0.11693];
pointC = [0.19797,0.09806];

%Define the Wslu
Wslu=0.90682;

%Define gravity cst
g=9.81;

%Calculate the value of Frsu
Frsu=(2*Tewu*cos(tethaA*pi/180)*(pointC(1,2)-pointA(1,2))+2*Tewu*sin(tethaA*pi/180)*↙
(pointC(1,1)-pointA(1,1))-Mc+Wslu*g*pointC(1,1))/(pointC(1,1)-pointB(1,1));

%Calculate the value of Fcy
Fcy=-2*Tewu*sin(tethaA*pi/180)-Wslu*g+Frsu;

%Calculate the value of Fdx
Fdx=(2*Tewu*cos(tethaC*pi/180)+2*Tewu*sin(tethaD*pi/180)-Fcx)/2;

%Define the Whju
Whju=0.59988;

%Calculate the value of Fdy
Fdy=(2*Tewu*sin(tethaC*pi/180)+2*Tewu*cos(tethaD*pi/180)+Whju*g-Fcy)/2;

%Define tethaE
tethaE=50;

%Calculate Fex
Fex=Tewu*cos(tethaE*pi/180)-Tewu*sin(tethaD*pi/180);

%Define weight of pulley
Wsmallpulley=0.00491;

%Calculate Fey
```

```
Fey=Tewu*cos(tethaD*pi/180)-Tewu*sin(tethaE*pi/180)+Wsmallpulley*g;

%Calculate Fgx
Fgx=-Tewu*cos(tethaE*pi/180)+Fex+Fdx;

%Define Wtlu
Wtlu=0.64483;

%Calculate Fgy
Fgy=Frsu/2+Wtlu*g+Fdy-Fey-Tewu*sin(tethaE*pi/180);

%Define points D,E,F,G,H
pointD=[0.20243,0.26568];
pointE=[0.20044,0.20952];
pointF=[-0.01809,-0.05729];
pointG=[-0.09359,-0.15016];
pointH=[-0.09353,-0.04919];

%Calculate Mg
Mg=-Frsu/2*(pointH(1,1)-pointG(1,1))+Wtlu*g*pointG(1,1)-Tewu*sin(tethaE*pi/180)*(pointF↙
(1,1)-pointG(1,1))+Tewu*cos(tethaE*pi/180)*(pointF(1,2)-pointG(1,2))-Fex*(pointE(1,2)-↙
pointG(1,2))-Fey*(pointE(1,1)-pointG(1,1))-Fdx*(pointD(1,2)-pointG(1,2))+Fdy*(pointD(1,1)↙
-pointG(1,1));

%Calculate the value of Fix
Fix=Fgx;

%Define the Wslu
Wslu=0.29978;

%Calculate Fiy
Fiy=Fgy+Wslu*g;

%Define tethaI
tethaI=15;

%Calculate the axial force Fiaxial
Fiaxial=Fiy*cos(tethaI*pi/180)-Fix*sin(tethaI*pi/180);

%Calculate the shear force Fishear
Fishear=+Fiy*sin(tethaI*pi/180)+Fix*cos(tethaI*pi/180);

%Calculate load shearing in kg
Loadsharingleg=Fiaxial/9.81;

%Calculate the axial force on load cell arrangement
Wsluloadcell=0.87999;
Faxialloadcell=(Fgy+Wsluloadcell*g)*cos(tethaI*pi/180)-Fix*sin(tethaI*pi/180);
Fshearloadcell=+(Fgy+Wsluloadcell*g)*sin(tethaI*pi/180)+Fix*cos(tethaI*pi/180);
%Calculate the moment at the loadcell
pointG=[-0.05042,0.30188];
```

```
pointJ=[0.01523,-0.06350];

Mloadcell=Mg-Fgy*(pointJ(1,1)-pointG(1,1))-Fgx*(pointG(1,2)-pointJ(1,2))-↙
Wsluloadcell*g*pointJ(1,1);
end
```



```
function [SPRINGEXTENSION,TIME] = PlotExoskeletonWinters()
%The function plots the progression of exoskeleton for 1 GC
 % Ask user to select an excel file
[filename,pathname]=uigetfile('*.xlsx');

%Read the time vector
TIME=xlsread(filename,'TIME');

% Read and store the position of markers placed on right leg.
RIGHTHIP=xlsread(filename,'RIGHTHIP');
RIGHTKNEE=xlsread(filename,'RIGHTKNEE');
RIGHTANKLE=xlsread(filename,'RIGHTANKLE');
RIGHTTOE=xlsread(filename,'RIGHTTOE');
RIGHTHEEL=xlsread(filename,'RIGHTHEEL');

% Read and store the position of markers placed on left leg.
LEFTHIP=xlsread(filename,'LEFTHIP');
LEFTKNEE=xlsread(filename,'LEFTKNEE');
LEFTANKLE=xlsread(filename,'LEFTANKLE');
LEFTTOE=xlsread(filename,'LEFTTOE');
LEFTHEEL=xlsread(filename,'LEFTHEEL');

% Read the position of the BUTTOCK
BUTT=xlsread(filename,'BUTT');

%Determine the size of TIME matrix
%Determine the size of dataset
sz=size(TIME);
numberframe=sz(1,1);

% Determine the angles of thigh, shank and foot in radians of right leg
RIGHTTETHATHIGHT=zeros(numberframe,1);
RIGHTTETHASHANK=zeros(numberframe,1);
RIGHTTETHAFOOT=zeros(numberframe,1);
for i=1:numberframe
%Compute the angle of  right thigh
    RIGHTTETHATHIGHT(i,1)=atan((RIGHTHIP(i,2)-RIGHTKNEE(i,2))/((RIGHTHIP(i,3)-RIGHTKNEE↙
(i,3))));

    %Compute the angle of right shank
    RIGHTTETHASHANK(i,1)=atan((RIGHTKNEE(i,2)-RIGHTANKLE(i,2))/((RIGHTKNEE(i,3)-↙
RIGHTANKLE(i,3))));

    %Compute the angle of right sole of foot
    RIGHTTETHAFOOT(i,1)=atan((RIGHTHEEL(i,2)-RIGHTTOE(i,2))/((RIGHTHEEL(i,3)-RIGHTTOE(i,↙
3))));
end

%Determine the angle of the right thigh and righ exothigh in degees
RIGHTTHIGHTANGLE=zeros(numberframe,1);
for i=1:numberframe
```

```
    %If tetha angle of thigh is negative, it needs to be corrected and
    %converted

    if RIGHTTETHATHIGHT(i,1)<0
    RIGHTTHIGHTANGLE(i,1)=(pi+RIGHTTETHATHIGHT(i,1))*180/pi;
    end

    %If tetha angle of thigh is positive, it needs to be converted

    if RIGHTTETHATHIGHT(i,1)> 0
      RIGHTTHIGHTANGLE(i,1)=(RIGHTTETHATHIGHT(i,1))*180/pi;
    end

end

% Determine the angle of right shank and right exo shank in degrees
RIGHTSHANKANGLE=zeros(numberframe,1);
for i=1:numberframe

    %If tetha angle of shank is negative, it needs to be corrected and
    %conveted
    if RIGHTTETHASHANK(i,1)<0
       RIGHTSHANKANGLE(i,1)=(pi+RIGHTTETHASHANK(i,1))*180/pi;
    end

    %If tetha angle of shank is positive, it needs to be converted
    if RIGHTTETHASHANK(i,1)>0
    RIGHTSHANKANGLE(i,1)=(RIGHTTETHASHANK(i,1))*180/pi;
    end

end

%Determine the angle of sole of foot in degrees
RIGHTFOOTANGLE=zeros(numberframe,1);
for i=1:numberframe
   RIGHTFOOTANGLE(i,1)=(RIGHTTETHAFOOT(i,1)+pi)*180/pi;
end

% Determine the angles of thigh, shank and foot in radians of right leg
LEFTTETHATHIGHT=zeros(numberframe,1);
LEFTTETHASHANK=zeros(numberframe,1);
LEFTTETHAFOOT=zeros(numberframe,1);
for i=1:numberframe
%Compute the angle of  right thigh
    LEFTTETHATHIGHT(i,1)=atan((LEFTHIP(i,2)-LEFTKNEE(i,2))/((LEFTHIP(i,3)-LEFTKNEE(i,↙
3))));

    %Compute the angle of right shank
    LEFTTETHASHANK(i,1)=atan((LEFTKNEE(i,2)-LEFTANKLE(i,2))/((LEFTKNEE(i,3)-LEFTANKLE(i,↙
3))));
```

```
    %Compute the angle of right sole of foot
    LEFTTETHAFOOT(i,1)=atan((LEFTHEEL(i,2)-LEFTTOE(i,2))/((LEFTHEEL(i,3)-LEFTTOE(i,3))));
end

%Determine the angle of the right thigh and righ exothigh in degees
LEFTTHIGHTANGLE=zeros(numberframe,1);
for i=1:numberframe

    %If tetha angle of thigh is negative, it needs to be corrected and
    %converted

    if LEFTTETHATHIGHT(i,1)<0
    LEFTTHIGHTANGLE(i,1)=(pi+LEFTTETHATHIGHT(i,1))*180/pi;
    end

    %If tetha angle of thigh is positive, it needs to be converted

    if LEFTTETHATHIGHT(i,1)> 0
      LEFTTHIGHTANGLE(i,1)=(LEFTTETHATHIGHT(i,1))*180/pi;
    end

end

% Determine the angle of right shank and right exo shank in degrees
LEFTSHANKANGLE=zeros(numberframe,1);
for i=1:numberframe

    %If tetha angle of shank is negative, it needs to be corrected and
    %conveted
    if LEFTTETHASHANK(i,1)<0
       LEFTSHANKANGLE(i,1)=(pi+LEFTTETHASHANK(i,1))*180/pi;
    end

    %If tetha angle of shank is positive, it needs to be converted
    if LEFTTETHASHANK(i,1)>0
    LEFTSHANKANGLE(i,1)=(LEFTTETHASHANK(i,1))*180/pi;
    end

end

%Determine the angle of sole of foot in degrees
LEFTFOOTANGLE=zeros(numberframe,1);
for i=1:numberframe
   LEFTFOOTANGLE(i,1)=(LEFTTETHAFOOT(i,1)+pi)*180/pi;
end

%Place the right and left exoankle
Ltoeexoankle=18.88/100;

RIGHTEXOANKLE=zeros(numberframe,2);
```

```
for i=1:numberframe
RIGHTEXOANKLE(i,1)= RIGHTTOE(i,3)+Ltoeexoankle*cos(RIGHTFOOTANGLE(i)*pi/180);
RIGHTEXOANKLE(i,2)= RIGHTTOE(i,2)+Ltoeexoankle*sin(RIGHTFOOTANGLE(i)*pi/180);
end

LEFTEXOANKLE=zeros(numberframe,2);
for i=1:numberframe
LEFTEXOANKLE(i,1)= LEFTTOE(i,3)+Ltoeexoankle*cos(LEFTFOOTANGLE(i)*pi/180);
LEFTEXOANKLE(i,2)= LEFTTOE(i,2)+Ltoeexoankle*sin(LEFTFOOTANGLE(i)*pi/180);
end


%Determine the right and left leg angle
RIGHTLEGTETHA=zeros(numberframe,1);
LEFTLEGTETHA=zeros(numberframe,1);
for i=1:numberframe
RIGHTLEGTETHA(i,1)=atan((RIGHTHIP(i,2)-RIGHTANKLE(i,2))/((RIGHTHIP(i,3)-RIGHTANKLE(i,↙
3))));
LEFTLEGTETHA(i,1)=atan((LEFTHIP(i,2)-LEFTANKLE(i,2))/((LEFTHIP(i,3)-LEFTANKLE(i,3))));
end

%Determine the angle of the right leg in degees
RIGHTLEGANGLE=zeros(numberframe,1);
for i=1:numberframe

    %If tetha angle of thigh is negative, it needs to be corrected and
    %converted

    if RIGHTLEGTETHA(i,1)<0
    RIGHTLEGANGLE(i,1)=(pi+RIGHTLEGTETHA(i,1))*180/pi;
    end

    %If tetha angle of thigh is positive, it needs to be converted

    if RIGHTLEGTETHA(i,1)> 0
      RIGHTLEGANGLE(i,1)=(RIGHTLEGTETHA(i,1))*180/pi;
    end

end

%Determine the angle of the right leg in degees
LEFTLEGANGLE=zeros(numberframe,1);
for i=1:numberframe

    %If tetha angle of thigh is negative, it needs to be corrected and
    %converted

    if LEFTLEGTETHA(i,1)<0
    LEFTLEGANGLE(i,1)=(pi+LEFTLEGTETHA(i,1))*180/pi;
    end
```

```
    %If tetha angle of thigh is positive, it needs to be converted

    if LEFTLEGTETHA(i,1)> 0
      LEFTLEGANGLE(i,1)=(LEFTLEGTETHA(i,1))*180/pi;
    end

end

% Determine the position of the shank based on rotation of leg for first 32
% frames
RIGHTEXOKNEE=zeros(numberframe,2);

%Define the initial angle between the shank and leg
shanknull=-15.41;

%Define the length of SLU
Lshank=480.60/1000;

%Determine the position of the right knee on the exoskeleton
for i=1:45
RIGHTEXOKNEE(i,1)=RIGHTEXOANKLE(i,1)+Lshank*cos((RIGHTLEGANGLE(i,1)+shanknull)*pi/180);
RIGHTEXOKNEE(i,2)=RIGHTEXOANKLE(i,2)+Lshank*sin((RIGHTLEGANGLE(i,1)+shanknull)*pi/180);
end

%Determine the SLU angle
RIGHTEXOSHANKANGLE=zeros(numberframe,1);
for i=1:45
RIGHTEXOSHANKANGLE(i,1)=atand((RIGHTEXOKNEE(i,2)-RIGHTEXOANKLE(i,2))/(RIGHTEXOKNEE(i,1)-↙
RIGHTEXOANKLE(i,1)));
if RIGHTEXOSHANKANGLE(i,1)<0
RIGHTEXOSHANKANGLE(i,1)=180+RIGHTEXOSHANKANGLE(i,1);
end

end

%Define the knee locking angle
Kneelockangle=114.73;

%Define the length of TLU
Lthigh=515.96/1000;

%Determine the TLU angle
RIGHTEXOTHIGHANGLE=zeros(numberframe,1);
for i=1:45
RIGHTEXOTHIGHANGLE(i,1)=270-(90-RIGHTEXOSHANKANGLE(i,1)+Kneelockangle);
end

%Determine the position of exohip for first set of points
RIGHTEXOHIP=zeros(numberframe,2);

for i=1:45
```

```
RIGHTEXOHIP(i,1)=RIGHTEXOKNEE(i,1)+Lthigh*cos((RIGHTEXOTHIGHANGLE(i,1))*pi/180);
RIGHTEXOHIP(i,2)=RIGHTEXOKNEE(i,2)+Lthigh*sin((RIGHTEXOTHIGHANGLE(i,1))*pi/180);
end

%Define the relative angle of SFU and TLU
RSUlockangle=54.31;

%Determine the angle of SFU
RIGHTEXOSEATANGLE=zeros(numberframe,1);
for i=1:45
RIGHTEXOSEATANGLE(i,1)=RSUlockangle-(180-RIGHTEXOTHIGHANGLE(i,1));
end

%Position the front SFU
Lcd=40.71/100;
RIGHTEXOSEAT=zeros(numberframe,2);
for i=1:29
  RIGHTEXOSEAT(i,1)=RIGHTEXOHIP(i,1)+Lcd*cos(RIGHTEXOSEATANGLE(i,1)*pi/180);
  RIGHTEXOSEAT(i,2)=RIGHTEXOHIP(i,2)+Lcd*sin(RIGHTEXOSEATANGLE(i,1)*pi/180);
end


%Loop equation used to determine the left SLU angle and left TLU angle
Angle1=zeros(numberframe,2);
Angle2=zeros(numberframe,2);
for i=1:45
syms x y
eqn1=Lshank*cos(x)+Lthigh*cos(y)==(RIGHTEXOHIP(i,1)-LEFTEXOANKLE(i,1));
eqn2=Lshank*sin(x)+Lthigh*sin(y)==(RIGHTEXOHIP(i,2)-LEFTEXOANKLE(i,2));
sol=solve([eqn1,eqn2],[x,y]);
Solx1=sol.x(1);
Soly1=sol.y(1);
Angle1(i,1)=double(Solx1)*180/pi;
Angle2(i,1)= double(Soly1)*180/pi;
Solx2=sol.x(2);
Soly2=sol.y(2);
Angle1(i,2)=double(Solx2)*180/pi;
Angle2(i,2)= double(Soly2)*180/pi;
end

%Define the left shankangle
LEFTEXOSHANKANGLE=zeros(numberframe,1);
for i=1:45
LEFTEXOSHANKANGLE(i,1)=Angle1(i,2);
end

%Define the left thigh angle
LEFTEXOTHIGHANGLE=zeros(numberframe,1);
for i=1:45
LEFTEXOTHIGHANGLE(i,1)=Angle2(i,2);
end
```

```
%Determine the position of left exo knee
LEFTEXOKNEE=zeros(numberframe,2);
for i=1:45
LEFTEXOKNEE(i,1)=LEFTEXOANKLE(i,1)+Lshank*cos(LEFTEXOSHANKANGLE(i,1)*pi/180);
LEFTEXOKNEE(i,2)=LEFTEXOANKLE(i,2)+Lshank*sin(LEFTEXOSHANKANGLE(i,1)*pi/180);
end

%Determine the seat angle based on left exothigh angle
for i=30:45
RIGHTEXOSEATANGLE(i,1)=RSUlockangle-(180-LEFTEXOTHIGHANGLE(i,1));
end

%Determine the position of exoseat when left leg is raising the SFU
for i=30:45
  RIGHTEXOSEAT(i,1)=RIGHTEXOHIP(i,1)+Lcd*cos(RIGHTEXOSEATANGLE(i,1)*pi/180);
  RIGHTEXOSEAT(i,2)=RIGHTEXOHIP(i,2)+Lcd*sin(RIGHTEXOSEATANGLE(i,1)*pi/180);
end

%Complete the angle of leftexothigh
for i=46:numberframe
count=i-45;
LEFTEXOTHIGHANGLE(i,1)=RIGHTEXOTHIGHANGLE(count,1);
end

%Complete the angle of leftexoknee
for i=46:numberframe
count=i-45;
LEFTEXOSHANKANGLE(i,1)=RIGHTEXOSHANKANGLE(count,1);
end

%Complete the angle of rightexothigh
for i=46:numberframe
count=i-45;
RIGHTEXOTHIGHANGLE(i,1)=LEFTEXOTHIGHANGLE(count,1);
end

%Complete the angle of rightexothigh
for i=46:numberframe
count=i-45;
RIGHTEXOSHANKANGLE(i,1)=LEFTEXOSHANKANGLE(count,1);
end

%Complete the right exoknee
for i=46:numberframe
RIGHTEXOKNEE(i,1)=RIGHTEXOANKLE(i,1)+Lshank*cos((RIGHTEXOSHANKANGLE(i,1))*pi/180);
RIGHTEXOKNEE(i,2)=RIGHTEXOANKLE(i,2)+Lshank*sin((RIGHTEXOSHANKANGLE(i,1))*pi/180);
end

%Place the left exo knee
for i=46:numberframe
```

```
LEFTEXOKNEE(i,1)=LEFTEXOANKLE(i,1)+Lshank*cos((LEFTEXOSHANKANGLE(i,1))*pi/180);
LEFTEXOKNEE(i,2)=LEFTEXOANKLE(i,2)+Lshank*sin((LEFTEXOSHANKANGLE(i,1))*pi/180);
end

% Plate the exohip
for i=46:numberframe
RIGHTEXOHIP(i,1)=LEFTEXOKNEE(i,1)+Lthigh*cos((LEFTEXOTHIGHANGLE(i,1))*pi/180);
RIGHTEXOHIP(i,2)=LEFTEXOKNEE(i,2)+Lthigh*sin((LEFTEXOTHIGHANGLE(i,1))*pi/180);
end

%Determine the rest of seat angle
for i=46:numberframe
    count=i-45;
RIGHTEXOSEATANGLE(i,1)=RIGHTEXOSEATANGLE(count,1);
end

%Determine the position of front of SFU
for i=46:numberframe
  RIGHTEXOSEAT(i,1)=RIGHTEXOHIP(i,1)+Lcd*cos(RIGHTEXOSEATANGLE(i,1)*pi/180);
  RIGHTEXOSEAT(i,2)=RIGHTEXOHIP(i,2)+Lcd*sin(RIGHTEXOSEATANGLE(i,1)*pi/180);
end


%Determine the length of segment EXOHIPSEAT
LEXOHIPSEAT=zeros(numberframe,1);
for i=1:90
LEXOHIPSEAT(i,1)=((RIGHTEXOSEAT(i,1)-RIGHTEXOHIP(i,1))^2+(RIGHTEXOSEAT(i,2)-RIGHTEXOHIP↙
(i,2))^2)^0.5;
end

%Determine the length of segment EXOSEATBUTT
LEXOSEATBUTT=zeros(numberframe,1);
for i=1:90
LEXOSEATBUTT(i,1)=((RIGHTEXOSEAT(i,1)-BUTT(i,3))^2+(RIGHTEXOSEAT(i,2)-BUTT(i,3))^2)^0.5;
end

%Determine the length of segment EXOHIPBUTT
LEXOHIPBUTT=zeros(numberframe,1);
for i=1:90
LEXOHIPBUTT(i,1)=((RIGHTEXOHIP(i,1)-BUTT(i,3))^2+(RIGHTEXOHIP(i,2)-BUTT(i,3))^2)^0.5;
end

%Determine the spring extension
SPRINGEXTENSION=zeros(numberframe,1);
for i=1:90
SPRINGEXTENSION(i,1)=LEXOSEATBUTT(i,1)+LEXOHIPBUTT(i,1)-LEXOHIPSEAT(i,1);
end

%Plot the data
figure
hold on
```

```
xlabel('Anterior / Posterior Position (m)')
ylabel('Superior / Inferior (m)')
for i=1:90
% Plot the right thigh
plot([RIGHTHIP(i,3),RIGHTKNEE(i,3)],[RIGHTHIP(i,2),RIGHTKNEE(i,2)],'r-o','LineWidth',1.5)

%Plot the right shank
plot([RIGHTKNEE(i,3),RIGHTANKLE(i,3)],[RIGHTKNEE(i,2),RIGHTANKLE(i,2)],'r-o','LineWidth',↙
1.5)

%Plot the right Ankle to Toe segment
plot([RIGHTANKLE(i,3),RIGHTTOE(i,3)],[RIGHTANKLE(i,2),RIGHTTOE(i,2)],'r-o','LineWidth',↙
1.5)

%Plot the right Ankle to Heel segment
plot([RIGHTANKLE(i,3),RIGHTHEEL(i,3)],[RIGHTANKLE(i,2),RIGHTHEEL(i,2)],'r-o','LineWidth',↙
1.5)

%Plot the right Heel to Toe segment
plot([RIGHTHEEL(i,3),RIGHTTOE(i,3)],[RIGHTHEEL(i,2),RIGHTTOE(i,2)],'r-o','LineWidth',1.5)

 % Plot the left thigh
plot([LEFTHIP(i,3),LEFTKNEE(i,3)],[LEFTHIP(i,2),LEFTKNEE(i,2)],'g-o','LineWidth',1.5)

%Plot the left shank
plot([LEFTKNEE(i,3),LEFTANKLE(i,3)],[LEFTKNEE(i,2),LEFTANKLE(i,2)],'g-o','LineWidth',1.5)

%Plot the left Ankle to Toe segment
plot([LEFTANKLE(i,3),LEFTTOE(i,3)],[LEFTANKLE(i,2),LEFTTOE(i,2)],'g-o','LineWidth',1.5)

%Plot the left Ankle to Heel segment
plot([LEFTANKLE(i,3),LEFTHEEL(i,3)],[LEFTANKLE(i,2),LEFTHEEL(i,2)],'g-o','LineWidth',1.5)

%Plot the left Heel to Toe segment
plot([LEFTHEEL(i,3),LEFTTOE(i,3)],[LEFTHEEL(i,2),LEFTTOE(i,2)],'g-o','LineWidth',1.5)

%Plot the BUTTOCK
plot(BUTT(i,3),BUTT(i,2),'k-o')

%Plot the right exoankle
plot(RIGHTEXOANKLE(i,1),RIGHTEXOANKLE(i,2),'b-o')

%Plot the left exoankle
plot(LEFTEXOANKLE(i,1),LEFTEXOANKLE(i,2),'m-o')

%Plot the right exo shank segment
plot([RIGHTEXOKNEE(i,1),RIGHTEXOANKLE(i,1)],[RIGHTEXOKNEE(i,2),RIGHTEXOANKLE(i,2)],'b-↙
o','LineWidth',1.5)

%Plot the right exo thigh segment
plot([RIGHTEXOHIP(i,1),RIGHTEXOKNEE(i,1)],[RIGHTEXOHIP(i,2),RIGHTEXOKNEE(i,2)],'b-↙
```

```
o','LineWidth',1.5)

% Plot the right seat segment
plot([RIGHTEXOSEAT(i,1),RIGHTEXOHIP(i,1)],[RIGHTEXOSEAT(i,2),RIGHTEXOHIP(i,2)],'b-
o','LineWidth',1.5)

%Plot the left exo shank segment
plot([LEFTEXOKNEE(i,1),LEFTEXOANKLE(i,1)],[LEFTEXOKNEE(i,2),LEFTEXOANKLE(i,2)],'m-
o','LineWidth',1.5)

%Plot the right exo thigh segment
plot([RIGHTEXOHIP(i,1),LEFTEXOKNEE(i,1)],[RIGHTEXOHIP(i,2),LEFTEXOKNEE(i,2)],'m-
o','LineWidth',1.5)

drawnow
pause(0.1)

end


end
```

```
function [RIGHTSEATPOSITION1,LEFTSEATPOSITION1,RIGHTSEAT1HEIGHTVARIATION,↙
LEFTSEAT1HEIGHTVARIATION,RIGHTSPRINGEXTENSION,LEFTSPRINGEXTENSION,↙
RIGHTLOADCELLMASSREADING,LEFTLOADCELLMASSREADING,GRFADJUST,VerticalGRF,↙
IncreaseVerticalGRF,TOTALLOADCELL,RIGHTSPRINGFORCE,LEFTSPRINGFORCE] =↙
AnalyzeSpringAlone()
%Function determine the load of load cells, position of seat, spring
%extension
% Ask user to select an excel file
[filename,pathname]=uigetfile('*.xlsx');

%Get data of markers placed on seat
RIGHTSEATPOSITION1=xlsread(filename,'RightSeat1');
%RIGHTSEATPOSITION2=xlsread(filename,'RightSeat2');
LEFTSEATPOSITION1=xlsread(filename,'LeftSeat1');

%Get data of spring on right leg
RIGHTLEGSPRINGLOW=xlsread(filename,'RightLegSpringLow');
RIGHTLEGSPRINGHIGH=xlsread(filename,'RightLegSpringHigh');

%Get data of spring on left leg
LEFTLEGSPRINGLOW=xlsread(filename,'LeftLegSpringLow');
LEFTLEGSPRINGHIGH=xlsread(filename,'LeftLegSpringHigh');

%Get data of load cell on right leg
RIGHTLEGLOADCELL=xlsread(filename,'LoadCellRight');

%Get data of load cell on left leg
LEFTLEGLOADCELL=xlsread(filename,'LoadCellLeft');

%Get data of GRF
GRF=xlsread(filename,'GRF');

%Determine the size of one matrix to be used
SIZEDATA=size(RIGHTSEATPOSITION1);
endpoint=SIZEDATA(1,1);

%Create an empty matrix for lenght of right spring
RIGHTSPRINGLENGTH=zeros(endpoint,1);

%Determine the lenght of right spring throughout trial
for i=1:endpoint
   RIGHTSPRINGLENGTH(i)=((RIGHTLEGSPRINGHIGH(i,1)-RIGHTLEGSPRINGLOW(i,1))^2+↙
(RIGHTLEGSPRINGHIGH(i,2)-RIGHTLEGSPRINGLOW(i,2))^2+(RIGHTLEGSPRINGHIGH(i,3)-↙
RIGHTLEGSPRINGLOW(i,3))^2)^0.5;
end

%Create an empty matrix for lenght of left spring
LEFTSPRINGLENGTH=zeros(endpoint,1);

%Determine the lenght of left spring throughout trial
for i=1:endpoint
```

```
   LEFTSPRINGLENGTH(i)=((LEFTLEGSPRINGHIGH(i,1)-LEFTLEGSPRINGLOW(i,1))^2+↙
(LEFTLEGSPRINGHIGH(i,2)-LEFTLEGSPRINGLOW(i,2))^2+(LEFTLEGSPRINGHIGH(i,3)-LEFTLEGSPRINGLOW↙
(i,3))^2)^0.5;
end

%Determine the initial lenght of right spring
RIGHTSPRINGINITIALLENGTH=RIGHTSPRINGLENGTH(1);

%Determine the initial lenght of left spring
LEFTSPRINGINITIALLENGTH=LEFTSPRINGLENGTH(1);

%Create two column matrix for spring extensions
RIGHTSPRINGEXTENSION=zeros(endpoint,1);
LEFTSPRINGEXTENSION=zeros(endpoint,1);

%Compute the spring extension of both spring
for i=1:endpoint

RIGHTSPRINGEXTENSION(i)=RIGHTSPRINGLENGTH(i)-RIGHTSPRINGINITIALLENGTH;
LEFTSPRINGEXTENSION(i)=LEFTSPRINGLENGTH(i)-LEFTSPRINGINITIALLENGTH;
end

%Ask user to define the zero lenght of right spring in cm
ZEROLENGTHRIGHTSPRING=input('Enter zero length of right spring in cm')/100;

% Ask user to define the initial length of right spring on exoskeleton in cm
INITIALLENGTHRIGHTSPRING=input('Enter the initial lenght of right spring in cm')/100;

%Ask user to define the spring constant
SPRINGCONSTANTRIGHTSPRING=input('Enter the spring constant in Nm');

%Compute the right spring force  based on initial dimension
RIGHTSPRINGFORCE=zeros(endpoint,1);
for i=1:endpoint
RIGHTSPRINGFORCE(i)=(INITIALLENGTHRIGHTSPRING+RIGHTSPRINGEXTENSION(i)-↙
ZEROLENGTHRIGHTSPRING)*SPRINGCONSTANTRIGHTSPRING;
end

%Ask user to define the zero lenght of right spring in cm
ZEROLENGTHRIGHTSPRING=input('Enter zero length of right spring in cm')/100;

% Ask user to define the initial length of right spring on exoskeleton in cm
INITIALLENGTHRIGHTSPRING=input('Enter the initial lenght of right spring in cm')/100;

%Ask user to define the spring constant
SPRINGCONSTANTRIGHTSPRING=input('Enter the spring constant in Nm');


%Compute the left spring force based on initial dimension
LEFTSPRINGFORCE=zeros(endpoint,1);
for i=1:endpoint
```

```
LEFTSPRINGFORCE(i)=(INITIALLENGTHLEFTSPRING+LEFTSPRINGEXTENSION(i)-ZEROLENGTHLEFTSPRING)
*SPRINGCONSTANTLEFTSPRING;
end

%Determine the load detected by the right load cell
RIGHTLOADCELLMASSREADING=zeros(endpoint,1);
for i=1:endpoint
RIGHTLOADCELLMASSREADING(i)=-0.6904*RIGHTLEGLOADCELL(i)+229.88;
end

%Determine the load detected by the left load cell
LEFTLOADCELLMASSREADING=zeros(endpoint,1);
for i=1:endpoint
LEFTLOADCELLMASSREADING(i)=-0.6904*LEFTLEGLOADCELL(i)+242.31;
end

%Determine the total load in both load cell
TOTALLOADCELL=LEFTLOADCELLMASSREADING+RIGHTLOADCELLMASSREADING;

% Determine the height variation of marker 1 on right side of seat unit
RIGHTSEAT1HEIGHTVARIATION=zeros(endpoint,1);
RIGHTSEAT1INITIALHEIGHT=RIGHTSEATPOSITION1(1,2);
for i=1:endpoint
RIGHTSEAT1HEIGHTVARIATION(i)=RIGHTSEATPOSITION1(i,2)-RIGHTSEAT1INITIALHEIGHT;
end

%Determine the height varion of marker 2 on right side of seat unit
RIGHTSEAT2HEIGHTVARIATION=zeros(endpoint,1);
 RIGHTSEAT2INITIALHEIGHT=RIGHTSEATPOSITION2(1,2);
 for i=1:endpoint
 RIGHTSEAT2HEIGHTVARIATION(i)=RIGHTSEATPOSITION2(i,2)-RIGHTSEAT2INITIALHEIGHT;
 end

% Determine the height variation of marker 1 on left side of seat unit
LEFTSEAT1HEIGHTVARIATION=zeros(endpoint,1);
LEFTSEAT1INITIALHEIGHT=LEFTSEATPOSITION1(1,2);
for i=1:endpoint
LEFTSEAT1HEIGHTVARIATION(i)=LEFTSEATPOSITION1(i,2)-LEFTSEAT1INITIALHEIGHT;
end

%Extract GRF for 100 sampling frequency, take values every 10 reading
GRFADJUST=zeros(endpoint,3);
GRFADJUST(1,1)=GRF(1,1);
GRFADJUST(1,2)=GRF(1,2);
GRFADJUST(1,3)=GRF(1,3);

for i=1:endpoint
    a=i*10+1;
GRFADJUST(i,1)=GRF(a,1);
GRFADJUST(i,2)=GRF(a,2);
GRFADJUST(i,3)=GRF(a,3);
```

```
end

%Represent vertical component in kg
VerticalGRF=-GRFADJUST(:,3)/9.81;

%Compute the increased GRF in kg
VerticalGRFInitial=VerticalGRF(1);
IncreaseVerticalGRF=VerticalGRF(:)-VerticalGRFInitial;

end
```

APPENDIX C: ETHICS APPROVAL

File Number: H02-17-02 **Date (mm/dd/yyyy):** 05/23/2017

Université d'Ottawa
Bureau d'éthique et d'intégrité de la recherche

University of Ottawa
Office of Research Ethics and Integrity

Ethics Approval Notice

Health Sciences and Science REB

Principal Investigator / Supervisor / Co-investigator(s) / Student(s)

First Name	Last Name	Affiliation	Role
Marc	Doumit	Engineering / Mecanical Engineering	Supervisor
Zlatko	Lovrenovic	Engineering / Mecanical Engineering	Student Researcher

File Number: H02-17-02

Type of Project: Master's Thesis

Title: Effectiveness of passive walking assist exoskeleton with upward assistance force

Approval Date (mm/dd/yyyy)	Expiry Date (mm/dd/yyyy)	Approval Type
05/23/2017	05/22/2018	Approval

Special Conditions / Comments:
N/A

APPENDIX D: ADDITIONNAL RESULTS

The following section presents all the additional results mentioned in the reports.

- Figure A-10 and Figure A-11 present the results of manual tests conducted on the final prototype using 6 different springs.

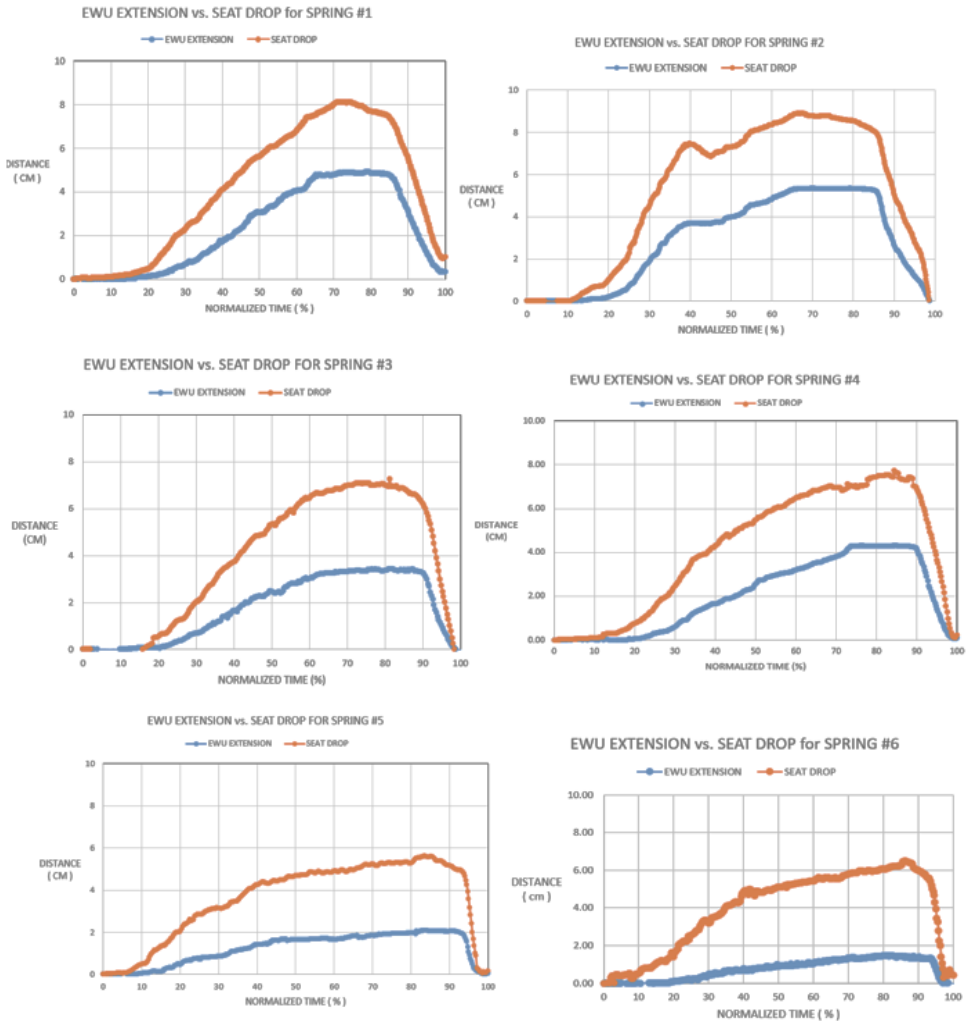

Figure A-10: Results value of ΔL_{SPRING} versus ΔY_{SEAT} for manual tests using 6 different springs.

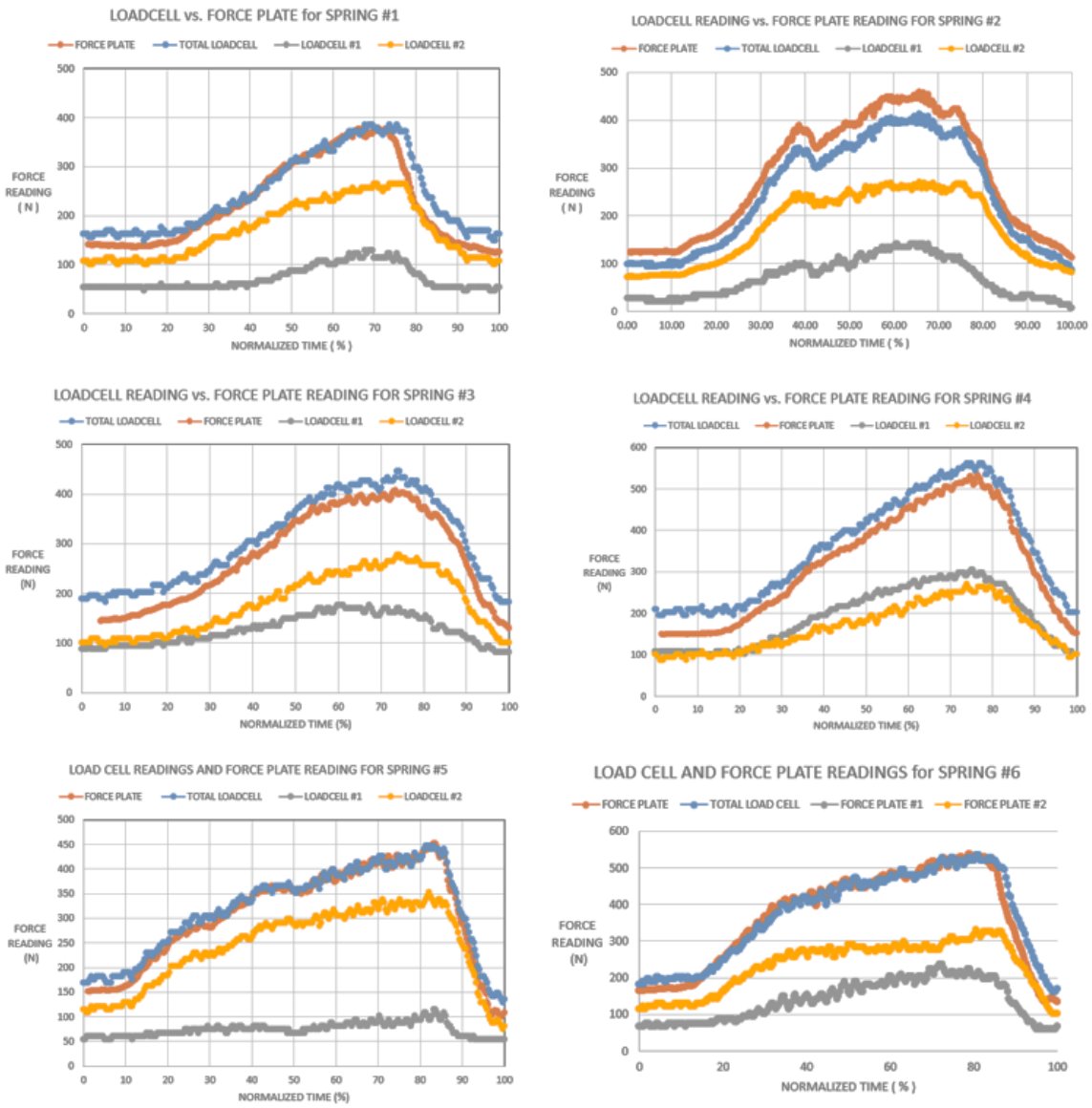

Figure A-11: Results values of force readings vs. normalized time for manual tests using 6 different springs.

- Figure A-12 presents the results of hip kinematics for all testing conditions.

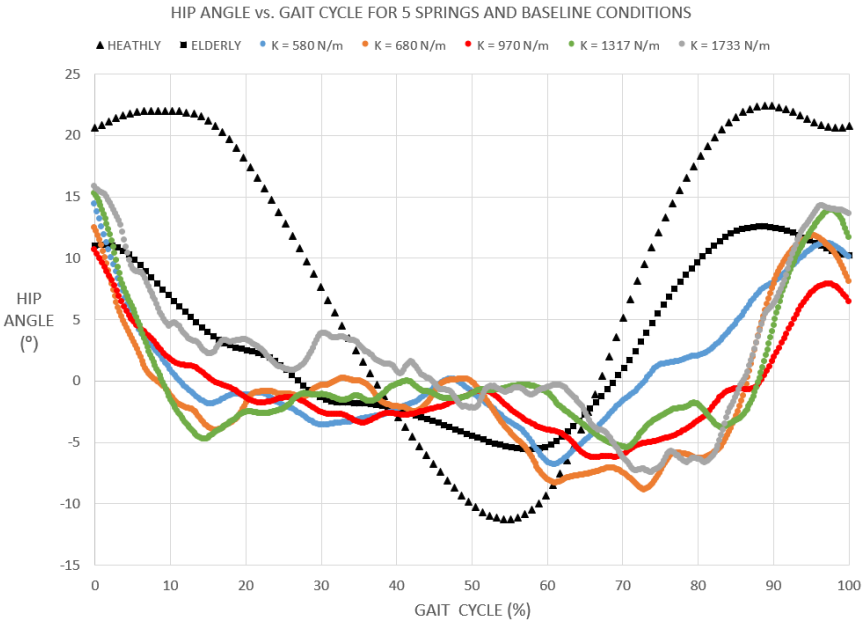

Figure A-12: Hip angle vs. gait cycle for all walking conditions.

- Figure A-13 presents the results of knee kinematics for all testing conditions.

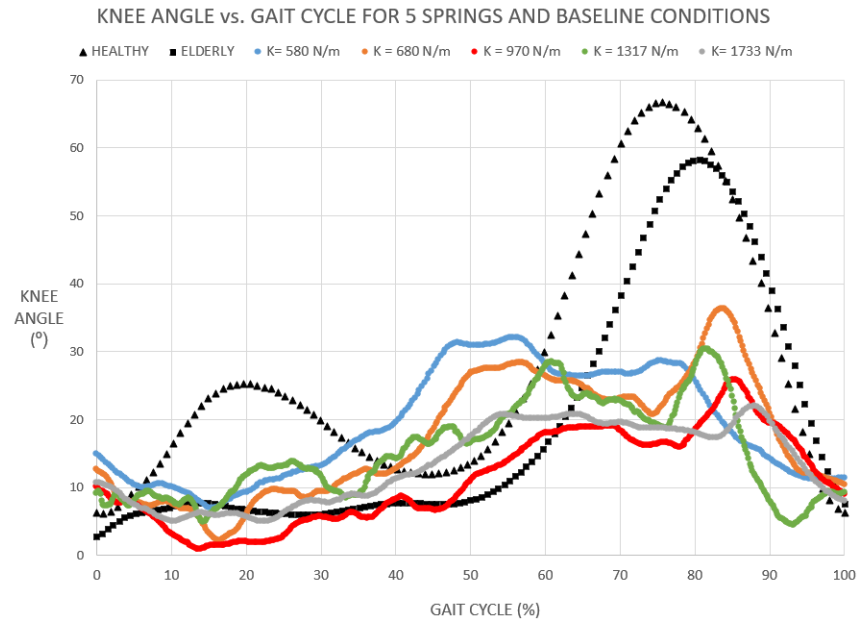

Figure A-13: Knee angle vs. gait cycle for all walking conditions.

- Figure A-14 presents the results of ankle kinematics for all testing conditions.

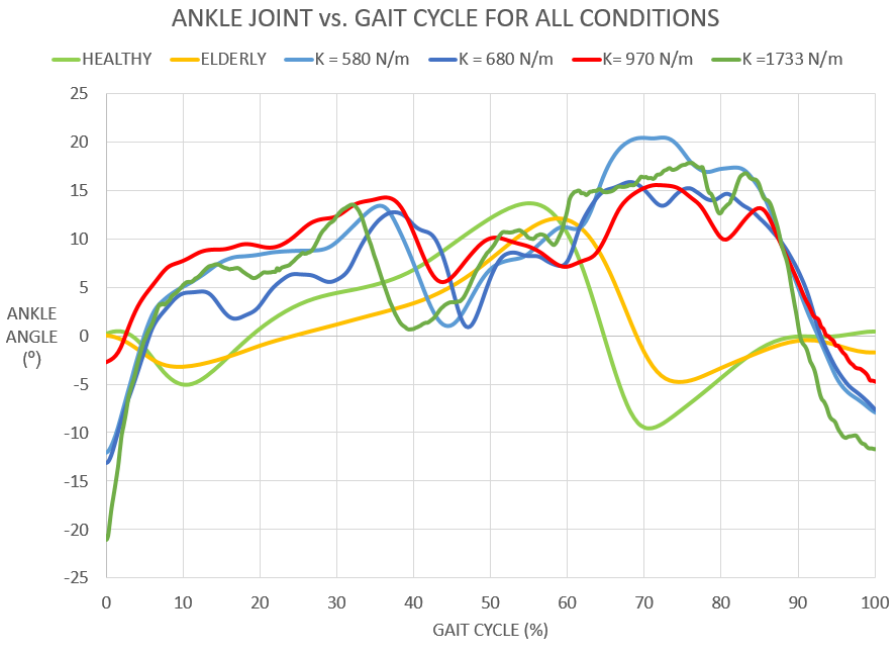

Figure A-14: Ankle angle vs. gait cycle for all walking conditions.

- Figure A-15 presents the results of vertical GRF for all testing conditions.

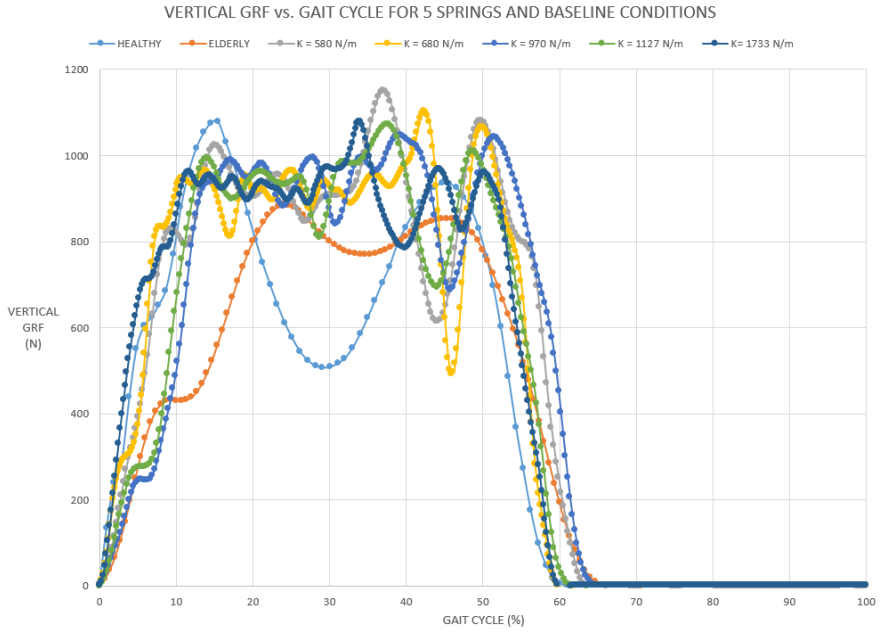

Figure A-15: Vertical GRF values vs. gait cycle for all walking conditions.